2009

Experimental Design, Synthesis and Application of Molecular Micelle Modified Polymeric Nanoparticles for Drug Delivery Systems and Free Radical Detection

Gabriela M. Ganea Visser
Louisiana State University and Agricultural and Mechanical College, gabiganea@yahoo.com

EXPERIMENTAL DESIGN, SYNTHESIS AND APPLICATION OF MOLECULAR MICELLE MODIFIED POLYMERIC NANOPARTICLES FOR DRUG DELIVERY SYSTEMS AND FREE RADICAL DETECTION

A Dissertation

Submitted to the Graduate Faculty of the
Louisiana State University and
Agricultural and Mechanical College
In partial fulfillment of the
Requirements for the degree of
Doctor of Philosophy

in

The Department of Chemistry

By
Gabriela M. Visser
B.S., University of Bucharest, Romania, 1997
M.S., University of Bucharest, Romania, 2004
December 2009

To my Romanian and Dutch families, my mother, Cristina, who is my continuous inspiration, my sister, Daniela, who empowers me with her strength, and my husband, Richard, whose unconditional love and support have kept me going on through this journey.

ACKNOWLEDGEMENTS

This work was accomplished with the support of many professors, students, and colleagues to whom I am deeply thankful.

Dr. Isiah M. Warner, for his tremendous patience, wisdom, and knowledge. Working in your research group was the best experience of my life. You helped me develop valuable skills that otherwise I would not have known. I greatly appreciate your guidance, ethics, enthusiasm and commitment to science.

Committee Members: Dr. Doug Gilman, Dr. Jack Losso, Dr. Cristina Sabliov, and **Dr. Ray Ferrell**, for their time and helpful discussions. Special thanks to Dr. Cristina Sabliov for her advice and great interest in my research, and Dr. Jack Losso, for his contribution in the cytotoxicity studies and our many discussions regarding antioxidants and natural products.

Dr. Sayo O. Fakayode, for sharing his knowledge in chemometrics and statistical analysis. I am convinced that my success has started when we discussed about my first experimental design.

Dr. Cornelus van Nostrum, for the collaboration work in his lab at Utrecht University, The Netherlands, as well as his critical and honest feedback.

Post doctoral researchers and graduate students of the Warner Research Group, for challenging me with questions in group meetings, brainstorming, laughs, friendship and support over the years.

Undergraduate students: Paulina Kolic, for her hard work during two summer semesters, helping me when I needed it the most, and **Abei Ishola** and **Stephen Maffett**, who found time to work on my projects between their tests and finals.

Karen Mcdonough, for her help in cell culture studies, including weekends and late nights.

Matthew Brown and **Ying Xiao**, for their assistance in microscopy.

TABLE OF CONTENTS

LIST OF TABLES

LIST OF FIGURES

LIST OF ABBREVIATIONS

Abbreviation	Name
17-AAG	17-allylamino-17-demethoxygeldanamycin
17-DAAG	17-dimethylaminoethylamino-17-demethoxy-geldanamycin
7-OH C3C	7-hydroxy coumarin 3-carboxylic acid
ANOVA	Analysis of variance
ATCC	American Tissue Culture Collection
BHA	4-methoxy-2-tert-butyl phenol
BHT	2,6 di-tert-butyl p-hydroxytoluene
C3C	Coumarin 3-carboxylic acid
C3C-poly-Nε-SUK	Coumarin 3-carboxylic acid functionalized poly (sodium *N*-undecenyl-Nε-Boc lysinate)
CCD	Central composite experimental design
CMC	Critical micelle concentration
DCC	*N,N'*-dicyclohexylcarbodiimide
DCM	Dichloromethane
DLS	Dynamic light scattering
DMAB	Dodecyl dimethyl ammonium bromide
DMF	Dimethyl formamide
DMSO	Dimethyl sulfoxide
DPPH	2,2-diphenyl-1-picrylhydrazyl
EE %	Entrapment efficiency
EHS	Environment Health and Safety

EPR	Electron Paramagnetic Resonance
FDA	Food and Drug Administration
FL	Fluorescence
IC	Internal conversion
ICX	Intersystem crossing
GSP	Glutathione peroxidase
HPLC	High Performance Liquid Chromatography
MLR	Multilinear regression
MTS	3-(4,5-dimethylthiazol-2-yl)-5-(3-carboxymethoxyphenyl)-2-(4-sulfo-phenyl)-2H-tetrazolium salt
NeR	Neutral red
NHS	*N*-hydroxysuccinimide
NNI	National Nanotechnology Initiative
NQO1	NADH quinone oxidoreductase
O/W	Oil-in-water emulsion
PDI	Polydispersity index
PEG	Poly (ethylene glycol)
PH	Phosphorescence
PLGA	Poly(lactide-co-glycolide)
Poly-Nε-Boc-SUK	Poly (sodium *N*-undecenyl-Nε-Boc lysinate)
Poly-SHG	Poly(sodium *N*-heptenyl-glycinate)
Poly-SDG	Poly(sodium *N*-decenyl-glycinate
Poly-SUA	Poly(sodium *N*-undecenyl-alaninate)
Poly-SUG	Poly (sodium *N*-undecenyl-glycinate)

Poly-SUL	Poly(sodium *N*-undecenyl-leucinate)
Poly-L-SULV	Poly (sodium *N*-undecenyl-L-leucyl-valinate)
Poly-SUS	Poly (sodium *N*-undecenyl sulfate)
Poly-SUV	Poly(sodium *N*-undecenyl-valinate)
PVA	Poly (vinyl alcohol)
Q10	Ubiquinone, coenzyme Q10
ROS	Reactive oxygen species
SDG	Sodium *N*-decenyl-glycinate
SDS	Sodium dodecyl sulfate
SECCA	Succinimidyl ester of coumarin 3-carboxylic acid
SHG	Sodium *N*-heptenyl-glycinate
SOD	Superoxide dismutase
SUA	Sodium *N*-undecenyl-alaninate
SUG	Sodium *N*-undecenyl-glycinate
SUL	Sodium *N*-undecenyl-leucinate
SUV	Sodium *N*-undecenyl-valinate
TBHQ	Tert-butyl hydroquinone
TEM	Transmission Electron Microscopy
TFA	Trifluoroacetic acid
TPGS	Tocopheryl polyethylene glycol succinate
TQ	Thymoquinone

ABSTRACT

Biodegradable and biocompatible polymeric nanoparticles such as poly (lactide-*co*-glycolide) (PLGA) nanoparticles have been extensively studied as drug delivery systems for a variety of pharmaceutical agents. Nanoparticle surface properties are primarily determined by the emulsifiers used in the synthesis process, which have a significant impact on nanoparticle physico-chemical and biological properties. Anionic amino acid – based molecular micelles were used in the emulsification process to prepare monodisperse, small (below 100 nm) PLGA nanoparticles with a well defined spherical shape. Such molecular micelle – modified nanoparticles were used as drug carriers for delivery of antioxidants. Thymoquinone is a natural antioxidant, and an emerging anticancer drug found in *Nigella sativa* black seed oil. Thymoquinone – loaded nanoparticles demonstrated improved properties when compared with the free drug, suggesting that such nanoparticle systems are promising candidates for antioxidant delivery and tumor growth inhibition. Furthermore, polymeric nanoparticles were used as sensors for detection of hydroxyl radicals. Ratiometric fluorescent molecular micelle – modified PLGA nanoparticles were designed using a reporting dye (coumarin – functionalized molecular micelle) present on their surface as well as a reference dye (neutral red) encapsulated into the polymeric matrix. The nanoparticles were able to detect hydroxyl radicals in a time and concentration dependent manner, and presented high selectivity for hydroxyl radicals as compared with other reactive oxygen species. In addition, the ratiometric fluorescent nanosensors were able to detect hydroxyl radicals in viable cells exposed to oxidative stress, allowing their potential use in the study of other living systems.

CHAPTER 1

INTRODUCTION

1.1 Nanotechnology and Drug Delivery Systems

If we were to build a scale of things, we would start by thinking about how big a planet is or how high we have to climb to the peak of a mountain. In contrast, we observe small objects around us such as the head of a pin (2 mm) or the width of a hair (50-150 μm). However, there is a smaller scale that we cannot see, the nanometer scale. For example, a double DNA strand is only a few nanometers in diameter. In addition, nanometer size materials offer unique properties. For example, quantum dots have size-dependent spectral properties, emitting light from blue to red and into the near-infrared. In the medical field, drug-loaded nanoparticles can target specific cells or can migrate through the blood brain barrier while the drug itself cannot.[1, 2] Therefore, science and technology are focused nowadays towards the nanometer scale, specifically to take advantage of such nanoscale properties.

The fabrication, characterization, and application of structures and devices having tunable properties determined by their nanometer size (≤100 nm) represent the discipline of nanotechnology.[3, 4] Nanotechnology is constructed on a strong foundation of cumulative efforts of chemists, biologists, physicists and engineers. Their goals include the discovery and the development of new and innovative technologies, assessment of social and health risk factors as well as sustainability for future generations.[5-7] Since the lecture of Richard Feynman entitled "There is plenty of room at the bottom" at CalTech in 1959, the development of nanotechnology has increased dramatically.[8-10] The transition from the macroscopic materials and devices to the nanoworld has been observed in many areas including material science, energy, agriculture, communications, environment, health care, and aerospace. Recently, a research group from the University of Arizona has developed an internet based database, called "nano mapper"

(http://www.nanomapper.eller.arizona.edu/), where one can search the number of patents related to nanotechnology published worldwide.[11] For example, using "nano" as keyword, the search results indicated that the United States Patent and Trademark Office has issued more than 3000 nano-patents. A significant number of patents was also released by the European and Japanese Patent Offices.

As a result of continuous growth in this field, more than 35 countries have initiated governmental funding programs related to nanotechnology. For example, the Japanese government allocated more than $800 million to nanotechnology projects in 2003, followed closely by the United States with approximately $774 million, representing six times more than in 1997.[12] In a report released by the National Nanotechnology Initiative (NNI), the central nanotechnology authority in the United States, the proposed NNI budget for 2010 is $1.64 billion. Such financial support was designated to contribute not only to the development of nanotechnology, but also to its impact on Environment, Health, and Safety (EHS).[13] Similarly, the European Commission Framework Programme proposed a total budget of 50 billion Euro for 2007-2013 that focuses on nanoscience, the production of new nanomaterials, and the development of nanotechnologies. In addition, multinational programs such as STAGE, NANOROADMAP, and FRAMINGNANO, have been developed for public engagement, education and communication throughout the European countries.[14]

One important area of nanotechnology is nanomedicine. It includes the investigation and the development of nanoscale surgery, tissue engineering, and drug delivery systems that lead to improved diagnosis and therapy.[1, 15] The efforts of the pharmaceutical industry have been directed towards new bioactive compounds that interact with biological molecules depending on local, sustained, or stimuli-triggered delivery.[16] Several important aspects of drug delivery systems are depicted in Figure 1.1. Active pharmaceuticals can be classified into four classes.

Class I includes compounds that have the highest permeability through cell membrane and the highest water solubility. In contrast, class IV drugs have the lowest bioavailability, and hardly reach the market. However, drugs from classes II and III possessing low bioavailability, determined by either low solubility or low permeability, are candidates for drug delivery systems.[17]

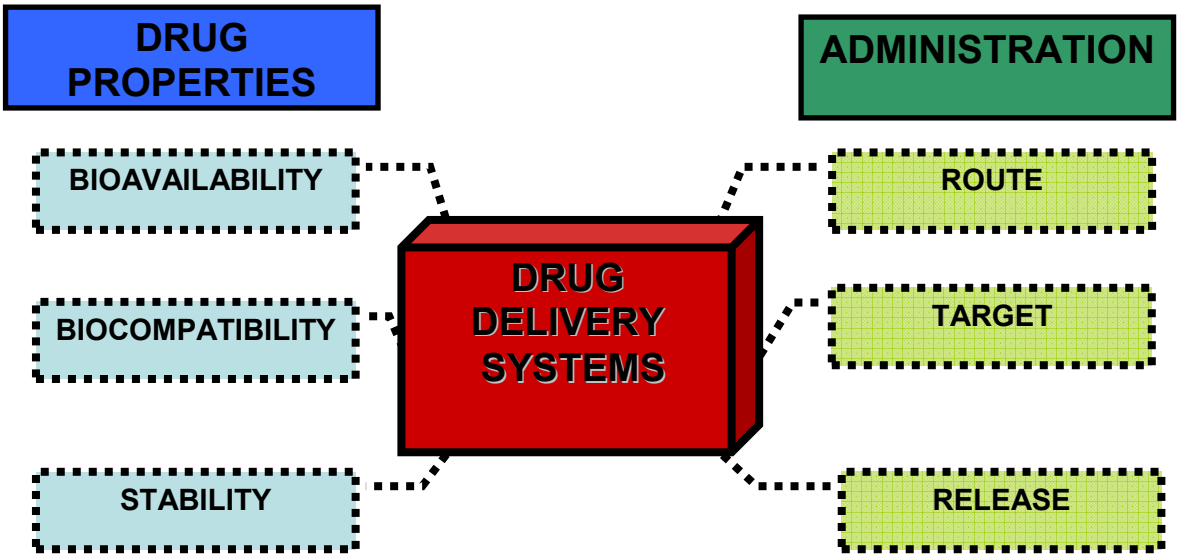

Figure 1.1 Principal characteristics of drug delivery systems.

In addition, biocompatible materials should be used as carriers in order to avoid inflammatory response and clearance from the body before reaching their site. Therefore, on one side, drug properties such as bioavailability, biocompatibility, and stability are relevant for the design of drug delivery systems that improve such properties. On the other side, questions such as how and where the drug is administered need to be addressed as well. Whether the drug delivery system is ingested or administered intravenously, targeted delivery becomes possible by functionalized surfaces that trigger direct responses from specific cells or intracellular components.[18-20]

Numerous pharmaceutical compounds can be delivered via various routes by use of nanoparticles. Oral drug administration is preferred based on patient convenience. However, many drugs are not resistant to the acidic environment present in the gastrointestinal tract. Therefore, intravenous administration is commonly used. In such cases, colloidal aqueous suspensions should contain submicron nanoparticles in order to avoid deposition and clogging of blood vessels.

Another important aspect of drug delivery systems is the release mechanism. For example, the drug can be delivered at a steady concentration over a period of time, or can present a burst release for a short period of time followed by constant release. In other cases, the drug can be released under the effect of external stimuli such as pH, temperature, and ionic strength. In addition, controlled drug delivery systems provide prolonged delivery at an optimum drug level as compared with a fluctuating free drug administration. Furthermore, drug delivery systems can be designed to target specific cells and tissues, and to provide drug protection against degradation. In addition, such systems lead to improved general comfort of the patient determined by reduced number of doses, and minimized undesirable side effects. [21-23]

1.2 Polymeric Nanoparticles as Drug Delivery Systems

There is a multitude of nanomaterials that can reach pharmaceutical performance of drug delivery systems. They include polymeric nanoparticles, solid lipid nanoparticles, cyclodextrins, liposomes, quantum dots, carbon nanotubes, and gold nanoparticles.[20, 24, 25] However, biodegradable materials are preferred specifically due to their biodegradability and compatibility with the human body. For example, poly (lactic acid), poly (glycolic acid), and their copolymer, poly (lactide-*co*-glycolide) (PLGA), are FDA approved biodegradable polymers previously used for scaffolds and tissue engineering. Nanoparticles prepared from such polymers would likely have less toxic effects than other nanomaterials used for preparation of drug carriers. In addition,

several other attractive properties such as degradation of the monomers through normal metabolic paths, versatility of preparation methods, and the variety of molecules to be delivered make PLGA nanoparticles the state of the art in drug delivery.[26, 27]

The market of polymeric nanoparticles used as drug delivery systems has expanded considerably in the last years. The first FDA approved drug delivery system was developed by TAP Pharmaceutical Products for prostate cancer treatment with leuprolide acetate using injectable PLGA microparticle system. Other drug delivery systems such as PLGA nanoparticles for human growth hormone delivery and albumin-stabilized nanoparticles for paclitaxel delivery are available on the market or in clinical trials.[27-29]

There are two types of polymeric nanoparticles: nanosheres and nanocapsules, as shown in Figure 1.2. A hydrophobic active agent can be entrapped in the polymeric matrix of nanospheres while a hydrophilic drug can be encapsulated into the nanocapsule core. In both cases, the drug can be adsorbed or chemically bound to the nanoparticle surface as well.[30-32] Using this variety of approaches, polymeric nanoparticles have been extensively investigated as delivery systems for anticancer drugs,[33, 34] gene therapy,[35] and protein delivery.[36]

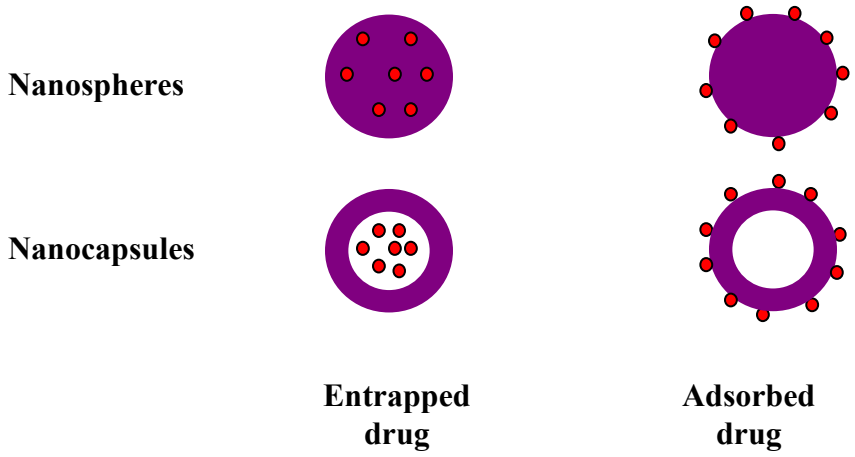

Figure 1.2 Nanospheres and nanocapsules as drug delivery systems.

1.2.1 Methods of Preparation

Polymeric nanoparticles can be prepared by a multitude of methods. [18, 37-39] Depending on the type of drug, preparation methods such as emulsion – evaporation and emulsion – diffusion can be specifically adopted for nanospheres incorporating hydrophobic drugs.[40-45] In addition, a double water-in-oil-in-water emulsion has been used for the encapsulation of water soluble active agents such as proteins and DNA.[46, 47]

Emulsification solvent evaporation is one of the most commonly used methods for the preparation of polymeric nanoparticles delivering hydrophobic drugs. A simple scheme of emulsification solvent evaporation method is illustrated in Figure 1.3. In this method, the polymer and the drug are dissolved in a water-immiscible organic solvent such as ethyl acetate, dichloromethane and chloroform. The organic phase is finely dispersed in a large aqueous phase containing an emulsifier, using high shear forces such as homogenization and sonication.

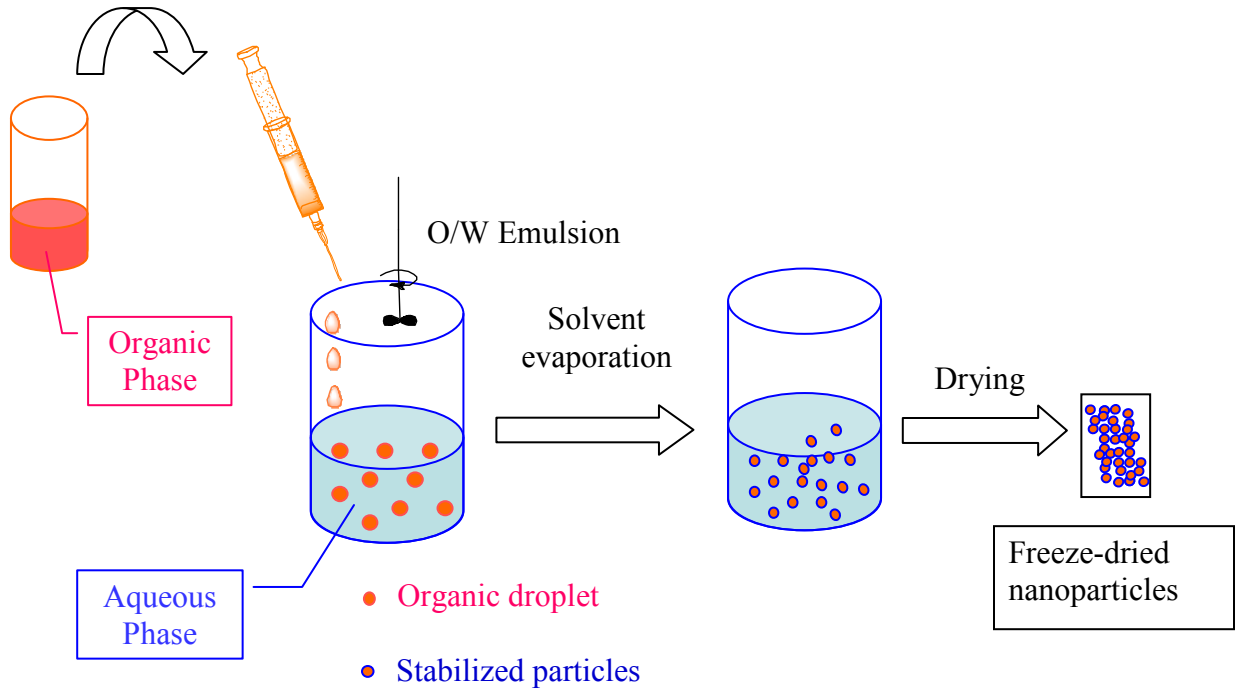

Figure 1.3 Basic principles of emulsification solvent evaporation method.

The organic solvent is then evaporated, leading to solidification of polymeric spheres. Parameters such as drug – polymer compatibility, the organic to aqueous phase ratio, evaporation speed as well as the intensity and time of homogenization play an important role in the synthesis of nanoparticles. For example, highly hydrophobic drugs can be encapsulated into polymers with a high content of lactide. In addition, a small organic to aqueous phase ratio often leads to small size nanoparticles. Removal of excess emulsifier and un-entrapped drug are critical aspects of nanoparticle synthesis as well. Therefore, purification by various methods such as dialysis and centrifugation follows the nanoparticle synthesis. For long term storage, nanoparticles are typically dried to powder form and re-suspended in aqueous media before use.

Other methods such as nanoprecipitation and diffusion can also be used for nanosphere preparation. The basic principle of these methods is similar to the one presented in Figure 1.3. However, they involve the use of a water miscible solvent and slow solvent evaporation in a larger aqueous phase. Particle sizes above 100 nm and poor drug entrapment limit such methods for their use in the preparation of polymeric nanoparticles.

1.2.2 Characterization of Polymeric Nanoparticles

The benefits of drug delivery systems based on polymeric nanoparticles are mainly determined by their physico-chemical properties such as particle size, zeta potential, shape and surface appearance as well as drug content and release. There are numerous methods for characterization of nanoparticles, as shown in Figure 1.4. For example, important aspects such as particle size, polydispersity, surface charge, and morphology are investigated by use of dynamic light scattering and imaging techniques. In contrast, separation techniques and spectroscopy can be used for the determination of drug content. In addition, toxicity and *in vitro* performance of nanoparticle-based drug delivery systems involve cell culture analyses. Several methods used in this dissertation are described below.

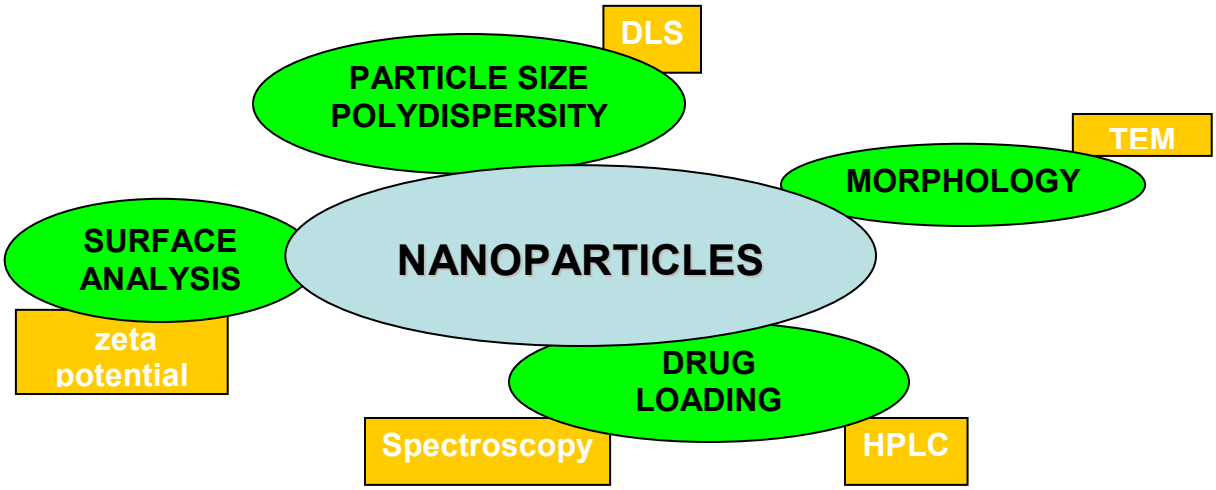

Figure 1.4 Methods for nanoparticle characterization. DLS – Dynamic Light Scattering; TEM – Transmission Electron Microscopy; HPLC – High Performance Liquid Chromatography.

1.2.2.1 Size and Polydispersity

Particle size and size distribution (polydispersity) are important characteristics of polymeric nanoparticles. Small nanoparticles of 100 nm are suitable for oral and parenteral administration and have better cellular uptake as compared to microparticles.[18, 35] Particle size is typically determined by use of dynamic light scattering, also known as photon correlation spectroscopy.

Dynamic light scattering (DLS) is based on variations in time of the intensity of scattered light from a monodisperse colloidal nanoparticle suspension. Such variations are the result of the nanoparticle translational and rotational Brownian motion in solution. The intensity of scattered photons is measured in channels that are further correlated. The correlation function, $g^{(1)}(\tau)$, is given by equation 1.1:

$$g^{(1)}(\tau) = \exp\left(-Dq^2(\tau)\right) \qquad 1.1$$

where τ is the decay time; $q = 4\pi n/\lambda_0 \sin\Theta/2$ is a scattering factor dependent on refractive index

n, incident light wavelength, λ_0, scattering angle ,Θ, and diffusion coefficient, *D*.[48]

The hydrodynamic radius of a nanoparticle, R_h (m), is determined based on the Stokes – Einstein formula (equation 1.2):

$$R_h = \frac{kT}{6\pi\eta D} \qquad 1.2$$

where *k* is Boltzmann constant (1.380×10^{-23} J K^{-1}); *T* is temperature (K); η is viscosity (Pa s^{-1}); and *D* is diffusion coefficient (m^2 s^{-1}).[3, 49]

Instrumentation for dynamic light scattering is simple and user-friendly (Figure 1.5). In principle, the light provided by a laser source passes through a sample containing nanoparticles. If a particle in solution is in the light path, it scatters light of whose intensity is further detected by a photomultiplier tube detector placed either at 90º or 173º. The backscatter detector at 173º represented in Figure 1.5 reduces interferences given by multiple scattering and large dust particles. The signal from the detector is transferred to a correlator that analyzes the time profile of the scattered light intensity. A computer processes this information and calculates the particle size (as diameter, Z_{ave}) based on the decay of correlation function in time. Polydispersity (as polydispersity index, PDI) is calculated as well and gives the size distribution of a nanoparticle sample. Monodisperse samples (PDI ~ 0.1) are represented by a narrow size distribution, whereas polydisperse samples (PDI > 0.1) would have broad size distribution including small nanoparticles as well as large nanoparticles and aggregates.[50]

1.2.2.2 Zeta Potential

The nanoparticle surface charge is critical for the stability of nanoparticle emulsion. If two particles would have no charge on the surface, they would likely coalesce. In contrast, highly positive or negative charged nanoparticles would remain suspended in solution for a longer period of time, based on their charge repulsion. For example, the positive ions of a solvent

attached to the surface of a negatively charged particle in suspension forms an ionic layer called the Stern layer. If this particle moves, the tightly attached positive charges (Stern layer) will move along with the particle. However, there is a diffuse layer at a certain distance from the surface of a particle where charges from the solvent are stationary.

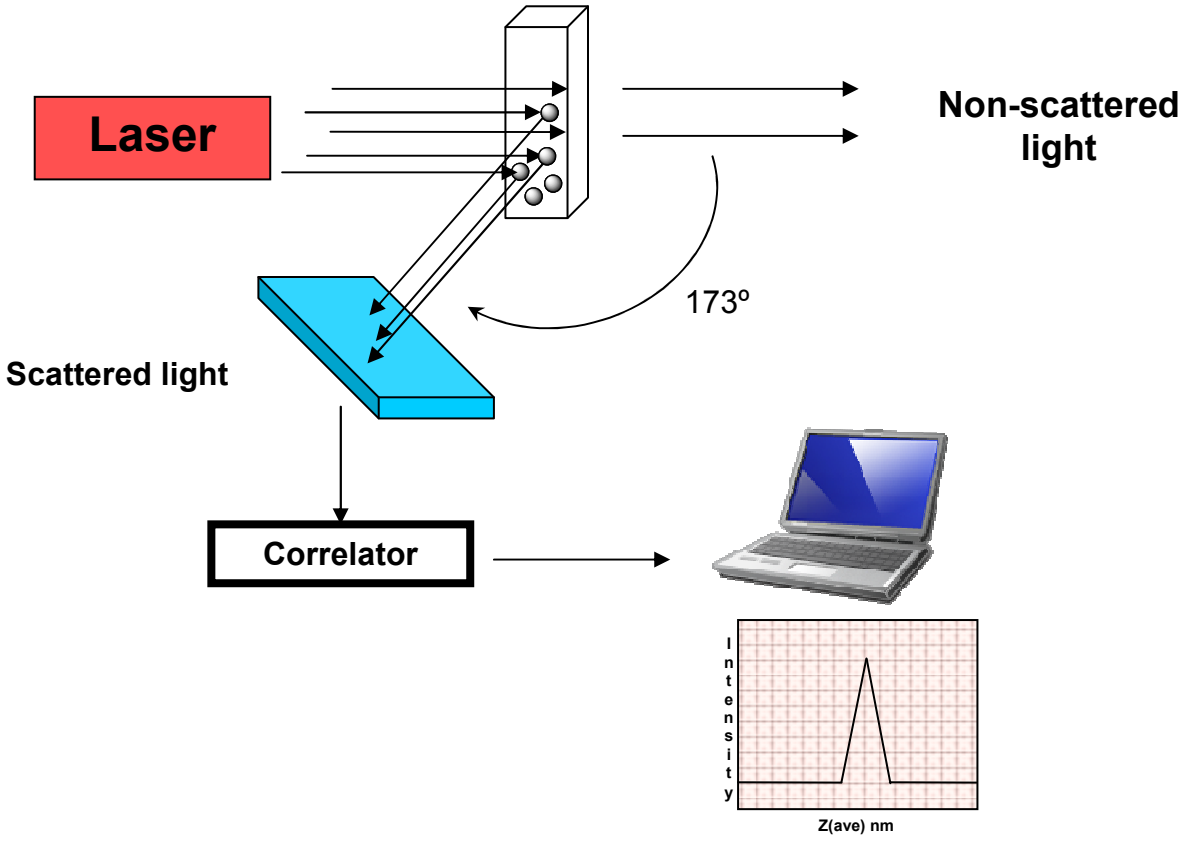

Figure 1.5 Dynamic light scattering instrumentation.

Zeta potential is an indicator of surface charge and is represented by the charge difference between Stern layer and stationary layer.[51] It is measured by laser Doppler anemometry that considers both scattered light and electrophoretic mobility of charged particles in a constant external electric field. The instrumentation is similar to the one presented in Figure 1.5. The difference is that an electric field is applied between two electrodes placed on the sides of a

capillary cell containing charged nanoparticles in suspension. Zeta potential is calculated based on the Henry equation (equation 1.3):

$$\mu_E = \frac{\zeta\ F(ka)}{6\pi\eta} \qquad 1.3$$

where μ_E is electrophoretic mobility ($cm^2v^{-1}s^{-1}$); ζ is zeta potential (mV); η is viscosity (Pa s^{-1}); *F(ka)* is Henry's function, approximated to 1.5 (Smoluchowski) for aqueous media and 1.0 (Huckel) for organic media.[49-51]

1.2.2.3 Morphology

Imaging techniques such as transmission electron microscopy, scanning electron microscopy and atomic force microscopy are typically used for the investigation of nanoparticle size, shape and uniformity. Transmission electron microscopy (TEM) is a powerful imaging technique commonly used in nanoparticle research, offering high resolution and great detail about nanoparticle morphology. It is based on the interactions of electrons generated by an electron gun with a thin layer of sample (≤ 100 μm) fixed on a small copper grid (3 mm).

There are two types of electrons detected in TEM, those transmitted through the sample that do not interact with the sample, and those that are scattered by a more dense material. Using this technique, a contrast TEM micrograph is formed on a phosphorous screen by light areas of transmitted electrons and dark areas of scattered electrons. A condenser system controls the intensity of the electron beam, whereas a series of lenses are used for the increase in magnification up to 200,000 times.[3, 52]

1.2.2.4 Drug Loading

Drug loading refers to the amount of encapsulated drug into the polymeric nanoparticles at the end of the synthesis process, after the elimination of excess drug that was not encapsulated. The drug loading is typically expressed as encapsulation efficiency representing the ratio

between the detected drug amount and the drug amount calculated based on the initial quantity added to the formulation. The expression for encapsulation efficiency is given by equation 1.4:

$$EE\ (\%) = \frac{drug_{calculated}}{drug_{theoretical}} \times 100 \qquad 1.4$$

where *EE %* is the encapsulation efficiency; $drug_{calculated}$ is the ratio between the amount of drug (mg) determined using analytical methods and the amount of nanoparticles (mg) taken for analysis; and $drug_{theoretical}$ the ratio between the amount of drug (mg) and the amount of polymer (mg) added initially to the formulation. The entrapment efficiency can be directly determined by dissolving a known amount of nanoparticles in appropriate solvents and analyzing the drug content. Alternatively, one can determine loses of polymer, drug and emulsifier during the nanoparticle synthesis, and calculate the drug loading by the difference.

The amount of encapsulated drug can be determined by various methods such as spectroscopy and separation techniques. For example, if the drug absorbs and emits light, then the drug loading can be easily determined by UV-Vis and fluorescence spectroscopy, respectively. In general, UV-Vis spectroscopy is a useful simple technique that is easy to use and widely available in research laboratories. Using this method, UV light passes through a transparent sample of known path length, and the transmitted or absorbed light is detected. The concentration of an analyte can be determined using Beer-Lambert's law as defined by equation 1.5:

$$A = \varepsilon bc \qquad 1.5$$

where *A* is absorbance (a.u.); *b* is path length (cm); *c* is analyte concentration (M); and ε is molar absorbtivity ($cm^{-1}\ M^{-1}$).

For direct determination of drug loading using UV-Vis spectroscopy, scattering light from the nanoparticle solution represents an important limitation. In addition, polymers usually

absorb light as well. If there is an overlap between the absorbance of the drug and the absorbance of other nanoparticle components, several sample preparation steps such as precipitation and filtration can be taken to eliminate such interferences. However, UV-Vis spectroscopy becomes useful for indirect determination of drug loading. In this case, drug loses in the purification steps such as centrifugation can be quantified and entrapment efficiency can be calculated by the difference. Typically, the determination of drug concentrations in the mM range is suitable for UV-Vis spectroscopy.

Fluorescence spectroscopy is a more sensitive technique in comparison to UV-Vis spectroscopy. When light comes in contact with a molecule in a ground state, it induces molecular excitation to an excited state of higher energy (excited state). The processes taking place in the excited state are represented by Jablonski diagram (Figure 1.6). Fluorescence (FL) occurs when the molecule is slowly relaxed to ground state emitting a photon that is further detected.

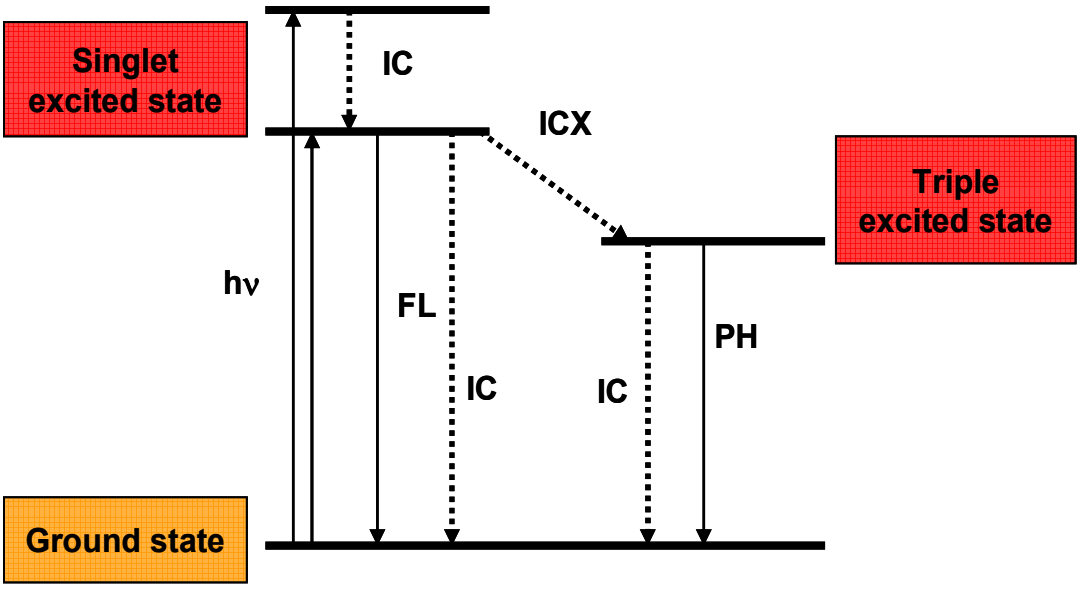

Figure 1.6 Jablonski Diagram representing the energy levels and processes of molecular excited state. FL – fluorescence; IC – internal conversion; ICX – intersystem crossing; PH – phosphorescence.

Processes such as internal conversion (IC) and intersystem crossing (ICX) are non-radiative energy transitions. In constrast, phosphorescence (PH) is a radiative process occurring by relaxation from a triple excited state. The components of UV-Vis and fluorescence spectroscopy instrumentation are schematically represented in Figure 1.7. They include a light source, gratings, a sample holder and a detector. The two instruments are comparable. However, fluorescence spectroscopy involves two gratings and a 90º angle configuration. Therefore, fluorescence spectroscopy is more sensitive, and can detect concentrations in the nanomolar range as compared to micromolar concentrations detected by UV-Vis spectroscopy.

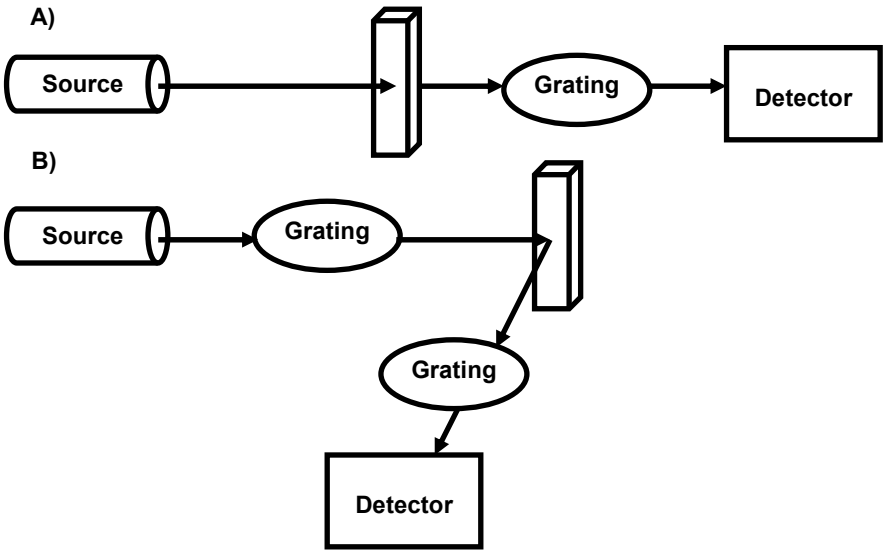

Figure 1.7 Instrumentation for spectroscopic methods. A) UV-Vis Spectroscopy; B) Fluorescence Spectroscopy.

Fluorescence spectroscopy has been used for determination of encapsulation efficiency of polymeric nanoparticles containing various fluorescent molecules that have been used for fluorescence imaging.[53] In addition, fluorescent anticancer drugs such as doxorubicin were encapsulated into polymeric nanoparticles, and the drug loading was determined by fluorescence spectroscopy.[54, 55]

Although spectroscopic techniques are useful in the determination of drug loading, complex matrices of nanoparticle formulations containing drugs, polymers, surfactants and other molecules would be difficult to analyze without preliminary sample preparation steps. In addition, many of the pharmaceutical compounds do not posses spectral properties, and, in some cases, the interferences from the polymer or other compounds present in formulation become significant. Instead, chromatographic separation techniques can be applied.

High performance liquid chromatography (HPLC) is commonly used in nanoparticle research for determination of drug composition. Using this method, each component is separated based on their partition between a solid stationary phase fixed inside a chromatographic column, and a liquid mobile phase passing through the column. Furthermore, separated components can be detected by a variety of detectors including UV-Vis, fluorescence, and electrochemical detectors. A typical HPLC system is depicted in Figure 1.8.

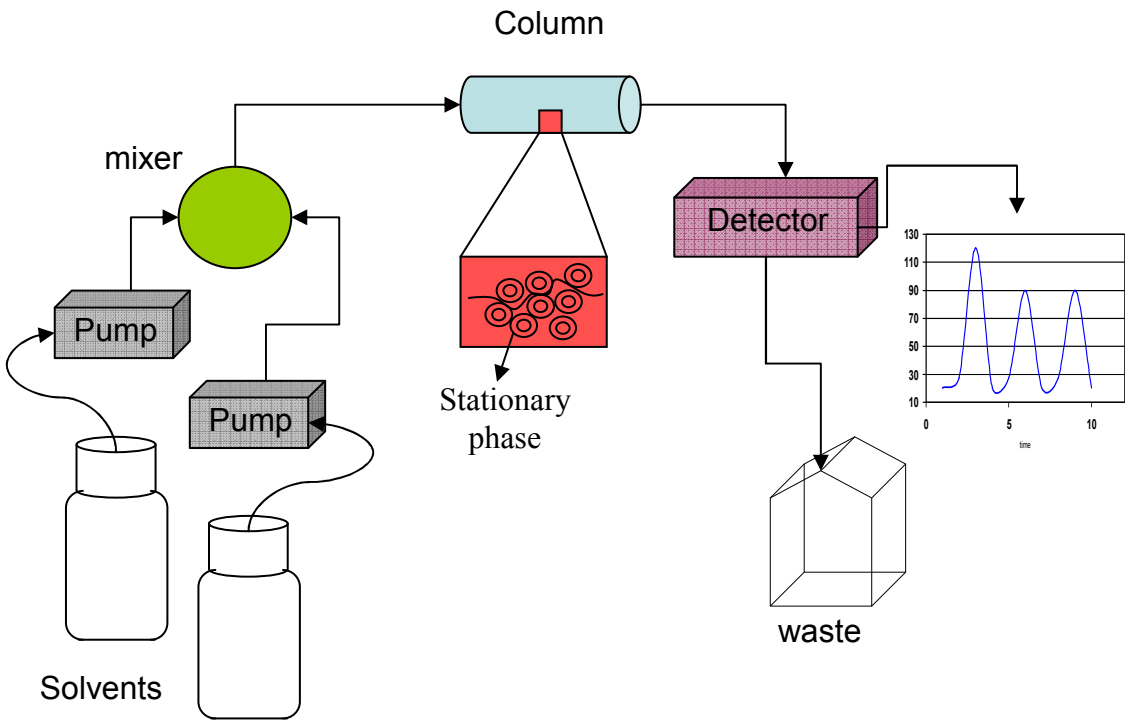

Figure 1.8 High performance liquid chromatography system.

The HPLC instrumentation includes the solvent containers, pumps and mixers for mobile phase preparation, a sample holder and injection system, the chromatographic column, and a detector. There are two modes that can be used for nanoparticle composition analysis: reversed phase and normal phase HPLC. The differences between these modes are shown in Table 1.1. In the reversed phase mode, stationary phase contains silica beads modified with alkyl chains of 4-18 carbons, whereas in normal phase hydrophilic compounds are simply adsorbed on the surface of silica packing.

Table 1.1 Differences between HPLC modes

Mode	Stationary phase	Mobile phase	Analytes
Reverse phase	Non-polar: Hydrocarbons (C4, C8, C18)	Polar: water, alcohols, acetonitrile	Non-polar (the least non-polar elutes first)
Normal phase	Polar: water, tri-ethylene glycol	Non-polar: hexanes, isopropyl ether	Polar (the least polar elutes first)

The polarity of the mobile phase is opposite to the one of the stationary phase, allowing partitioning of the analytes between these phases. The longer the analyte interacts with the stationary phase, the longer the retention time would be. Therefore, a chromatogram contains fast eluting peaks for non-interacting compounds at shorter times as well as interactive compounds at longer times.[56] Determination of a hydrophobic drug loading typically involves a reverse phase HPLC system. The selection of an appropriate solvent that allows complete nanoparticle dissolution is important in order to avoid further drug losses that would affect the entrapment efficiency. In addition, an adequate mobile phase that clearly separates all compounds present in the nanoparticle formulation and does not create any precipitation in the system should be used.

1.3 Molecular Micelles

Many nanoparticle preparation methods are based on the formation of oil-in-water (o/w) nanoemulsions that require the presence of an anionic, cationic, or non-ionic surfactant (emulsifier) dissolved in the aqueous phase. The surfactant adsorbs on the surface of organic droplets based on hydrophobic interactions consequently reducing the surface tension between the oil and the aqueous phases. For a surface tension near zero, a spontaneous emulsion is formed. An important aspect is the size of an emulsion droplet that depends on various factors including surfactant concentration and oil to water phases' ratio. For example, large droplets seem to coalesce easily while small droplets remain suspended in water for a longer period of time. In nanoparticle synthesis, nanoparticle size and size distribution are directly related to reduction and stability of emulsion droplet. Several emulsifiers such as sodium dodecyl sulfate (SDS), dodecyl dimethyl ammonium bromide (DMAB), poly (vinyl alcohol) (PVA), poly (ethylene glycol) (PEG), Pluronic, Tween, and tocopheryl polyethylene glycol succinate (TPGS) are used for such purposes.[57-61]

1.3.1 Comparison with Conventional Micelles

In general, surfactants are amphiphilic molecules that have both hydrophobic and hydrophilic groups. For example, SDS is a common anionic surfactant that has a hydrophobic alkyl chain (tail) and a negatively charged sulfate group as hydrophilic moiety (head). Other surfactants can be cationic such as DMAB, or neutral such as Triton X. In aqueous solution, surfactant molecules self-assemble into spherical micelles, rods and bilayers depending on the surfactant geometry and concentration.

The critical micellar concentration is defined as the concentration at which a micelle is formed, often observed by a sudden decrease of solution surface tension.[49] Micelles are in a dynamic equilibrium with the surfactant molecules, and any change in the environment can

disrupt their stability in solutions. In contrast, molecular micelles offer an advantageous alternative to conventional micelles, because of their enhanced stability, rigidity, and controllable size.[62] A comparison between conventional and molecular micelles is depicted in Figure 1.9. Molecular micelles present a CMC value of zero, as determined by the covalently bound micellar core, which eliminates the dynamic equilibrium between the monomers and the micelle, conferring enhanced stability. It should be noted that anionic molecular micelles such as poly (sodium *N*-undecenyl sulfate) (poly-SUS), poly (sodium *N*-undecenyl-glycinate) (poly-SUG) and poly (sodium *N*-undecenyl-L-leucyl-valinate) (poly-L-SULV) have been successfully used as alternatives to conventional micelles for pseudostationary phases in chromatographic separations.[62-64]

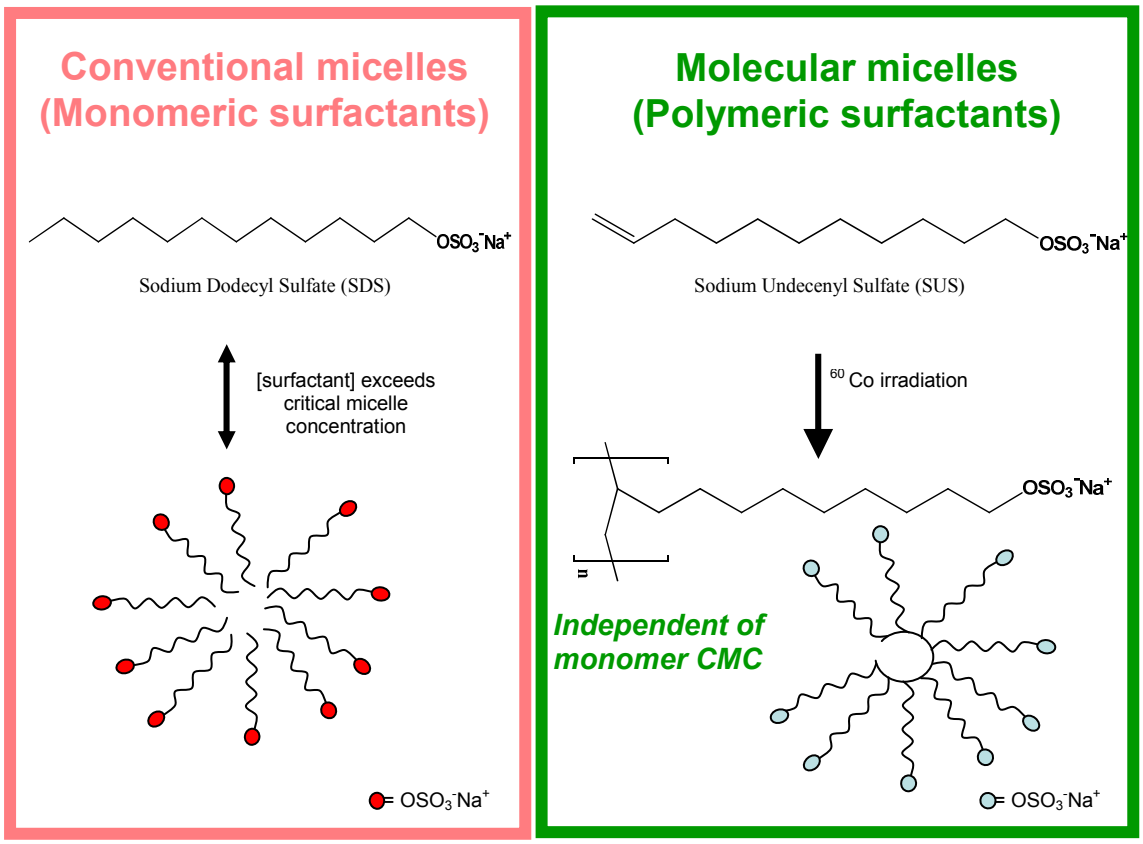

Figure 1.9 Comparison between conventional micelles and molecular micelles.

1.3.2 Molecular Micelles in Nanoparticle Synthesis

The importance of the emulsifier in the stability of emulsion is well established. However in case of nanoparticles used as drug delivery systems, the bulk emulsifier is removed, mainly because of its toxicity. In addition, the remaining emulsifier has to be at a low concentration in order to avoid toxic effects, but at a high enough concentration in order to allow re-suspension of nanoparticles in aqueous solution after purification and drying.

Sodium dodecyl sulfate (SDS) has also been used as an emulsifier in nanoparticle synthesis, and often leads to small particle sizes.[41] However, the stability of nanoparticle suspension is affected after SDS removal, by the formation of aggregates which are not able to re-suspend in an aqueous solution. In addition, the surfactant is efficient as emulsifier only at concentrations higher than the CMC, which limits the investigation of a wider range of concentrations. Poly (vinyl alcohol) (PVA) is one of the commonly used emulsifiers, which leads to the formation of high stable nanoparticles in solution.[40, 47] However, the residual PVA attached to the nanoparticle surface is difficult to remove and limits the nanoparticle cellular uptake and drug controlled release properties.[65]

1.4 Antioxidants

Nanomedicine and drug delivery systems have a direct impact on the improvement of disease treatment, especially in chemotherapy. In addition, disease prevention is an important aspect of our lives as we eat healthy and exercise in order to avoid illness. Antioxidants play a significant role in both disease prevention and treatment. The word “antioxidant” is often seen in the supermarkets on product labels from milk, soda, shampoo, and anti-wrinkle face cream. The questions of what an antioxidant is and what it does after it is used often remain unanswered. The term antioxidant would simply imply a compound that opposes oxidation. Indeed, in the case of aerobic organisms, oxidation is a normal metabolic process in which energy is produced through

a series of reactions that involve oxidants, i.e. free radicals. However, the overproduction of oxidants becomes deleterious, and therefore, is counterbalanced by the presence of antioxidants that act either as free radical suppressors or as scavengers.[66, 67] The types of free radicals and their roles are described in Section 1.5.

Antioxidants such as coenzyme Q10, enzymes superoxide dismutase (SOD) and glutathione peroxidase (GSP) are normally produced by the body. Other antioxidants come from diet and include vitamins, carotenoids, and minerals. Several examples of antioxidants are shown in Figure 1.10.[68] Natural antioxidants can be found in nuts, seed oil, vegetables, fruits spices, teas and animal products. Vitamin E is a generic name represented by a group of four tocopherols. liposoluble compounds found in fats and oils with various antioxidant activities, depending on their ability to donate the hydrogen from the hydroxyl group in lipid peroxidation. Flavonoids are another group of antioxidants found in most of the plant leaves and flowers. The presence of multiple hydroxyl groups determines an enhanced free radical scavenging activity. Other natural antioxidants, such as vitamin C (ascorbic acid) found in citrus, resveratrol found in grapes, and β-carotene found in carrots are also important antioxidants. Synthetic powerful antioxidants such as tert-butyl hydroquinone (TBHQ), 4-methoxy-2-tert-butyl phenol (BHA) and 2,6 di-tert-butyl p-hydroxytoluene (BHT) are hydrophobic and thermally stable, therefore used as antioxidants in vegetable oils. However, such compounds are strictly regulated because of their toxicity and more recently have been replaced with natural antioxidants.

1.4.1 Nutrition, Disease Prevention, and Therapy

The majority of antioxidants come from our diet. The term antioxidant is used often on many consumer products to label specific antioxidant benefits. The Food and Drug Administration (FDA) defines an antioxidant as a nutrient that possesses antioxidant activity, acting against free radicals. Such activity has to be supported by scientific evidence.

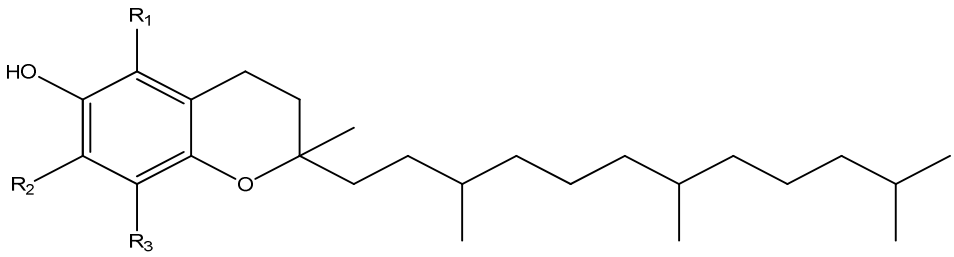

Tocopherols

Tocopherols	R_1	R_2	R_3
α	CH_3	CH_3	CH_3
β	CH_3	H	CH_3
γ	H	CH_3	CH_3
δ	H	H	CH_3

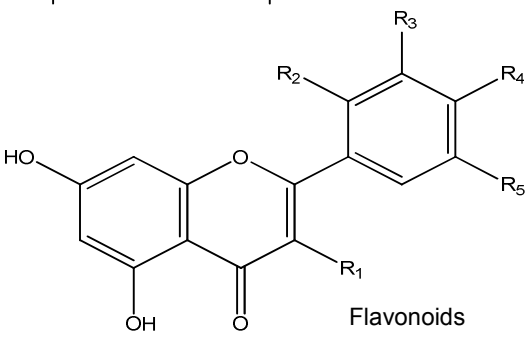

Flavonoids

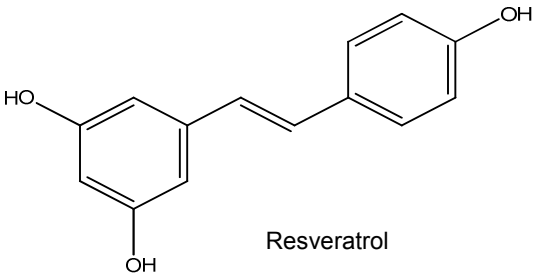

Resveratrol

Flavonoids	R_1	R_2	R_3	R_4	R_5
Chrysin	H	H	H	H	H
Luteolin	H	H	OH	OH	H
Quercetin	OH	H	OH	OH	H
Kaemferol	OH	H	H	OH	H

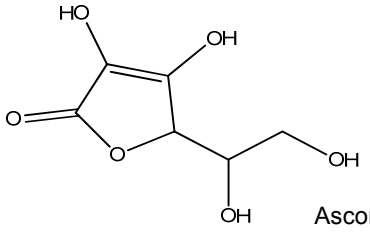

Ascorbic acid

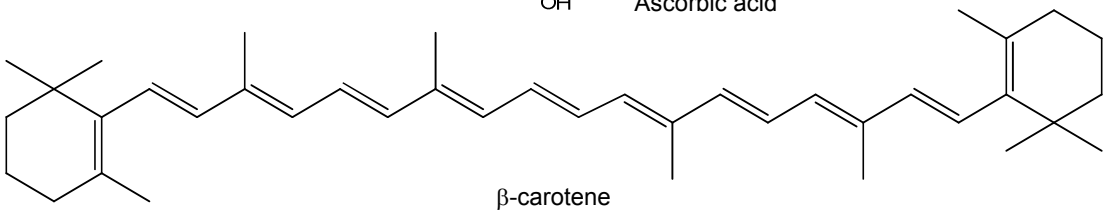

β-carotene

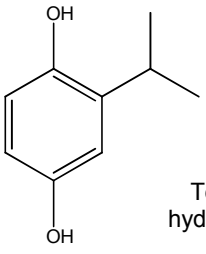

Tert-butyl hydroquinone

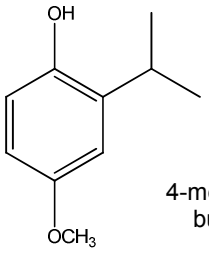

4-methoxy-2-tert-butyl phenol

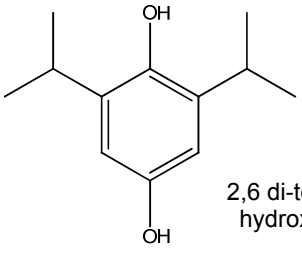

2,6 di-tert-butyl p-hydroxytoluene

Figure 1.10 Natural and synthetic antioxidants.

According to FDA, a "good source of antioxidants" is represented by a group of nutrients including vitamin C, vitamin E and carotenoids that are present in concentrations of 10 – 20 percent of their recommended daily intake value.[69] Besides a regular diet rich in fruits and vegetables that provide a daily antioxidant intake, dietary supplements are a source of antioxidants as well. In the recent years, a dramatic increase in the use of dietary supplements has been observed. It is estimated that in the United States there were over 290,000 dietary supplements on the market in 2005, with over $20 billion in sales, vitamins and minerals representing 34 percent of it.[70]

Phytonutrition becomes phytotherapy when a compound with nutritional value is used for the improvement of physiological functions.[71, 72] The use of plants and foods in the treatment of various conditions has been known for centuries in many regions of the world.[73-76] Today many of them are excellent sources for drug discovery. In addition, the implications of free radicals in the origin of disease provided an opportunity for the development of antioxidant alternative therapy for disease prevention and treatment. For example, antioxidants can reduce the incidence of cancer, help restoring the immune system, decrease the oxidation of low-density lipoprotein, and in some instances prevent the development of age-related cataract and macular degeneration.[70, 77, 78] In addition, the mechanism against disease depends on antioxidants type and structure. For example, enzymes such as superoxide dismutase and catalase inhibit the formation of superoxide anion radicals and hydrogen peroxide, while glutathione peroxidase and vitamin E participate in the decomposition of lipid peroxides.

1.4.2 Quinones

Quinones refer to a group of antioxidants that typically contain a benzoquinone structure, although several naphtoquinones and antraquinones have also antioxidant properties. Ubiquinone, also named coenzyme Q10 (Q10) is a well known endogenous antioxidant present

in the mitochondria where participates in the respiratory chain by reacting with superoxide anion radical as shown in Figure 1.11.[79, 80] The enzyme NADH quinone oxidoreductase (NQO1) catalyzes the transformation of quinone into semi-quinone radical that further accepts electrons from superoxide radical. Dihydroquinone is formed at the end of the cycle regenerating the benzoquinone. Deficiencies in Q10 and damages of mitochondrial DNA are the main cause of genetic mitochondrial diseases. [81, 82] Currently, the administration of Q10 supplements is the first of line therapy for the treatment of mitochondrial encephalomyopathies.

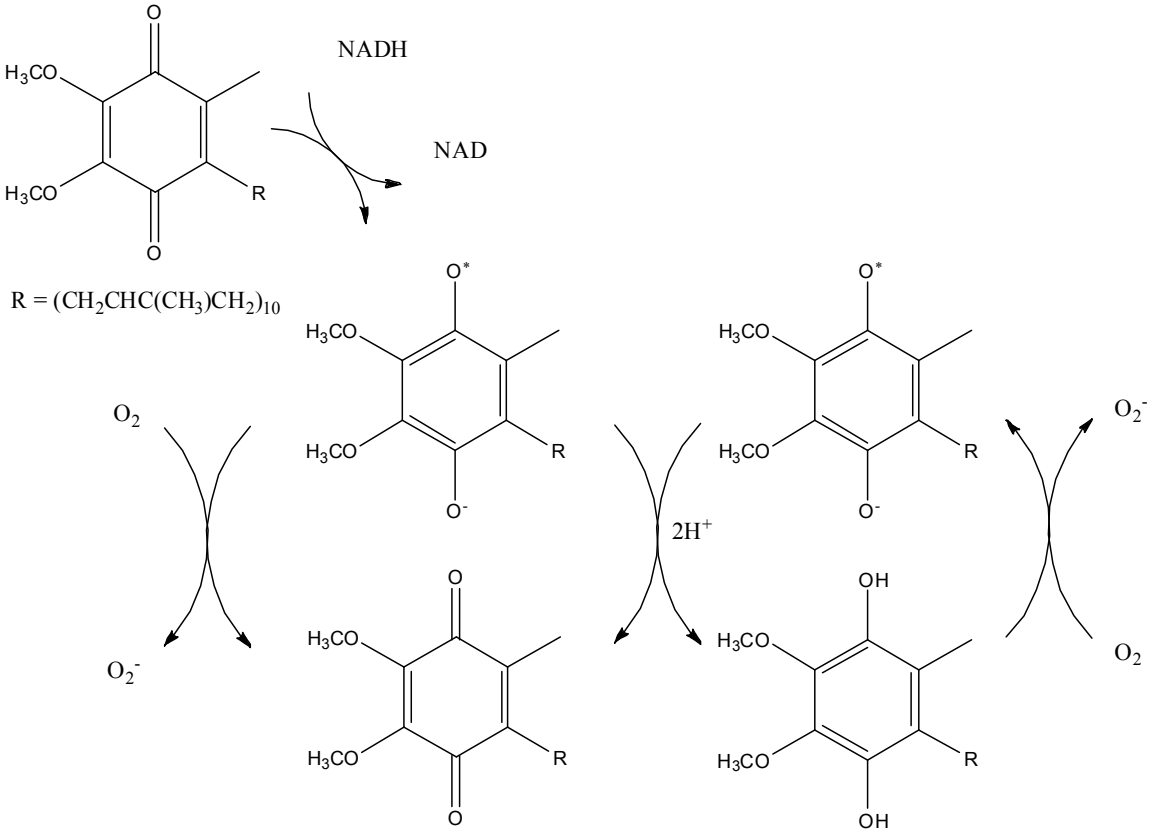

Figure 1.11 Role of coenzyme Q10 in respiratory chain.

In recent years, benzoquinone-based inhibitors of NQO1 have been developed for cancer treatment, favored by the high concentration of this enzyme in some types of cancer as well as

the hypoxic conditions of the solid tumors.[80, 83] Mitomycin C (Figure 12.A) is a classical NQO1 inhibitor and has been used as chemotherapeutic agent for a variety of cancers including head, neck, breast and prostate. However, its lack of specificity for cancer cells accompanied by strong and uncontrollable side effects limit the benefits of this drug. Alternatively, a better NQO1 substrate with reduced side effects, EOquin (Figure 12.B) is currently used for treatment of superficial bladder cancer. Another class of benzoquinone anticancer drugs is represented by benzoquinone ansamycins (Figure 12.C). They are cyclic compounds that bind to heat shock protein 90, one of the most abundant chaperone proteins that is overexpressed in cancer cells.[84] Numerous clinical trials involve therapy with two benzoquinone ansamycins: 17-allylamino-17-demethoxygeldanamycin (17-AAG) and 17-dimethylaminoethylamino-17-demethoxy-geldanamycin (17-DAAG). They are used either alone or in combination with other anticancer drugs for the treatment of advanced solid tumors, metastatic renal carcinoma and chemotherapy refractory breast cancer.[85]

Natural alkylated and cyclic benzoquinones found in plant extracts presented cytotoxic effects against various cancer cell lines.[86, 87] Thymoquinone (Figure 12.D) is the major constituent of *Nigella sativa* black seed oil, a medicinal plant from the *Ranunculaceae* family, which has been used for centuries in Africa, Europe, and Asia for treatment of many diseases including inflammation, asthma, hypertension, and gastrointestinal conditions. [88] *Nigella sativa* black seed oil as well as its major constituent, thymoquinone, display antioxidant properties by acting as free radical scavengers. [89, 90] Thymoquinone exhibits a protective antioxidant effect against the severe side effects caused by doxorubicin, an anticancer drug, that can generate congestive heart failure after chemotherapy.[91, 92] Furthermore, thymoquinone is an emerging anticancer drug, showing cytotoxic activities for a series of cancer cell lines including colorectal, ovarian, leukemia, and breast cells. [93-95]

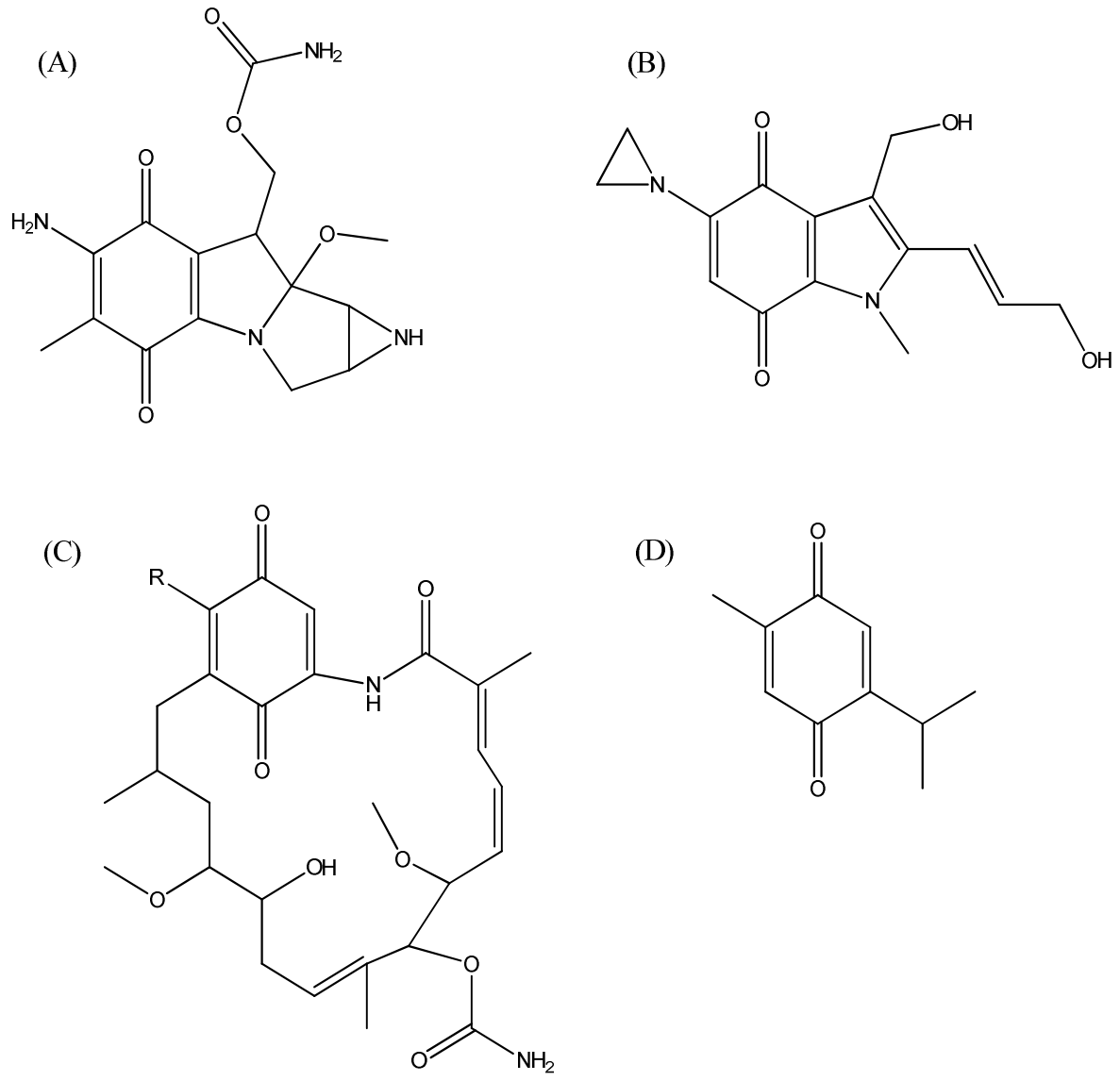

Figure 1.12 Benzoquinone – based anticancer drugs.

1.4.3 Antioxidant Delivery

Despite their great antioxidant and anticancer activities, many antioxidants are not soluble in aqueous media. Their administration is limited by low dose concentrations, use of organic solvents, and reduced bioavailability. On the other side, their stability, specificity, metabolism and clearance are factors to consider after administration. In recent years, controlled delivery of antioxidants has allowed a new approach for cancer therapy, cardiovascular diseases,

neurodegenerative diseases, and ageing. [96-99] Novel antioxidant-loaded drug delivery systems such as polymeric nanoparticles have been identified as alternatives that should provide long-term delivery, prevent antioxidant degradation, and increase pharmaceutical activity of such antioxidants.[97, 99]

Several studies have reported nanoparticle-based drug delivery systems for controlled delivery of antioxidants, including nanoparticles for delivery of the flavonoids such as quercetin, and natural antioxidant ellagic-acid.[100-103] Other nanoparticles were designed for the delivery of coenzyme Q10that improved stability and cellular uptake.[104-106] In other studies, "nanocurcumin" was prepared using polymeric nanoparticles for controlled delivery of natural curcumin, with improved solubility and anticancer properties of curcumin.[107, 108]

1.5 Free Radicals

1.5.1 Oxidative Stress and Free Radicals

The production of energy by aerobic organisms takes place by the oxidation of biological substrates in the presence of oxygen. The complete oxygen reduction occurs in mitochondria and involves a series of radical intermediates such as superoxide anion radical ($^{\bullet}O_2^-$), hydroxyl radical ($HO^{\bullet}$), $^1O_2$ (singlet oxygen) and non radical species, such as hydrogen peroxide (H_2O_2), as shown in Figure 1.13.[66]

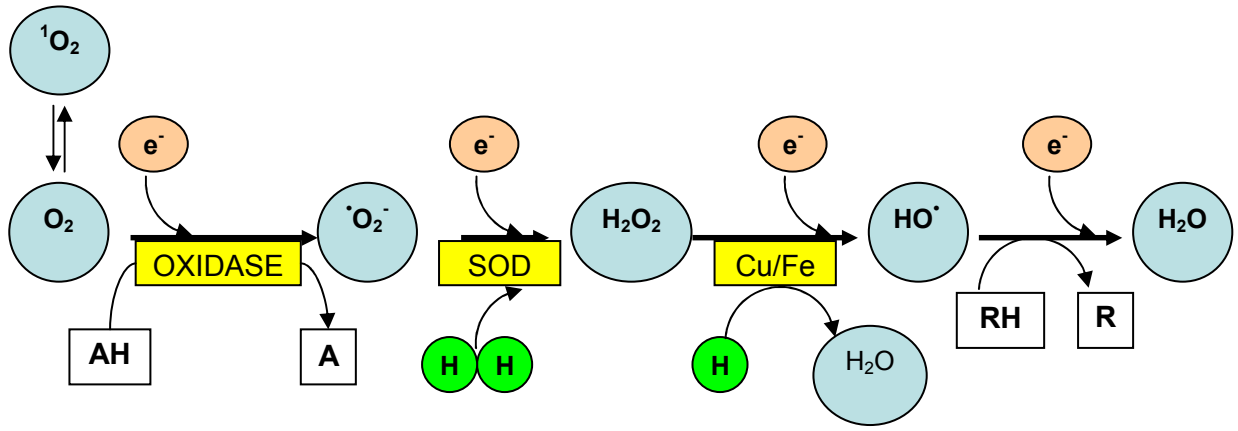

Figure 1.13 Generation of reactive oxygen species.

These species are collectively named as reactive oxygen species (ROS). Other species including reactive nitrogen species and chlorous radicals participate in oxidation reactions as well. Although such reactions are well controlled, sometimes incomplete substrate oxidation and partial oxygen reduction occur and lead to an excess of free radicals. Such excess is typically counterbalanced by antioxidants able to react with ROS and inactivate them.

If an imbalance exists between the production of radical species and the level of antioxidants, then the organisms face the undesired situation of oxidative stress. In contrast, if there is an excess of antioxidants, reductive stress takes place. Figure 1.14 graphically represents the balance between the ROS and antioxidants, moving towards radical species in the case of oxidative stress and towards antioxidants for reductive stress. Excessive production of radical species can lead to alteration of cellular functions responsible for cardiovascular diseases, neurodegenerative diseases, diabetes, cancer, joint diseases, and aging.[109-114]

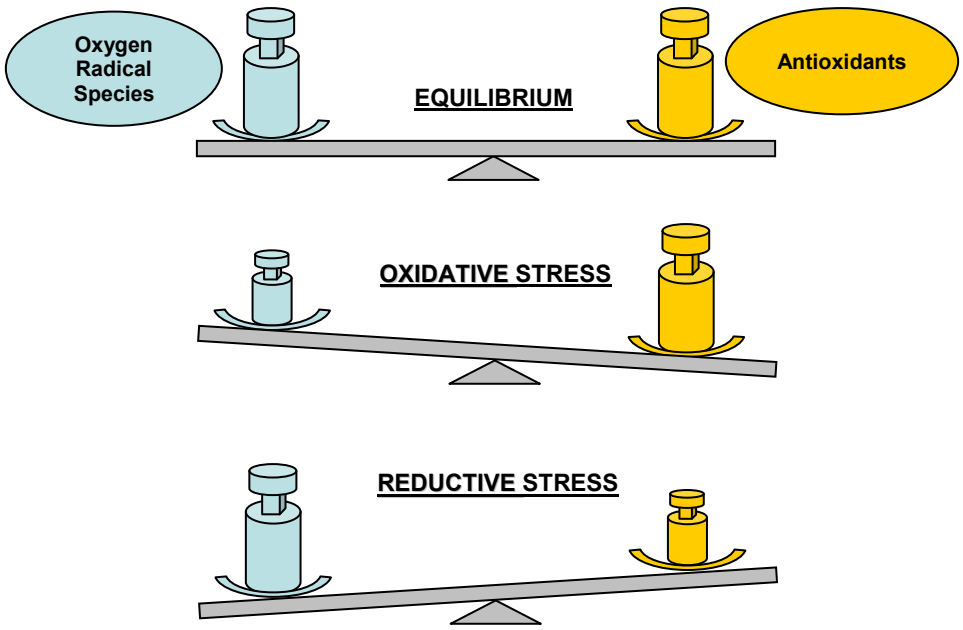

Figure 1.14 The balance between reactive oxygen radical species and antioxidants.

In comparison with other radicals, hydroxyl radical is particularly dangerous. It can be produced at cellular levels by Fenton and Habber-Weiss reactions of hydrogen peroxide with transition metals such as iron and copper (1.10 and 1.11).[67, 113]

$$H_2O_2 + Fe^{2+} \rightarrow Fe^{3+} + HO^- + OH^\bullet \quad 1.10$$

$$H_2O_2 + Cu^{+} \rightarrow Cu^{2+} + HO^- + OH^\bullet \quad 1.11$$

The hydroxyl radical has a short half-life, and is considered the most aggressive free radical, mainly due to its high reactivity. It is able to react with lipids, amino acids, proteins, DNA, and sugars at extremely high rates, leading to cell damage and even cell death.[115] Other sources such as ozone and ionization radiation lead to hydroxyl radical generation as well.

1.5.2 Methods for Free Radical Detection

Numerous methods have been developed for oxidative stress detection, and are summarized in Figure 1.15. They are focused on the identification and quantification of the oxidative stress biomarkers, the determination of antioxidant activity, as well as direct or indirect detection of radicals.[67, 109] Biomarkers are a good indication of oxidative stress, although they are disease specific. Many of them require long and cumbersome procedures for the exact assessment of oxidative stress levels, especially in the early stages of a disease. Methods for antioxidant quantification are based on scavenging ability of an antioxidant and enzymatic activity of enzymes involved in the respiratory chain, i.e. SOD, catalase, peroxidases.

Reactive oxygen species can be directly detected by Electron Paramagnetic Resonance (EPR) spectroscopy, based on their electron transfer to nitroso compounds that are stable paramagnetic adducts. Although highly sensitive, EPR is limited by the stability of adducts and instrumentation accessibility. Alternatively, fluorescence spectroscopy is a highly sensitive method used for the detection of reactive oxygen species (ROS). In the literature, fluorescent dyes have been given extensive attention for ROS indirect detection.[116-118]

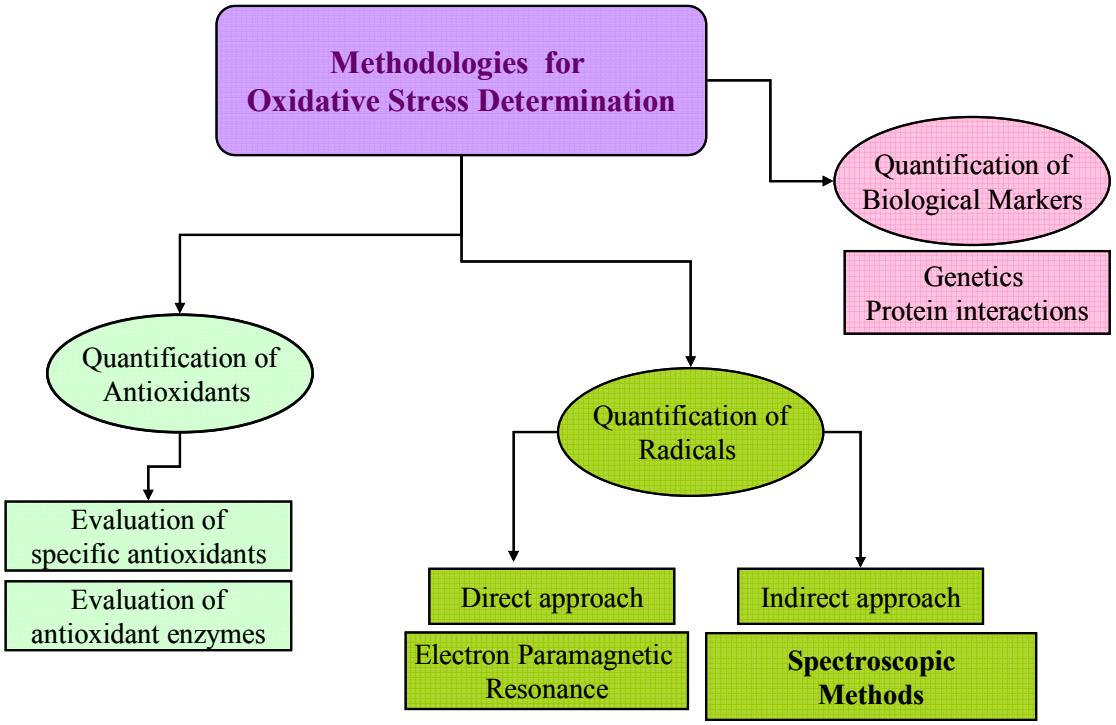

Figure 1.15 Methods of detection for oxidative stress.

1.5.3 Free Radical Fluorescent Sensors

Compared to other methods, fluorescence sensors are promising tools providing several advantages such as high specificity, localized information at the target site, spectral and microscopical detection. A list of common fluorescent probes and the radicals they react with is presented in Table 1.2. Several dihydro-probes, including 2'7'-dichlorodihydro-fluorescein, dihydro-rhodamine and dihydro-calcein are used for total ROS determination, mainly because they are not specific for a particular radical.[119]

Other more specific fluorophores such as hydroethidine were used for the detection of superoxide anion radical. Hydroxyl radical can be detected by hydroxylation reaction of aromatic compounds. Specifically, coumarin 3-carboxylic acid (C3C) has been used as fluorescent sensor for detection of hydroxyl radical. This probe reacts with hydroxyl radical and undergoes hydroxylation at position C7 of the coumarin structure, producing a highly fluorescent

compound, 7-hydroxy coumarin 3-carboxylic acid.[120-122] Because C3C has an available carboxylic group in the C3 position, it can be easily coupled with other groups via peptide bond synthesis. Therefore, other coumarin derivatives such as the succinimidyl ester of C3C, phospholipid liked coumarins, and C3C – derivatized amino acids and peptides were used for the detection of hydroxyl radicals.[123-125]

Table 1.2 Free radical fluorescent sensors

Fluorophore	**$^{\bullet}O_2^-$**	**$^1O_2$**	**$OH^{\bullet}$**	**H_2O_2**
Hydroethidine	√			
1,3-Diphenylisobenzofuran	√	√		
Homovanillic acid				√
2,7-Dichlorodihydrofluorescein diacetate			√	√
Dihydrorhodamine 123				√
N-Acetyl-3,7-dihydroxyphenoxazine				√
9,10-Dimethylanthracene		√		
2-[6-(4V-amino)phenoxy-3H-xanthen-3-on-9-yl] benzoic acid			√	
Coumarin-3-carboxylic acid			√	

Although fluorescent probes can be used to detect hydroxyl radicals, several limitations should be taken into consideration. For example, the changes in the fluorescence intensity of a single fluorophore that reacts with a specific radical can be affected by variations in radical and probe concentrations, instrumental artifacts and environmental factors such as temperature and pH. In addition, *in vitro* imaging becomes challenging if the probe reacts with molecules present in the cellular media, photobleaches or generates other secondary radicals.[126] A novel approach for detection of hydroxyl radicals is the use of fluorescence ratiometric detection that likely eliminates such limitations. In this case, the intensity ratio of two probes is directly proportional

with analyte concentration independently of aforementioned factors. Such ratiometric fluorescent sensors were reported for the detection of hydrogen peroxide and hydroxyl radicals using coumarin-coupled dyes.[127, 128] An alternative approach is the use of ratiometric nanoparticles. In Chapter 4 of this dissertation, ratiometric PLGA nanoparticles were used for the detection of hydroxyl radicals. The reporting signal is given by a coumarin-functionalized molecular micelle while the reference signal is given by neutral red loaded nanoparticles.

1.6 Chemometrics and Optimization Design

Chemometrics is a relatively new discipline developed only 30-35 years ago along with the advances in computing, fast data collection and the increasing importance of analytical data in industry. Chemometrics simply refers to analysis and interpretation of instrumental data. For examples, the optimum conditions of a chemical reaction are found by analyzing the effects of reagent concentrations and environmental reaction conditions on the yield of products. In chromatographic separation of various pharmaceuticals pattern recognition defines groups of compounds from the same origin. In addition, chemometric approaches facilitate the spectroscopic quantification of reagents and products of a chemical reaction or the components of a complex biological sample.

It is always advantageous to plan and design experiments ahead of time. Using this approach, four major components of experimental design can be defined as follows:[129]

1) Screening. A large number of parameters such as concentration of reagents, temperature, and pH can be investigated in order to identify the most important ones.
2) Optimization. The truly optimum conditions of a chemical process can be found. For example, the highest yield of a reaction was found 80 % for a temperature of 20 ºC, at a pH of 7. However, applying an optimization design, the reaction yield was found 95 % at a temperature of 30 ºC and a pH of 6.

3) Time saving. As an expansion of small scale screening and optimization, time saving becomes important on an industrial scale where the relationships between structures and measured properties must be quantified in real time.

4) Quantitative modeling. Based on collected experimental data and chemometric analysis, models can be developed and predict future experiments.

In the process of experimental design, one establishes **factors** – the input controllable parameters – such as pH, temperature, and concentration, and measures the **responses** – the output parameters – such as yield, resolution, efficiency. These factors can be investigated at different levels denoted negative for the lowest, zero for the middle and positive for the highest.[130] The response can be described in a simple case by equation 1.12 where it strictly depends on one factor and defined as single linear regression. In case of multiple interactions, the response can be described by a multi-linear regression given by equation 1.13.

$$y = b_0 + bx \tag{1.12}$$

$$y = b_0 + b_1x_1 + b_2x_2 + ... + b_nx_n \tag{1.13}$$

where y is the response; x_n are the factors; b_0 is the intercept; and b_n are the coefficients that indicate the extent of x-y dependency. the goal of an experimental design being to find the coefficients b and a matrix D containing all factors and responses. In addition, a model is defined based on the experimental data and it is able to predict the response as a function of investigated factors.

There are several optimization experimental designs commonly used by chemists. They are graphically represented in Figure 1.16. Factorial design is the simplest design and usually used for screening in order to find the main factors that affect the response. A more comprehensive optimization design is the central composite design. This design includes a factorial design and a star design that allows the investigation of both linear and quadratic

factors. Another useful design is represented by Box-Behnken design in which the levels of the investigated factors are central as compared to positive and negative levels used by the other designs. This allows for a reduced number of experiments, consequently reducing the time, but maintaining the benefits of an experimental design. Both central composite and Box-Behnken designs include central samples for reproducibility purposes, where all factors are set at level zero.

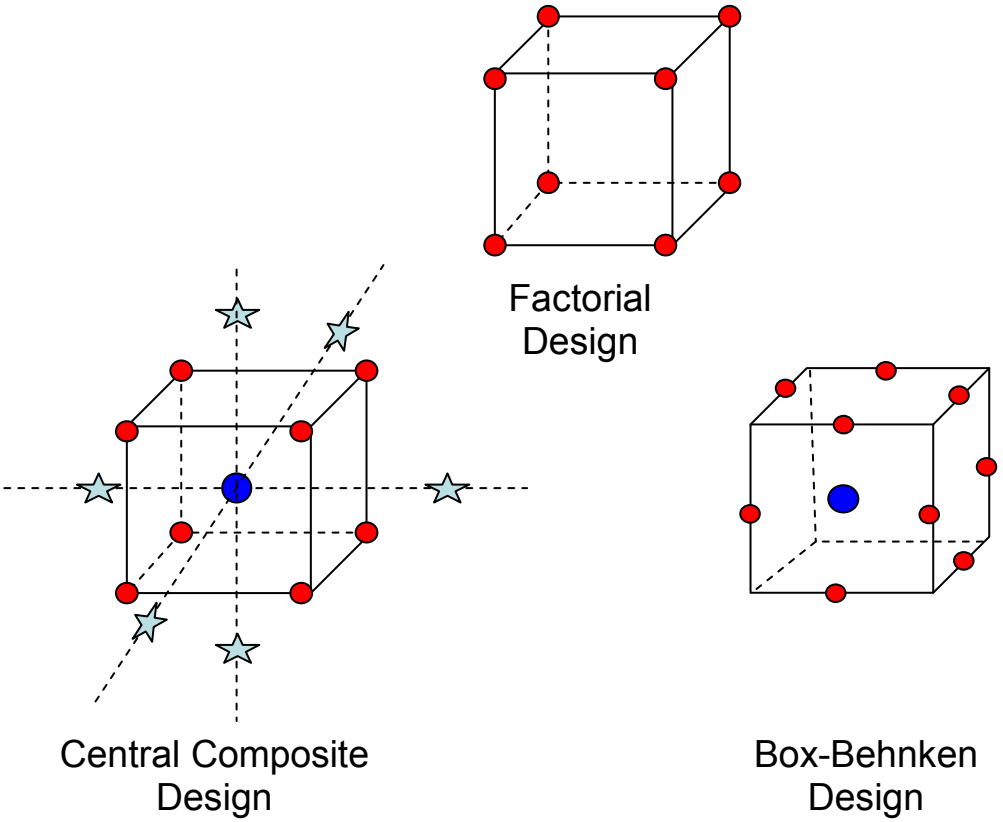

Figure 1.16 Types of optimization designs.

In nanoparticle synthesis, optimization experimental design is an extremely useful tool.[131-135] In many nanoparticle formulations, factors such as polymer concentration, drug concentration, solvent ratio, emulsifier type and concentration as well as drug properties and concentration added to the formulation contribute significantly to the properties of nanoparticles.

Therefore, it is important to strictly control such factors in order to obtain the desired particle size, polydispersity, and drug entrapment efficiency.

1.7 Scope of Dissertation

Polymeric nanoparticles are useful tools in drug delivery and nanomedicine. In particular, polymeric nanoparticles modified with various molecular micelles offer advantages in terms of particle size and polydispersity control, as well as properties related to biological and analytical purposes. A general description of nanoparticle synthesis and characterization methods is presented in the first chapter of this dissertation. In addition, the roles of antioxidants and free radicals in nutrition and disease prevention are described. The use of polymeric nanoparticles for delivery of antioxidants as well as the detection methods for free radicals are introduced in Chapter 1 as well.

In the second chapter of this dissertation, a chemometric central composite experimental design (CCD) was used to optimize the synthesis of poly (D,L lactide-*co*-glycolide) (PLGA) nanoparticles by emulsification solvent evaporation using anionic molecular micelles, such as poly (sodium *N*-undecenyl sulfate) (poly-SUS), poly (sodium *N*-undecenyl-glycinate) (poly-SUG) and poly (sodium *N*-undecenyl-L-leucyl-valinate) (poly-L-SULV) as well as conventional emulsifiers, such as anionic sodium dodecyl sulfate (SDS) and non-ionic poly (vinyl alcohol) (PVA). The individual and combined effects of PLGA concentration, emulsifier concentration, homogenization speed, and sonication time (design variables) on particle size and polydispersity index (responses) were investigated using multivariate analysis. A quadratic model was used to predict the properties of molecular micelle - modified PLGA nanoparticles demonstrating the advantage of using optimization design in the synthesis of polymeric nanoparticles.

Molecular micelle – modified PLGA nanoparticles were used for the delivery of thymoquinone, an antioxidant and anticancer drug. In the third chapter of this dissertation,

anionic amino acid - based molecular micelles were used as emulsifiers in the synthesis of thymoquinone (TQ) – loaded PLGA nanoparticles by use of an emulsification solvent evaporation method. The optimum TQ entrapment efficiency was found for poly-SUG – modified PLGA nanoparticles using a Box-Behnken experimental design. In addition, other structurally related molecular micelles having various amino acid head groups and different hydrophobic carbon chain lengths were also examined as emulsifiers. Furthermore, other properties of TQ-loaded nanoparticles were investigated, including drug release, total antioxidant activity, and cytotoxicity against breast normal and cancer cells.

Molecular micelle – modified polymeric nanoparticles can be used not only for delivery of antioxidants, but as analytical nanosensors for detection of free radicals. In Chapter 4 of this dissertation, neutral red (NeR) loaded PLGA nanoparticles were synthesized by emulsification solvent evaporation using molecular micelles such as poly (sodium N-undecenyl-Nε-lysinate) (poly-Nε-SUK) functionalized with coumarin 3-carboxylic acid (C3C) as emulsifier. Such nanoparticles were able to detect hydroxyl radicals based on a ratiometric fluorescence detection scheme. The product of the reaction between the coumarin functionalized molecular micelle and hydroxyl radicals, 7-hydroxy coumarin 3-carboxylic acid (7-OH C3C) represented the reporting dye, while NeR was the reference dye. C3C-poly-Nε-SUK – modified NeR-loaded nanoparticles were able to detect hydroxyl radicals in simulated samples as well as biological samples exposed to oxidative stress.

The research presented in this dissertation demonstrates the utility of molecular micelles in nanoparticle synthesis, their versatility that conferred tunable properties for drug loaded nanoparticles, and their ability to offer functional groups for analytical purposes. Molecular micelle – modified nanoparticles are not only an example of drug delivery systems, but nanosensors that can be used for detection of various molecules.

1.8 References

1 Moghimi, S. M.; Hunter, A. C.; Murray, J. C. *Faseb Journal* **2005**, *19*, 311-330.

2 Greenfield, S. A. *Trends in Biotechnology* **2005**, *23*, 34-41.

3 Hornyak, G. L.; Dutta, J.; Tibbals, H. F.; Rao, A. K. *Introduction to nanoscience* **2008**, Taylor & Francis Group, Boca Raton, Florida, 3-58.

4 Hornyak, G. L.; Moore, J. J.; Tibbals, H. F.; Dutta, J. *Fundamentals of nanotechnology* **2008**, Taylor & Francis Group, Boca Raton, Florida, 3-52.

5 Roco, M. C. *Environmental Science & Technology* **2005**, A106-A112.

6 Roco, M. C.; Bainbridge, W. S. *Journal of Nanoparticle Research* **2002**, *4*, 281-295.

7 Roco, M. C.; Bainbridge, W. S. *Journal of Nanoparticle Research* **2005**, *7*, 1-13.

8 Goddard III, W. A.; Brenner, D. W.; Lyshevski, S. E.; Iafrate, G. J. **2003**, CRC Press, Boca Raton, Florida, 1-1 - 1-9.

9 Devreese, J. T. *MRS Bulletin* **2007**, *32*, 718-724.

10 Madia, W. J.; Pearson, E. W. *Metallurgical and Materials Transactions B-Process Metallurgy and Materials Processing Science* **2006**, *37*, 683-696.

11 Li, X.; Hu, D.; Dang, Y.; Chen, H.; Roco, M. C.; Larson, C. A.; Chan, J. *Journal of Nanoparticle Research* **2009**, *11*, 529-552.

12 Roco, M. C. *Current Opinion in Biotechnology* **2003**, *14*, 337-346.

13 The National Nanotechnology Initiative *Supplement to the President's 2010 Budget* **2009**, www.nano.gov.

14 Hullman, A. *European Comission* **2008**, http://cordis.europa.eu/nanotechnology.

15 Ebbesen, M.; Jensen, T. G. *Journal of Biomedicine and Biotechnology* **2006**, 1-11.

16 Park, K.; Mrsny, R. J. *Controlled drug delivery: present and future* **2000**, *752*, ACS Symposium Series, 2-12.

17 Svenson, S. *Carrier-Based Drug Delivery* **2002**, *879*, ACS Symposium Series, 2-23.

18 Hans, M. L.; Lowman, A. M. *Current Opinion in Solid State and Materials Science* **2002**, *6*, 319-327.

19 Broz, P.; Hunziker, P. *Nanomaterials for Medical Diagnosis and Therapy* **2007**, Wiley-VCH Verlag GmbH, Germany, 189-254.

20 Khademhosseini, A.; Langer, R. *Nanobiotechnology, SBE Special Edition* **2006**, 38-41.

21 Ha, C. S.; Gardella, J. A. *Chemical Reviews* **2005**, *105*, 4205-4232.

22 Ju, X. J.; Xie, R.; Yang, L. H.; Chu, L. Y. *Expert Opinion on Therapeutic Patents* **2009**, *19*, 683-696.

23 Torchilin, V. P. *Advanced Drug Delivery Reviews* **2006**, *58*, 1532-1555.

24 Kayser, O.; Lemke, A.; Hernandez-Trejo, N. *Current Pharmaceutical Biotechnology* **2005**, *6*, 3-5.

25 Vogelson, C. T. *Modern Drug Discovery* **2001**, *4*, 49-52.

26 Anderson, J. M.; Shive, M. S. *Advanced Drug Delivery Reviews* **1997**, *28*, 5-24.

27 Bala, I.; Hariharan, S.; Kumar, M. N. V. R. *Critical Reviews in Therapeutic Drug Carrier Systems* **2004**, *21*, 387-422.

28 Riehemann, K.; Schneider, S. W.; Luger, T. A.; Godin, B.; Ferrari, M.; Fuchs, H. *Angewandte Chemie-International Edition* **2009**, *48*, 872-897.

29 Haley, B.; Frenkel, E. *Urologic Oncology-Seminars and Original Investigations* **2008**, *26*, 57-64.

30 Allemann, E.; Gurny, R.; Doelker, E. *European Journal of Pharmaceutics and Biopharmaceutics* **1993**, *39*, 173-191.

31 Kumar, M. N. V. R. *Journal of Pharmacy & Pharmaceutical Sciences* **2000**, *3*, 234-258.

32 Shikanov, A.; Kumar, N.; Domb, A. J. *Israel Journal of Chemistry* **2005**, *45*, 393-399.

33 Brannon-Pepas, L.; Blanchette, J. O. *Advanced Drug Delivery Reviews* **2004**, *56*, 1649-1659.

34 Brigger, I.; Dubernet, C.; Couvreur, P. *Advanced Drug Delivery Reviews* **2002**, *54*, 631-651.

35 Panyam, J.; Labhasetwar, V. *Advanced Drug Delivery Reviews* **2003**, *55*, 329-347.

36 Delie, F.; Blanco-Prieto, M. J. *Molecules* **2005**, *10*, 65-80.

37 Moinard-Checot, D.; Chevalier, Y.; Briancon, S.; Fessi, H.; Guinebretiere, S. *Journal of Nanoscience and Nanotechnology* **2006**, *6*, 2664-2681.

38 Quintanar-Guerrero, D.; Alleman, E.; Fessi, H.; Doelker, E. *Drug Develoment and Industrial Pharmacy* **1998**, *24*, 1113-1128.

39 Astete, C. E.; Sabliov, C. M. *Journal of Biomaterials Science, Polymer Edition* **2006**, *17*, 247-289.

40 Song, C. X.; Labhasetwar, V.; Murphy, H.; Qu, X.; Humphrey, W. R.; Shebuski, R. J.; Levy, R. J. *Journal of Controlled Release* **1997**, *43*, 197-212.

41 Birnbaum, D. T.; Kosmala, J. D.; Brannon-Pepas, L. *Journal of Nanoparticle Research* **2000**, *2*, 173-181.

42 Mu, L.; Feng, S.-S. *Pharmaceutical Research* **2003**, *20*, 1864-1872.

43 Kumar, M. N. V. R.; Bakowsky, U.; Lehr, C. M. *Biomaterials* **2004**, *25*, 1771-1777.

44 Panyam, J.; Williams, D.; Dash, A.; Leslie-Pelecky, D.; Labhasetwar, V. *Journal of Pharmaceutical Sciences* **2004**, *93*, 1804-1814.

45 Win, K. Y.; Feng, S.-S. *Biomaterials* **2006**, *27*, 2285-2291.

46 Bilati, U.; Alleman, E.; Doelker, E. *Journal of Microencapsulation* **2005**, *22*, 205-214.

47 Jiao, Y. Y.; Ubrich, N.; Marchand-Arvier, M.; Vigneron, C.; Hoffman, M.; Maincent, P. *Drug Delivery* **2001**, *8*, 135-141.

48 Santhakumaran, L. M.; Chen, A.; Pillai, T. T.; He, H.; Thomas, T. J. *Nanofabrication towards biomedical applications* **2005**, Wiley-VCH Verlag GmbH, Germany, 253-287.

49 Birdi, K. S. *CRC Press, Boca Raton, FL* **2009**, *3rd edition*, 340-350.

50 Malvern-Instruments *Mano317* **2005**, 14-11 - 14-18.

51 Schmitz, K. S. *Academic Press, San Diego, CA* **1990**, 321-327.

52 Goodhew, P. J.; Humphreys, J.; Beanland, R. *Electron Microscopy and Analysis* **2001**, *3rd edition*, Taylor & Francis Group, New York, 66-121.

53 Panyam, J.; Sahoo, S. K.; Prabha, S.; Bargar, T.; Labhasetwar, V. *International Journal of Pharmaceutics* **2003**, *262*, 1-11.

54 Jeong, Y.-I.; Choi, K.-C.; Song, C.-E. *Archives of Pharmaceutical Research* **2006**, *29*, 712-719.

55 Kang, S. I.; Na, K.; Bae, Y. H. *Colloids and Surfaces, A: Physicochemical and Engineering Aspects* **2003**, *231*, 103-112.

56 Skoog, D. A.; Holler, F. G.; Nieman, T. A. *Principles of instrumental analysis* **1998**, Thomson Learning, Inc. 5th edition 300-328; 538-543; 725-767.

57 Choi, M. S.; Park, E. S.; Chi, S. C.; Shin, B. C. *Journal of Korean Pharmaceutical Sciences* **2004**, *34*, 177-183.

58 Zhang, Z. P.; Feng, S. S. *Biomacromolecules* **2006**, *7*, 1139-1146.

59 Mu, L.; Feng, S. S. *Pharmaceutical Research* **2003**, *20*, 1864-1872.

60 Hariharan, S.; Bhardwaj, V.; Bala, I.; Sitterberg, J.; Bakowsky, U.; Ravi Kumar, M. N. V. *Pharmaceutical Research* **2006**, *23*, 184-195.

61 Win, K. Y.; Feng, S.-S. *Biomaterials* **2005**, *26*, 2713-2722.

62 Shamsi, S. A.; Palmer C.P.; Warner, I. M. *Analytical Chemistry* **2001**, *73*, 140A-149A.

63 Haddadian, F.; Shamsi, S. A.; Warner, I. M. *Electrophoresis* **1999**, *20*, 3011-3026.

64 Kapnissi-Christodoulou, C. P.; Zhu, X.; Warner, I. M. *Electrophoresis* **2003**, *24*, 3917-3934.

65 Sahoo, S. K.; Panyam, J.; Prabha, S.; Labhasetwar, V. *Journal of Controlled Release* **2002**, *82*, 105-114.

66 Sorg, O. *Comptes Rendus Biologies* **2004**, *327*, 649-662.

67 Kohen, R.; Nyska, A. *Toxicologic Pathology* **2002**, *30*, 620-650.

68 Pokorny, J.; Yanishlieva, N.; Gordon, M. *Antioxidants in food* **2001**, CRC Press LLC, Boca Raton, Forida, 87-249.

69 Food and Drug Administration *Federal Register Final Rule - 62 FR 49868* **1997**, *62*, 49868-49881.

70 Milbury, P. E.; Richer, A. C. *Understanding the antioxidant controversy: scrutinizing the "fountain of youth"* **2008**, Praeger Publishers, Westport, Connecticut, 1-14.

71 Bland, J. S. *Alternative Therapies* **1996**, *2*, 73-76.

72 Zhou, B.; Liu, Z.-L. *Pure Applied Chemistry* **2005**, *77*, 1887-1903.

73 Guarrera, P. M. *Fitoterapia* **2003**, *74*, 515-544.

74 Pal, S. K. *Current Science* **2002**, *82*, 518-524.

75 Helton, L. R. *J Cult Divers* **1996**, *3*, 123-128.

76 Darshan, S.; Doreswamy, R. *Phytotherapy Research* **2004**, *18*, 343-357.

77 Borek, C. *Integrative cancer therapies* **2004**, *3*, 333-341.

78 Garewal, H. S. *Antioxidants and disease prevention* **1997**, CRC Press LLC, Boca Raton, Florida, 3-177.

79 Trumpower, B. L. *Journal of Bioenergetics and Biomembranes* **1981**, *13*, 1-24.

80 Gutierrez, P. L. *Frontiers in Bioscience* **2000**, *5*, 629-638.

81 Horvath, R.; Gorman, G.; Chinnery, P. F. *Neurotherapeutics* **2008**, *5*, 558-568.

82 Quinzii, C. M.; Lopez, L. C.; Naini, A.; DiMauro, S.; Hirano, A. *Biofactors* **2008**, *32*, 113-118.

83 Alcain, F. J.; Villalba, J. M. *Expert Opinion on Therapeutic Patents* **2007**, *17*, 649-665.

84 Snader, K. M. *Anticancer agents from natural products* **2005**, CRC Press Boca Raton, Florida, 339-356.

85 Neckers, L.; Neckers, K. *Expert Opin Emerg Drugs* **2005**, *10*, 137-149.

86 Dettrakul, S.; Surerum, S.; Rajviroongit, S.; Kittakoop, P. *Journal of Natural Products* **2009**, *72*, 861-865.

87 Muhammad, I.; Takamatsu, S.; Walker, L. A.; Mossa, J. S.; Fong, H. H. S.; El-Feraly, F. S. *Phytotherapy Research* **2003**, *17*, 887-891.

88 Salem, M. L. *International Immunopharmacology* **2005**, *5*, 1749-1770.

89 Badary, O. A.; Taha, R. A.; El-Din, A. M. G.; Abdel-Wahab, M. H. *Drug and Chemical Toxicology* **2003**, *26*, 87-98.

90 Burits, M.; Bucar, F. *Phytotherapy Research* **2000**, *14*, 323-328.

91 Badary, O. A.; Abdel-Naim, A. B.; Adel-Wahab, M. H.; Hamada, F. M. A. *Toxicology* **2000**, *143*, 219-226.

92 Nagi, M. N.; Mansour, M. A. *Pharmacological Research* **2000**, *41*, 283-289.

93 Gali-Muhtasib, H.; Roessner, A.; Schneider-Stock, R. *International Journal of Biochemistry & Cell Biology* **2006**, *38*, 1249-1253.

94 Shoieb, A. M.; Elgayyar, M.; Dudrick, P. S.; Bell, J. L.; Tithof, P. K. *International Journal of Oncology* **2003**, *22*, 107-113.

95 Gali-Muhtasib, H.; Diab-Assaf, M.; Boltze, C.; Al-Hmaira, J.; Hartig, R.; Roessner, A.; Schneider-Stock, R. *International Journal of Oncology* **2004**, *25*, 857-866.

96 Sheu, S. S.; Nauduri, D.; Anders, M. W. *Biochimica Et Biophysica Acta-Molecular Basis of Disease* **2006**, *1762*, 256-265.

97 Kaur, I. P.; Kapila, M.; Agrawal, R. *Ageing Research Reviews* **2007**, *6*, 271-288.

98 Ratnam, D. V.; Ankola, D. D.; Bhardwaj, V.; Sahana, D. K.; Kumar, M. *Journal of Controlled Release* **2006**, *113*, 189-207.

99 Dziubla, T.; Muro, S.; Muzykantov, V. R.; Koval, M. *Oxidative Stress, Disease and Cancer* **2006**, 1023-1043.

100 Wu, T. H.; Yen, F. L.; Lin, L. T.; Tsai, T. R.; Lin, C. C.; Cham, T. M. *International Journal of Pharmaceutics* **2008**, *346*, 160-168.

101 Zhang, Y.; Yang, Y.; Tang, K.; Hu, X.; Zou, G. *Journal of Applied Polymer Science* **2008**, *107*, 891-897.

102 Bala, I.; Bhardwaj, V.; Hariharan, S.; Sitterberg, J.; Bakowsky, U.; Kumar, M. *Nanotechnology* **2005**, *16*, 2819-2822.

103 Bala, I.; Bhardwaj, V.; Hariharan, S.; Kharade, S. V.; Roy, N.; Kumar, M. N. V. R. *Journal of Drug Targeting* **2006**, *14*, 27-34.

104 Ankola, D. D.; Viswanad, B.; Bhardwaj, V.; Ramarao, P.; Ravi Kumar, M. N. V. *European Journal of Pharmaceutics and Biopharmaceutics* **2007**, *67*, 361-369.

105 Hsu, C.-H., Coenzyme Q10 nanoparticles engineered from microemulsion precursors for oral delivery, 2004.

106 Nehilla, B. J.; Bergkvist, M.; Popat, K. C.; Desai, T. A. *International Journal of Pharmaceutics* **2008**, *348*, 107-114.

107 Bisht, S.; Feldmann, G.; Soni, S.; Ravi, R.; Karikar, C.; Maitra, A.; Maitra, A. *Journal of Nanobiotechnology* **2007**, 5:3.

108 Kurzrock, R.; Li, L.; Mehta, K.; Aggarwai, B. B.; Liposomal curcumin for treatment of cancer: WO/2004/080396, 2004, pp 66.

109 Dalle-Donne, I.; Rossi, R.; Colombo, R.; Giustarini, D.; Milzani, A. *Clinical Chemistry (Washington, DC, United States)* **2006**, *52*, 601-623.

110 Molavi, B.; Mehta Jawahar, L. *Current opinion in cardiology* **2004**, *19*, 488-493.

111 Passi, S.; Gianni, G.; Cocchi, M. *Progress in Nutrition* **2006**, *8*, 241-256.

112 Manea, A.; Constantinescu, E.; Popov, D.; Raicu, M. *Journal of Cellular and Molecular Medicine* **2004**, *8*, 117-126.

113 Goetz, M. E.; Luch, A. *Cancer Letters* **2008**, *266*, 73-83.

114 Afonso, V.; Champy, R.; Mitrovic, D.; Collin, P.; Lomri, A. *Joint, Bone, Spine* **2007**, *74*, 324-329.

115 Halliwell, B.; Gutteridge, J. M. C. *Free radicals in biology and medicine* **1989**, Oxford University Press, 2nd edition, 1-81.

116 Gomes, A.; Fernandes, E.; Lima, J. L. F. C. *Journal of Biochemical and Biophysical Methods* **2005**, *65*, 45-80.

117 Soh, N.; Imato, T. *Current Bioactive Compounds* **2006**, *2*, 409-430.

118 Soh, N. *Analytical and Bioanalytical Chemistry* **2006**, *386*, 532-543.

119 Keller, A.; Mohamed, A.; Droese, S.; Brandt, U.; Fleming, I.; Brandes, R. P. *Free Radical Research* **2004**, *38*, 1257-1267.

120 Manevich, Y.; Held, K. D.; Biaglow, J. E. *Radiation Research* **1997**, *148*, 580-591.

121 Martin-Aragon, S.; Benedi, J.; Villar, A. *Phytotherapy Research* **1996**, *10*, S75-S78.

122 Newton, G. L.; Milligan, J. R. *Radiation Physics and Chemistry* **2006**, *75*, 473-478.

123 Makrigiorgos, G. M.; Baranowska-Kortylewicz, J.; Bump, E.; Sahu, S. K.; Berman, R. M.; Kassis, A. I. *International Journal of Radiation Biology* **1993**, *63*, 445-458.

124 Soh, N.; Makihara, K.; Ariyoshi, T.; Seto, D.; Maki, T.; Nakajima, H.; Nakano, K.; Imato, T. *Analytical Sciences* **2008**, *24*, 293-296.

125 Ghosh, S. C.; Auzenne, E.; Farquhar, D.; Klostergaard, J. *Bioconjugate Chemistry* **2007**, 731-735.

126 Bartosz, G. *Clinica Chimica Acta* **2006**, *368*, 53-76.

127 Albers, A. E.; Okreglak, V. S.; Chang, C. J. *Journal of American Society* **2006**, 9640-9641.

128 Soh, N.; Makihara, K.; Sakoda, E.; Imato, T. *Chemical Communications (Cambridge, United Kingdom)* **2004**, 496-497.

129 Brereton, R. G. *Applied chemometrics for scientists* **2007**, John Wily & Sons, West Sussex, England, 1-62.

130 Otto, M. *Chemometrics. Statistics and computer application in analytical chemistry* **1999**, Wiley-VCH GmbH, Germany, 81-116.

131 Prakobvaitayakit, M.; Nimmannit, U. *AAPS PharmSciTech* **2003**, *4*, 1-9.

132 Dillen, K.; Vandervoort, J.; Van den Mooter, G.; Verheyden, L.; Ludwig, A. *International Journal of Pharmaceutics* **2004**, *275*, 171-187.

133 Vandervoort, J.; Ludwig, A. *International Journal of Pharmaceutics* **2002**, *238*, 77-92.

134 Ganea, G. M.; Sabliov, C. M.; Ishola, A. O.; Fakayode, S. O.; Warner, I. M. *Journal of Nanoscience and Nanotechnology* **2008**, *8*, 280-292.

135 Duan, Y.; Sen, X.; Wang, Q.; Liu, J.; Zhang, Z. *Journal of Materials Science: Materials in Medicine* **2006**, *17*, 559-563.

CHAPTER 2

EXPERIMENTAL DESIGN AND MULTIVARIATE ANALYSIS FOR OPTIMIZING POLY (D,L-LACTIDE-*CO*-GLYCOLIDE) (PLGA) NANOPARTICLE SYNTHESIS USING MOLECULAR MICELLES*

2.1 Introduction

Significant advances in the application of nanotechnology in the medical field have been recently witnessed, particularly relevant to the improvements in pharmaceuticals' bioavailability and delivery. Controlled drug delivery systems offer an excellent alternative to the free drug administration, providing a constant drug concentration in the bloodstream within the efficient therapeutic range, for a prolonged period of time. The benefits of such systems include a reduced number of doses, minimizing the undesirable side effects and adverse reactions, leading to improved general comfort of the patient.[1-3]

Biodegradable polymeric nanoparticles are attractive drug delivery systems because of their biocompatibility and degradation through normal metabolic pathways, the wide variety of preparation methods, high encapsulation efficiency, and sustained drug release in time. Numerous pharmaceutical compounds can be delivered via various routes by use of nanoparticles. For example, the active agent can be entrapped in the polymeric matrix (nanospheres), encapsulated into a nanocapsule structure, and adsorbed or chemically bound to the nanoparticle surface.[4-6] Using this variety of approaches, polymeric nanoparticles have been extensively investigated as delivery systems in cancer therapy,[7, 8] gene therapy,[9] and protein delivery.[10] Poly (lactic acid), poly (glycolic acid) and their copolymer poly (lactide-*co*-glycolide) (PLGA) are the most commonly used biocompatible and biodegradable polymers in the preparation of nanoparticle drug carriers.[11, 12] Various methods are available for polymeric nanoparticle synthesis, including emulsification solvent diffusion, dialysis, salting-out, and

* Reproduced with permission from Journal of Nanoscience and Nanotechnology (Appendix V)

nanoprecipitation.[13-15] Emulsification solvent evaporation is commonly used for the preparation of polymeric nanoparticles, where either a single oil-in-water (O/W) emulsion is prepared for the entrapment of hydrophobic active agents [16-21] or, a double water-in-oil-in-water (w/o/w) emulsion is used for the encapsulation of water soluble active agents.[22, 23]

Nanoparticle synthesis is a challenging process involving many variables which affect the nanoparticle physico-chemical properties relevant to the performance of polymeric nanoparticles as drug delivery systems. For example, particle size, polydispersity, and surface charge are critical characteristics for the biological applications of polymeric drug carriers.[24, 25] Chemometric experimental design is an emerging field in nanoparticle synthesis which can be employed for the evaluation of individual effects as well as combined effects of the preparation variables on the nanoparticle characteristics. The influence of polymer concentration, emulsifier type and concentration, phase ratio, and drug concentration is typically studied on particle size, size distribution, surface properties, entrapment efficiency, and drug release properties.[26-30] By use of chemometric experimental design with a reduced number of experiments one can establish the optimal conditions which lead to the desired characteristics of polymeric nanoparticles. Central composite design is an excellent choice for nanoparticle synthesis in comparison to other experimental design approaches, such as full or fractional factorial designs, because of its ability to provide the linearity as well as the curvature of the responses as a function of the design variables.[27, 28]

Many nanoparticle preparation methods involve the presence of an anionic, cationic, or non-ionic emulsifier dissolved in the aqueous phase. The role of the emulsifier is typically to stabilize the emulsion and consequently to reduce the particle size and improve the size distribution. Poly (vinyl alcohol) (PVA) is one of the commonly used emulsifiers which leads to the formation of nanoparticles with a small size.[16, 23] However, the residual PVA attached to the

nanoparticle surface is difficult to remove and limits the nanoparticle cellular uptake and drug controlled release properties [31]. Sodium dodecyl sulfate (SDS) has also been used as an emulsifier in nanoparticle synthesis, and often leads to small particle sizes. However, the stability of nanoparticle suspension is affected after SDS removal, by the formation of aggregates which are not able to re-suspend in an aqueous solution.[17] In certain cases, the surfactant emulsifier is efficient only at concentrations higher than the critical micelle concentration (CMC), which limits the investigation of a wider range of concentrations.

Molecular micelles offer an advantageous alternative to conventional micelles, such as SDS, because of their enhanced stability, rigidity, and controllable size[32] Furthermore, molecular micelles present a CMC value of zero, as determined by the covalently bound micellar core, which eliminates the dynamic equilibrium between the monomers and the micelle. Thus, the formation of monodispersed polymeric nanoparticles may be achievable at a low emulsifier concentration, using molecular micelles. It should be noted that anionic molecular micelles such as poly (sodium *N*-undecenyl sulfate) (poly-SUS), poly (sodium *N*-undecenyl-glycinate) (poly-SUG) and poly (sodium *N*-undecenyl-L-leucyl-valinate) (poly-L-SULV) have been successfully used as alternatives to conventional micelles for pseudostationary phases in chromatographic separations.[32-34]

In this study, we report the use molecular micelles as potential emulsifiers in the synthesis of polymeric nanoparticles.[35] The first objective of the present study was to synthesize PLGA nanoparticles using three molecular micelles (poly-SUS, poly-SUG and poly-L-SULV) and two conventional emulsifiers (SDS and PVA) by use of the emulsification solvent evaporation method. Secondly, an investigation of the effect of four formulation parameters (design variables) on particle size and size distribution (responses) was performed using a central composite experimental design (CCD) and multivariate analysis. The design variables used in

this study were PLGA concentration, emulsifier concentration, homogenization speed, and sonication time. In addition, the experimental values of selected formulations for each emulsifier were compared with the predicted values given by the model. Finally, the optimal experimental conditions were selected based on CCD, in order to synthesize PLGA nanoparticles having the minimum particle sizes and minimum PDI values. The optimal nanoparticle suspensions were further purified by use of dialysis and then freeze-dried. The changes in their physico-chemical properties such as particle size, polydispersity index (PDI), and zeta potential were monitored before dialysis, after dialysis, and after freeze-drying. The morphology of the dried PLGA nanoparticles prepared with molecular micelles as emulsifiers was investigated using transmission electron microscopy (TEM).

2.2 Experimental

2.2.1 Materials

Poly (D,L-lactide-*co*-glycolide) (PLGA, lactide:glycolide 50:50, MW 40,000-75,000), poly (vinyl alcohol) (PVA, average MW 9,000-10,000, 80 % hydrolyzed), sodium dodecyl sulfate (SDS), undecylenic acid, ω-undecylenyl alcohol, glycine, ethyl acetate, hydrochloric acid, chlorosulfonic acid, sodium carbonate, and sucrose were purchased from Sigma-Aldrich (St. Louis, MO, USA). *N*-hydroxysuccinimide (NHS), *N,N'*-dicyclohexylcarbodiimide (DCC), and pyridine were purchased from Fluka (Milwaukee, WI, USA). Isopropyl alcohol, tetrahydrofuran, and ethyl ether were purchased from EMD Chemicals Inc. (Gibbstown, NJ, USA). LL-leucyl-valinate was purchased from Bachem Bioscience Inc. (King of Prussia, PA, USA). Sodium bicarbonate and sodium hydroxide were purchased from Fisher Scientific (Pittsburgh, PA, USA). Butyl alcohol was purchased from Mallinckrodt (Hazelwood, MO, USA). Doubly-distilled deionized water was obtained from an ELGA PURELAB Ultra water polishing system (US Filter, Lowell, MA, USA).

2.2.2 Synthesis of Molecular Micelles

A sulfate based molecular micelle, poly (sodium *N*- undecenyl sulfate) (poly-SUS), was prepared according to Bergstrom's procedure [36], modified by Shamsi et al.[37] A general synthesis scheme is presented in Appendix I. The micelles poly (sodium *N*- undecenyl-glycinate) (poly-SUG) and poly (sodium *N*- undecenyl-L-leucyl-valinate) (poly-L-SULV) were synthesized according to the procedure described by Macossay et al.[38] The chemical structures of the molecular micelles are presented in Figure 2.1.

2.2.3 Nanoparticle Synthesis

PLGA nanoparticles were synthesized by use of an emulsification solvent evaporation method. Briefly, appropriate amounts of PLGA were dissolved in 2.5 mL ethyl acetate to form an organic phase. The aqueous phase was prepared by dissolving various amounts of emulsifiers, molecular micelles (poly-SUS, poly-SUG and poly-L-SULV) or conventional surfactants (SDS and PVA), in 10 mL water. The organic phase was then added dropwise to the aqueous phase under stirring conditions using a homogenizer (model 398, Biospec Products, Inc., Racine, WI, USA) at different speeds, resulting in a single o/w emulsion. The emulsion droplets were further reduced by sonication using a probe ultrasound processor (model VC750, Sonics and Materials Inc., Newton, CT, USA), operating at an amplitude intensity of 30 %, for periods of time ranging from 5 minutes to 20 minutes. The solvent was evaporated using a rotary evaporator (Büchirotovapor R-200, Brinkmann Instruments, Inc., Westbury, NY, USA).

2.2.4 Central Composite Experimental Design and Multivariate Analysis

The effects of four design variables on particle size and size distribution were simultaneously investigated using a central composite design (CCD). The design variables were the PLGA concentration, stabilizer concentration, homogenization speed, and sonication time.

All other parameters were held constant. The CCD and resultant data analysis were performed using Unscrambler 9.1.2 software (Camo, Corvallis, OR, USA, version 9.1.2)

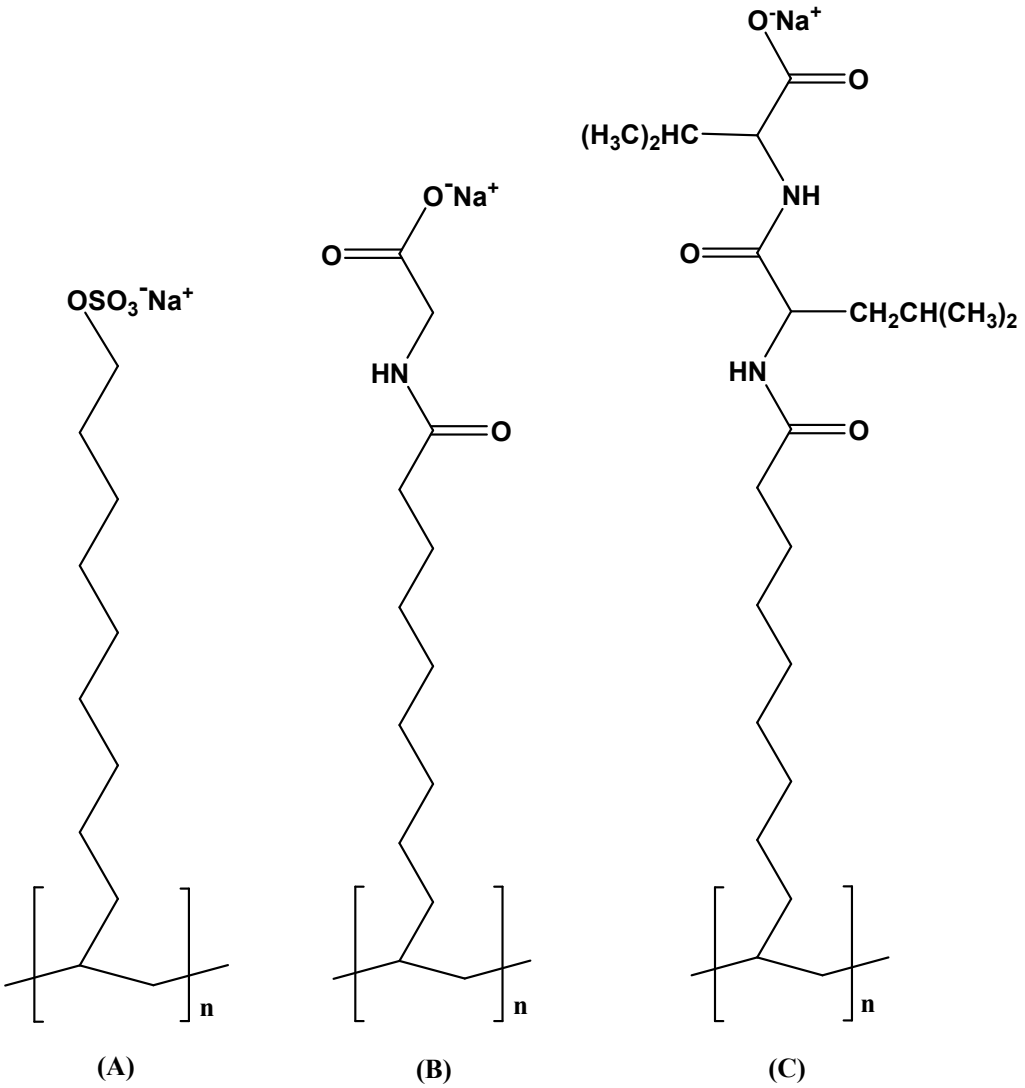

Figure 2.1 Chemical structure of investigated molecular micelles. (A) poly (sodium N-undecenyl sulfate) (poly-SUS); (B) poly (sodium N- undecenyl-glycinate) (poly-SUG); (C) poly (sodium N- undecenyl-leucyl-valinate) (poly-L-SULV).

The optimal experimental conditions necessary to synthesize PLGA nanoparticles having the minimum particle sizes and minimum PDI values were determined by use of CCD for each of the investigated emulsifiers. The levels of the investigated design variables are presented in

Table 2.1. The experimental design involved a total of 29 experiments, with 5 central level samples to evaluate the reproducibility of the nanoparticle synthesis.

Table 2.1 Levels of design variables investigated in the central composite design

Design Variable	**Levels**				
PLGA concentration (% (w/v))	0.5	2.0	3.5	5.0	6.5
Emulsifier concentration (% (w/v))	0.05	0.1	0.55	1.0	1.5
Homogenization speed (rpm)	5,000	10,000	15,000	20,000	25,000
Sonication time (min)	0	5	10	15	20

2.2.5 Nanoparticle Purification

In order to verify the changes in particle size and PDI after synthesis, the optimal formulations were further purified by dialysis and freeze-dried. The PLGA nanoparticle suspension was introduced in a Spectra/Por Float-A-Lyzer tube (cellulose ester membrane, MWCO 100,000 Da, Spectrum Laboratories, Inc., Rancho Dominguez, CA, USA) prepared according to the manufacturer's instructions and placed in a 4 liter volume of water under magnetic stirring for 24 hours (the external water was completely replaced after 12 hours). Dialyzed nanoparticle suspensions were further lyophilized (Freezone Plus 6, Labconco, Kansas City, MO, USA) in the presence of 2 % (w/v) sucrose as a cryoprotectant. The dried nanoparticles were re-suspended in water at 0.1 % (w/v) concentration for the investigation of their physico-chemical properties.

2.2.6 Nanoparticle Characterization

The average particle diameter (Z_{ave}) and size distribution indicated by the polydispersity index (PDI) were measured by use of dynamic light scattering (DLS) (Zetasizer NanoZS,

Malvern Instrumets Ltd., Malvern, UK) and reported as intensity distribution. For each measurement, appropriate volumes of nanoparticle suspension were transferred into a disposable polystyrene cuvet for particle size and PDI determinations. Nanoparticle surface charge indicated by zeta potential was measured by use of laser doppler anemometry (Zetasizer NanoZS, Malvern Instrumets Ltd., Malvern, UK) using a capillary cell. The reported values of particle size, PDI, and zeta potential represent an average of 3 measurements performed at 25 ºC, for each batch of nanoparticle suspensions. The nanoparticle morphologies were investigated using transmission electron microscopy (TEM) (JEOL 100CX, JEOL USA Inc., Peabody, MA, USA) operating at 80kV. A drop of nanoparticle suspension was dried at room temperature on a carbon coated copper grid and negatively stained with a 2 % uranyl acetate solution, to create a contrast image, prior to imaging.

2.3 Results and Discussions

2.3.1 Optimization of Nanoparticle Synthesis

In the present study, PLGA nanoparticles were synthesized by use of an emulsification solvent evaporation method using molecular micelles poly-SUS, poly-SUG and poly-L-SULV as well as conventional emulsifiers (SDS and PVA). In aqueous solution, micelles self-assemble into spherical shape structures having a hydrophobic core and a hydrophilic surface formed by functional head groups. Polymerization of such species produces molecular micelles [32].

The proposed mechanism of nanoparticle synthesis using molecular micelles is schematically represented in Figure 2.2. The PLGA polymer is first dissolved in an organic phase. The water soluble molecular micelles contribute to the formation of dispersed organic droplets containing PLGA, under homogenization and sonication conditions. After formation of an emulsion, the organic solvent is evaporated and the PLGA nanoparticles are purified and freeze-dried as previously described in the experimental section.

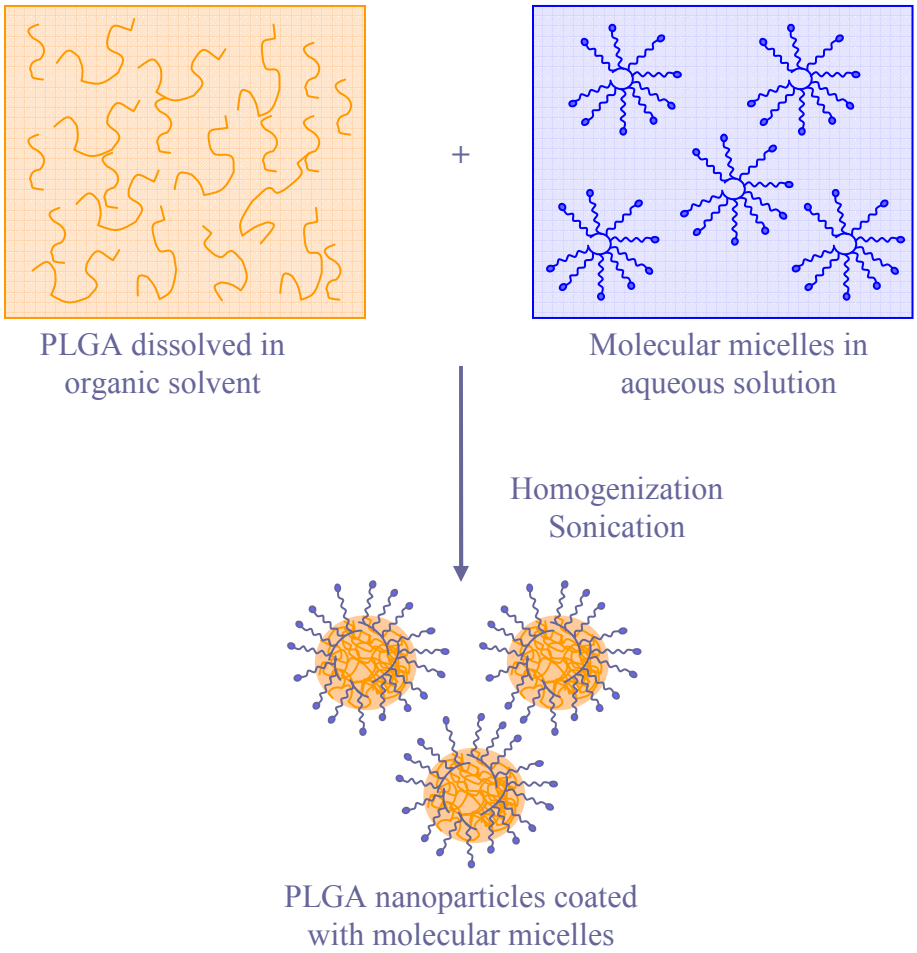

Figure 2.2 Proposed mechanism of PLGA nanoparticle formation by use of emulsification solvent evaporation using molecular micelles as emulsifiers.

The results of nanoparticle synthesis using SDS, PVA, poly-SUS, poly-SUG and poly-L-SULV under various experimental conditions are presented in Table 2.2. The experimental conditions for all experiments used in central composite design are listed in Appendix II. A multivariate analysis in the form of a multilinear regression (MLR) was used to correlate the nanoparticle synthetic parameters (design variables) with the nanoparticle size and PDI (responses). MLR was used for regression modeling since no colinearity was found between the design variables used in this study. In addition, the number of design variables (4) was smaller than the experimental runs (29).

Table 2.2 The responses (particle size and PDI) used in the central composite design

Exp. No.	SDS		PVA		Poly-SUS		Poly-SUG		Poly-L-SULV	
	Z_{ave} (nm)	PDI	Z_{ave} (nm)	PDI	Z_{ave} (nm)	PDI	Z_{ave} (nm)	PDI	Z_{ave} (nm)	PDI
1	48.8	0.140	162.3	0.047	125.0	0.125	85.4	0.113	143.0	0.114
2	52.2	0.122	162.3	0.042	115.0	0.098	84.4	0.149	113.0	0.128
3	55.4	0.145	137.7	0.051	115.0	0.148	78.0	0.106	121.0	0.123
4	56.3	0.145	131.0	0.039	114.0	0.114	90.1	0.148	117.0	0.120
5	47.9	0.393	112.3	0.049	69.3	0.142	66.2	0.162	77.7	0.172
6	44.8	0.242	115.0	0.042	101.0	0.102	66.9	0.137	89.9	0.153
7	65.2	0.117	290.7	0.175	129.0	0.075	122	0.061	136.0	0.067
8	54.1	0.112	158.7	0.035	115.0	0.130	88.9	0.082	144.0	0.133
9	60.5	0.132	369.0	0.246	153.0	0.063	185.0	0.192	156.0	0.069
10	46.6	0.178	168.0	0.044	113.0	0.128	99.6	0.117	122.0	0.122
11	61.8	0.137	194.0	0.022	140.0	0.097	115.0	0.111	142.0	0.122
12	61.7	0.131	322.0	0.178	155.0	0.065	158.0	0.073	145.0	0.077
13	47.0	0.181	139.0	0.038	117.0	0.129	85.9	0.123	122.0	0.141
14	72.7	0.138	274.3	0.188	169.0	0.105	200.0	0.110	167.0	0.069
15	53.7	0.124	158.7	0.028	108.0	0.103	90.9	0.096	105.0	0.109
16	50.3	0.130	174.3	0.035	108.0	0.124	95.2	0.101	123.0	0.113
17	51.4	0.145	172.0	0.053	111.0	0.111	102.0	0.117	129.0	0.119
18	2530.0	1.000	664.0	0.590	548.0	0.736	719.0	0.811	2130.0	0.971
19	54.8	0.173	123.7	0.043	103.0	0.127	66.3	0.121	114.0	0.125
20	51.8	0.132	177.3	0.027	109.0	0.140	90.6	0.097	125.0	0.117
21	45.4	0.180	115.7	0.035	89.0	0.158	69.3	0.134	107.0	0.133
22	80.0	0.151	402.7	0.279	162.0	0.075	155.0	0.078	171.0	0.068
23	51.2	0.140	182.7	0.027	112.0	0.125	89.5	0.098	121.0	0.117
24	56.5	0.157	308.3	0.194	124.0	0.081	126.0	0.059	128.0	0.054
25	97.4	0.142	445.0	0.297	173.0	0.097	156.0	0.085	157.0	0.084
26	50.8	0.261	134.7	0.026	91.7	0.155	63.8	0.125	130.0	0.124
27	50.6	0.158	177.7	0.039	114.0	0.118	86.8	0.104	124.0	0.104
28	92.4	0.126	627.0	0.330	168.0	0.061	165.0	0.081	186.0	0.082
29	85.8	0.124	400.7	0.308	159.0	0.090	146.0	0.089	172.0	0.072

Note: H. speed – homogenization speed; S. time – sonication time.

Both the linear regression and quadratic regression models were developed for nanoparticle synthesis. Better regression models were obtained using quadratic regression. Hence, the quadratic model was used for data analysis. The quadratic regression equation used for correlation between design variables and responses is described by equation 2.1, i.e.

$$y = b_0 + b_1X_1 + b_2X_2 + b_3X_3 + b_4X_4 + +b_{12}X_1X_2 + b_{13}X_1X_3 + b_{14}X_1X_4 + \\ + b_{23}X_2X_3 + b_{24}X_2X_4 + b_{34}X_3X_4 + +b_{11}X_1^2 + b_{22}X_2^2 + b_{33}X_3^2 + b_{44}X_4^2 \quad 2.1$$

where y is the measured response, particle size (Z_{ave}, nm), or PDI; X_1 is the PLGA concentration (% (w/v)); X_2 is the emulsifier concentration (% (w/v)); X_3 is the homogenization speed (rpm); X_4 is the sonication time (minutes); b_0 is the intercept; $b_{1\text{-}4}$ are the regression coefficients for the linear terms; $b_{12,\ 13,\ 14,\ 23,\ 24,\ 34}$ are the regression coefficients describing the interactions between two variables; and $b_{11\text{-}44}$ are the regression coefficients for the quadratic terms.

Analysis of variance (ANOVA) was further used to evaluate the levels of significance of each design variable and their interactions on the responses. The design variables were considered significant for a p-value ≤ 0.05. The p-values obtained from ANOVA and the regression coefficients of the design variables were calculated and are listed in Table 2.3 as an example for particle size in case of molecular micelles. X_1 is PLGA concentration (% (w/v)); X_2 is emulsifier concentration (% (w/v)); X_3 is homogenization speed (rpm); X_4 is sonication time (min). A complete ANOVA analysis is presented in Appendix III. Generally, PLGA concentration and emulsifier concentration were found to be the most significant variables influencing the particle size and size distribution. The other two variables, homogenization speed and sonication time, had comparatively higher p-values, indicating less influence on the responses (particle size and PDI). However, for a small homogenization speed and a sonication

time of zero, the responses were significantly higher than the other formulations used in the experimental design.

2.3.1.1 Factors Affecting Particle Size

Particle size is an important characteristic of polymeric nanoparticles. Small nanoparticles are suitable for oral and parenteral administration and have better cellular uptake.[9, 13] In this study, the particle size was found to be dependent on the emulsifier type as well as the investigated formulation parameters.

Table 2.3 Results of analysis of variance for particle size (molecular micelles)

Particle size (Z_{ave})						
	Poly-SUS		**Poly-SUG**		**Poly-L-SULV**	
Design variables	*p* value	regression coefficients	*p* value	regression coefficients	*p* value	regression coefficients
Intercept	0.00	126.14	0.00	134.69	0.00	139.01
X_1	0.00	8.77	0.00	5.47	0.00	9.94
X_2	0.00	-52.20	0.00	-76.95	0.00	-49.84
X_3	0.83	0.00	0.25	0.00	0.12	0.00
X_4	0.01	-1.35	0.00	-1.54	0.00	-1.99
X_1X_2	0.44	-1.60	0.51	1.34	0.59	-0.54
X_1X_3	0.70	0.85	0.32	2.24	0.15	-1.76
X_1X_4	0.29	2.16	0.05	4.32	0.00	4.01
X_2X_3	0.49	-1.43	0.79	-0.53	0.00	3.77
X_2X_4	0.26	2.15	0.03	4.55	0.00	-4.40
X_3X_4	0.32	1.99	0.18	2.79	0.06	2.23
X_1^2	0.49	-1.19	0.63	0.86	0.01	-2.80
X_2^2	0.00	9.70	0.00	10.72	0.00	10.75
X_3^2	0.80	0.44	0.09	3.21	0.37	0.79
X_4^2	0.12	2.98	0.03	4.68	0.45	0.78

When SDS was used as the emulsifier, a particle size below 100 nm was obtained. In contrast, the particle size was always higher than 100 nm in the experiments using PVA. Comparatively, the nanoparticle synthesis using molecular micelles as emulsifiers, resulted in nanoparticles with sizes larger than the ones obtained using SDS, but smaller than those obtained using PVA. Among the three investigated molecular micelles, consistently smaller nanoparticle sizes were obtained with poly-SUG, followed by poly-SUS and poly-L-SULV. The reduced sizes obtained using molecular micelles can be explained by the self-assembling structure of molecular micelles in aqueous solution, having a polar group oriented to the micellar surface and a hydrocarbon tail within the micelle, similarly to a conventional micelle, such as SDS. However, the polymerized molecular micelles do not have a CMC and thus create a hydrophobic environment where the organic droplets can be accommodated during the homogenization and sonication processes.

The response surface was further used to investigate the influence of design variables on particle size and size distribution. In general, comparatively smaller nanoparticle sizes were obtained at low PLGA concentration and at high emulsifier concentration. However, for constant PLGA concentration and emulsifier concentration, an increase in nanoparticle size was obtained at low sonication times and low homogenization speeds.

The response surface corresponding to particle size as a function of design variables is represented in Figure 2.3. When SDS was used as the emulsifier (Figure 2.3.A), the minimum particle size range (42.4 – 54.8 nm) was obtained for PLGA concentrations below 6 % (w/v) and SDS concentration between 0.1 and 1.1 % (w/v). However, for an SDS concentration smaller than 0.1 % (w/v) and larger than 1.1 % (w/v), the particle size increased with the increase of PLGA concentration. The homogenization speed and sonication time, had a different effect on the particle size. The smallest particle size range (45.7 – 49.2 nm) was obtained for a

homogenization speed higher than 20,000 rpm and a sonication time higher than 10 minutes. In contrast, the largest particle size was obtained for a homogenization speed of 5,000 rpm and a sonication time of 20 minutes.

The response surface for PVA (Figure 2.3.B) showed a minimum particle size range (85.5 – 172.4 nm) for a large PVA concentration range, from 0.3 to 1.5 % (w/v). However, at PVA concentrations below 0.3 % (w/v), the particle size increased with an increase in PLGA concentration. Similarly to other emulsifiers, the maximum particle size was obtained for emulsifier concentration smaller than 0.1 % (w/v) and PLGA concentrations higher than 5 % (w/v). The particle size surface response for PVA represented for homogenization speed and sonication time indicated a minimum particle size range (147.4 – 177.6 nm) at sonication times between 8 and 18 minutes, irrespective of homogenization speed. However, the particle size increased at low and high extremes of sonication time and homogenization speed ranges. Despite this flexibility, a particle size below 100 nm could not be achieved using PVA, within the ranges of investigated design variables.

Similar response surfaces were obtained for the investigated molecular micelles in terms of PLGA concentration and emulsifier concentration (Figures 2.3.C, 2.3.D, 2.3.E). The minimum particle size ranges for poly-SUS (72.7 – 94.2 nm), poly-SUG (47.8 – 69.5 nm) and poly-L-SULV (73.8 – 95.7 nm) were obtained for an emulsifier concentration between 0.5 and 1.5 % (w/v) and a PLGA concentration below 2 % (w/v) for poly-SUS and poly-L-SULV and below 3.5 % (w/v) for poly-SUG. For concentrations of molecular micelles smaller than 0.5 % (w/v), the particle size increased and reached a maximum for a PLGA concentration higher than 5 % (w/v). When the particle size was represented as a function of homogenization speed and sonication time, the minimum particle size range was highly influenced by the type of molecular micelle. In the case of poly-SUS, the minimum particle size range (105.6 – 111.7 nm) was

present at homogenization speeds lower than 18,000 rpm and sonication times higher than twelve minutes. Although poly-SUS and SDS have similar chemical structures, the strong forces induced in the homogenization and sonication processes seemed to disturb the equilibrium of SDS micelles in solution, thereby increasing the particle size. In contrast, poly-SUS micelles are stable micelles even at high shear forces, resulting in a minimum size range at high sonication times.

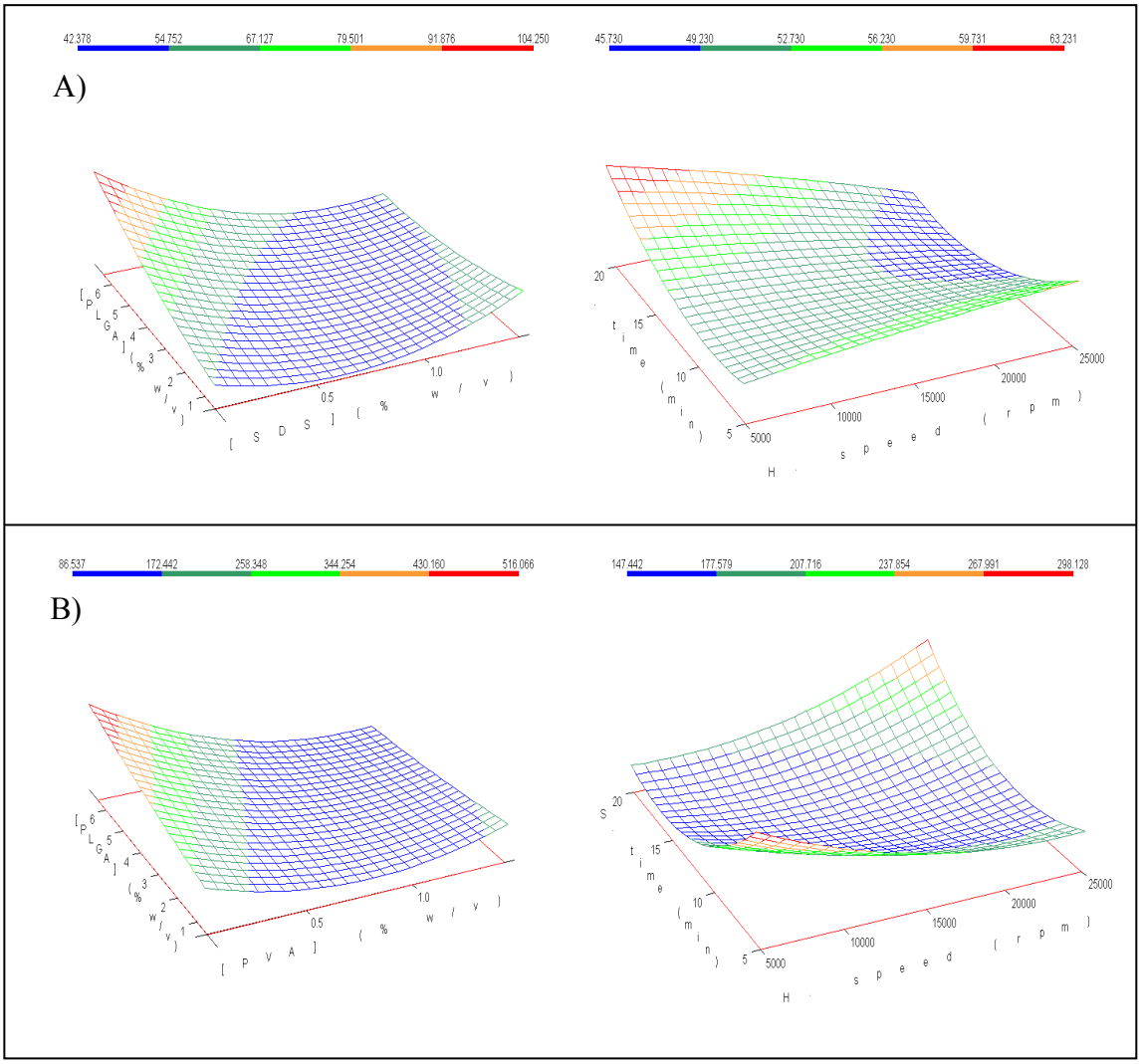

Figure 2.3 Response surface corresponding to particle size for PLGA nanoparticles prepared with A) SDS; B) PVA C) poly-SUS; D) poly-SUG; E) poly-L-SULV (right side – response surface for PLGA concentration and emulsifier concentration; and left side – response surface for homogenization time and sonication speed).

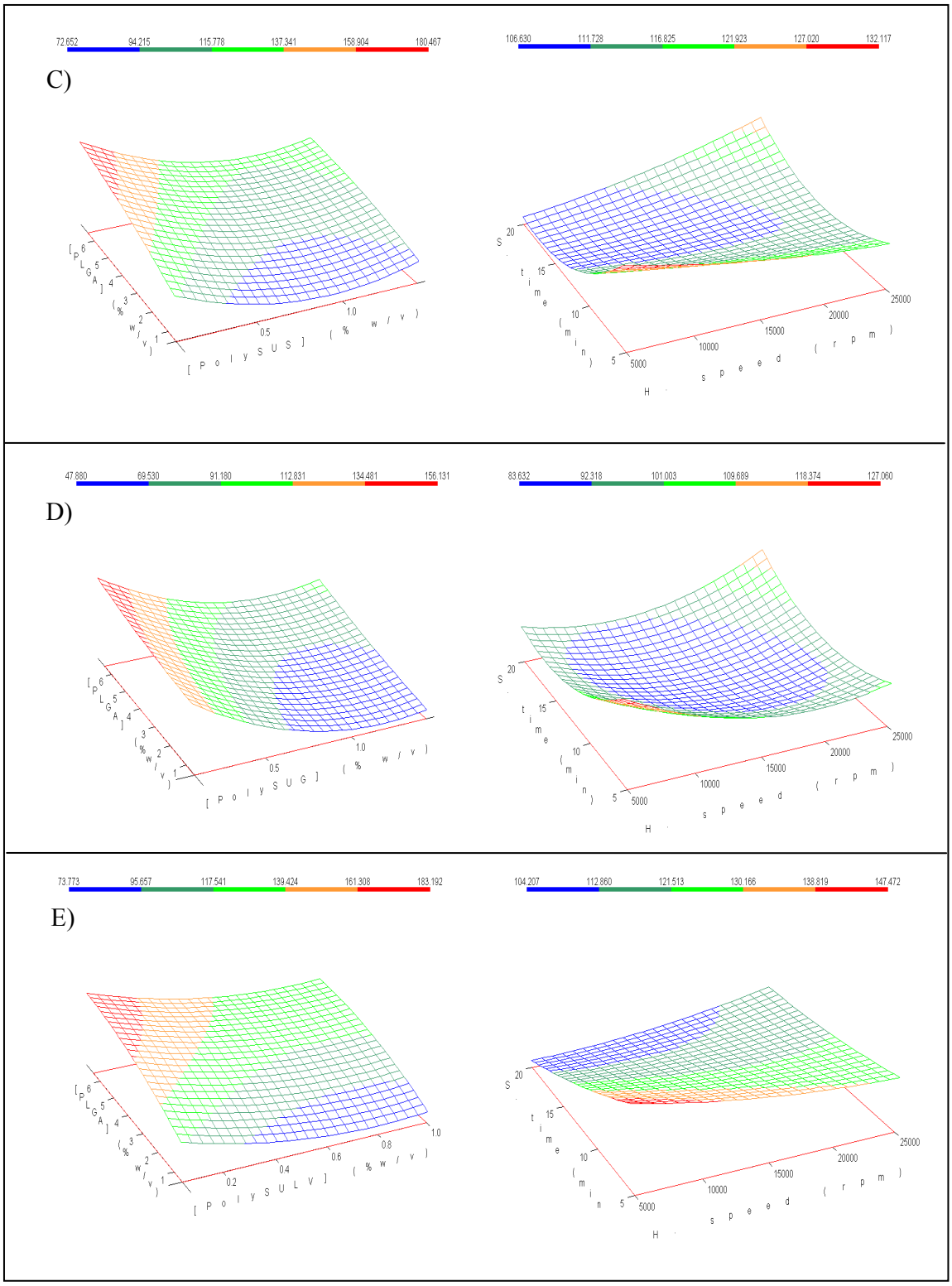

Figure 2.3 Continued.

In the case of poly-SUG, the minimum size range (83.6 – 92.3 nm) was achieved in the center of homogenization speed and sonication time ranges, i.e. 15,000 rpm and 15 minutes respectively. Extreme values, high or low, led to an increase in particle size. When poly-L-SULV was used as the emulsifier, the response surface showed a minimum range (104.2 – 112.8 nm) for long sonication times, between 17 and 20 minutes, and small homogenization speeds, from 5,000 to 15,000 rpm. However, the maximum particle size range similar for all molecular micelles and was obtained for small homogenization speeds, below 10,000 rpm, and short sonication times of 5-6 minutes.

2.3.1.2 Factors Affecting Polydispersity

Polydispersity, represented by the polydispersity index (PDI), is an indication of the particle size distribution. Nanoparticle suspensions are close to monodisperse for small values of PDI, typically below 0.100, and they become more polydisperse as the PDI value increases over 0.200.[28] In the nanoparticle synthesis involving the use of SDS as an emulsifier, the experimental PDI values ranged from 0.122 to 0.393, while the use of PVA as an emulsifier resulted in nanoparticles with experimental PDI values ranging from 0.022 to 0.330. Compared to conventional micelles, consistently smaller PDI values were obtained when molecular micelles were used as emulsifiers. The smallest experimental PDI values of 0.054, 0.059 and 0.061 were obtained when poly-L-SULV, poly-SUG and poly-SUS were used as emulsifiers, respectively. Smaller experimental PDI values obtained for molecular micelles, as compared to conventional micelles, are probably the result of their stability and uniform size in solution, as we earlier hypothesized. This leads to monodisperse suspensions in all experimental formulations using molecular micelles as emulsifiers.

The effect of design variables on the PDI response surface is represented in Figure 2.4. Although the PDI varied within a wide range, it generally decreased with a decrease of

emulsifier concentration and an increase in PLGA concentration. In contrast, PDI values decreased with a decrease of homogenization speed and an increase in sonication time. In terms of PLGA concentration and emulsifier concentration, the PDI produced a concave response surface for SDS, PVA, and the molecular micelles poly-SUG and poly-L-SULV. For the latter molecular micelles (Figures 2.4.D, 2.4.E), a minimum range was obtained at small emulsifier concentration, below 0.2 % (w/v), and PLGA concentration from 0.5 to 5.5 % (w/v).

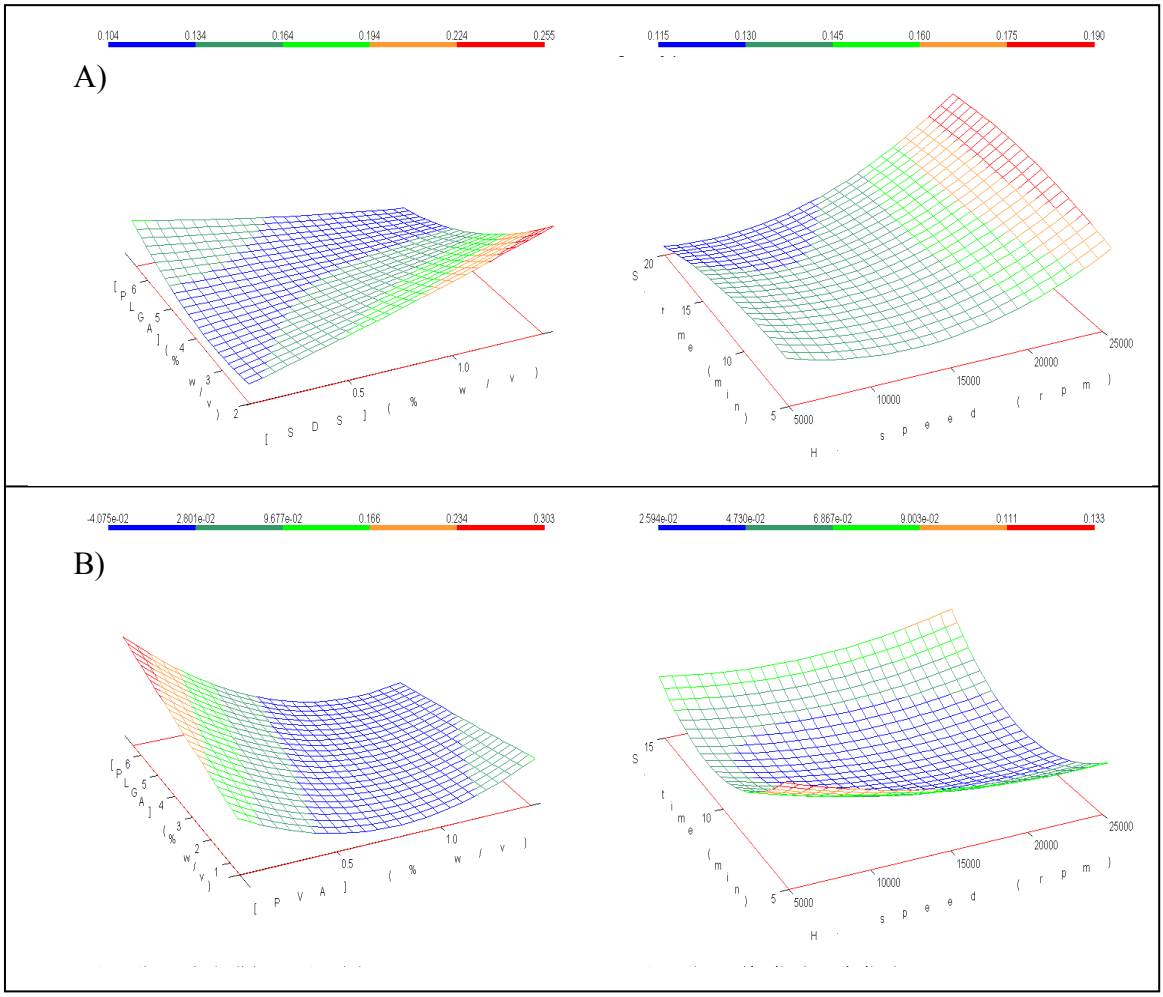

Figure 2.4 Response surface corresponding to polydispersity index for PLGA nanoparticles prepared with A) SDS; B) PVA; C) poly-SUS; D) poly-SUG; E) poly-L-SULV(right side – response surface for PLGA concentration and emulsifier concentration; and left side – response surface for homogenization time and sonication speed).

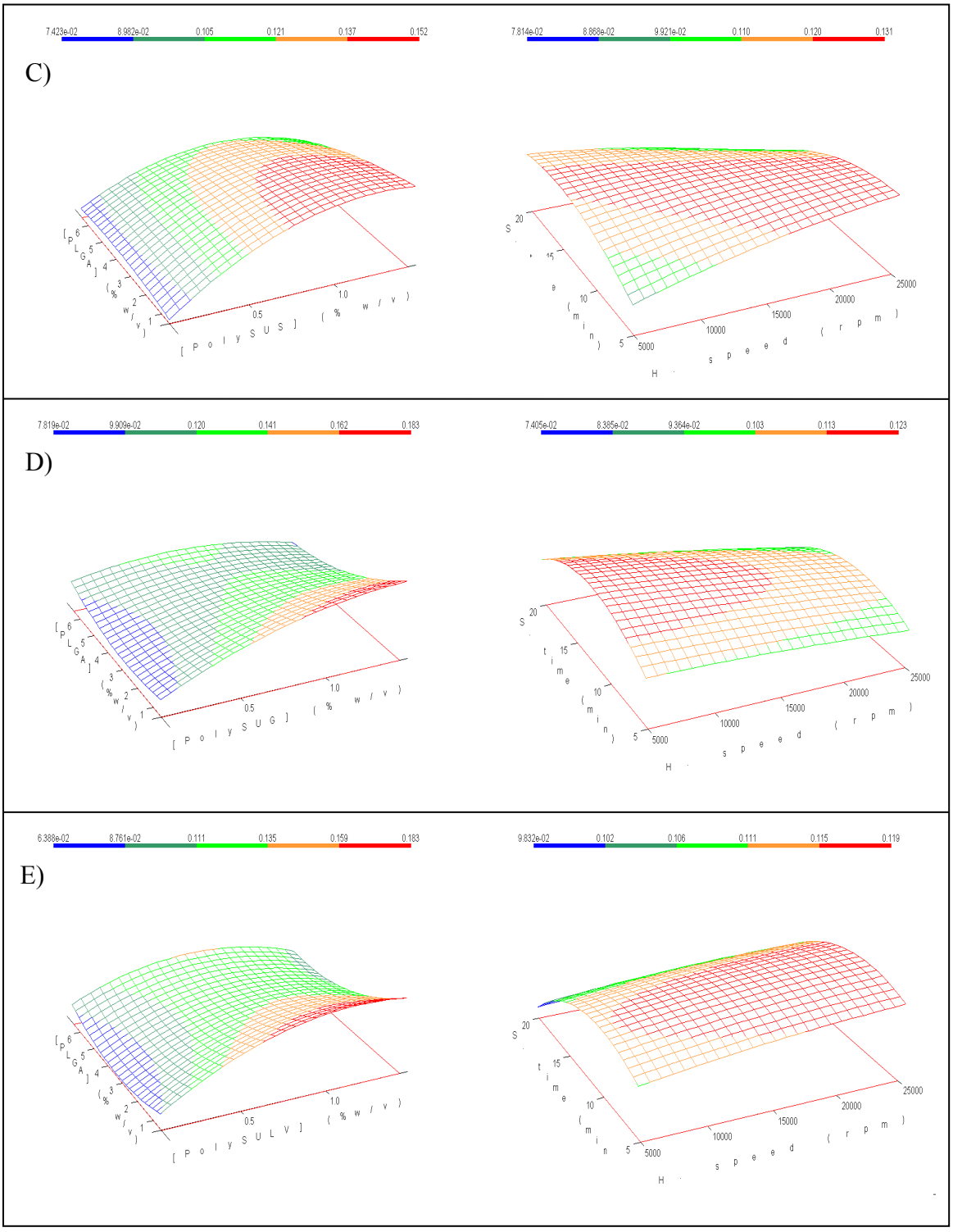

Figure 2.4 Continued.

For SDS (Figure 2.4.A), this range was extended towards high SDS concentrations and high PLGA concentrations. In the case of PVA (Figure 2.4.B), the minimum PDI range was obtained for PVA concentrations between 0.5 and 1.5 % (w/v) and PLGA concentrations from 0.5 to 6.5 % (w/v). However, at PVA concentrations below 0.5 % (w/v), the PDI value increased with an increase of PLGA concentration. The response surface for poly-SUS (Fig. 2.4.C) was opposite to the ones for the other emulsifiers and seemed to be independent of PLGA concentration and highly dependent on poly-SUS concentration. In this case, the minimum PDI range was obtained for a poly-SUS concentration below 0.2 % (w/v), irrespective of PLGA concentration. However, for emulsifier concentration higher than 0.2 % (w/v), the PDI value increased with the increase of poly-SUS concentration. When the PDI response surface was represented as a function of homogenization speed and sonication time, the molecular micelles presented similar convex surfaces with a minimum situated at high homogenization speeds and high sonication times. The only exception was poly-L-SULV, where the minimum PDI was obtained for high homogenization speed (20,000 rpm), irrespective of the sonication time. In contrast, the PDI surface response was concave for SDS and PVA. However, the minimum range was located at different values of design variables. In the case of SDS, the smallest PDI values were obtained for homogenization speeds lower than 15,000 rpm and sonication times longer than fifteen minutes. For PVA, the minimum PDI range was obtained for homogenization speeds between 10,000 and 25,000 rpm and sonication times between 8 and 12 minutes.

2.3.1.3 Validation of the Regression Model

The CCD used in this study was designed to have five replicates of central samples in order to evaluate the reproducibility of the nanoparticle synthesis. In general, one would expect that the percentage relative standard deviation for particle size would be significantly smaller as compared to percentage relative standard deviation for PDI, simply because of their different

orders of magnitude. In the case of particle size, the percentage relative standard deviation of the five replicated central samples ranged from 1.5 % for SDS to 4.5 % for poly-SUG, indicating high reproducibility for the nanoparticle synthesis. In contrast, the percentage relative standard deviation for PDI had higher values, from 7.4 % for poly-L-SULV to 20.1 % for poly- SUG.

In order to verify the predictive ability of the regression model, the experiments resulting in nanoparticles having a minimum particle size and a minimum PDI value, respectively, were selected for each emulsifier and reproduced in triplicate. The average values for particle size and PDI experimentally obtained from DLS were compared to the particle size and PDI values predicted by the model. The experimental and predicted values of particle size and PDI and their percentage relative errors are shown in Table 2.4. In general, the predictive ability of the model was better when molecular micelles were used as emulsifiers. Their percentage relative errors for particle size ranged from -7.8 % for poly-SUS to -16.1 % for poly-SUG, indicating a good predictability of the model for molecular micelles. In the case of the PDI values, the percentage relative error ranged from -3.8 % for poly-L-SULV to -23.9 % for poly-SUG. However, in the case of conventional emulsifiers SDS and PVA, the percentage relative errors were smaller than those for the PDI values of the molecular micelles, but significantly higher for the particle sizes.

2.3.2 Characterization of Optimally Synthesized PLGA Nanoparticles

2.3.2.1 Particle Size and Size Distribution

PLGA nanoparticle synthesis was optimized by use of CCD. The optimal conditions required to synthesize PLGA nanoparticles having the minimum particle size and minimum PDI were selected based on the location of the minimum ranges for particle size and PDI given by the quadratic model. In order to verify the changes in nanoparticle physico-chemical characteristics after synthesis, the optimal PLGA nanoparticle formulations were further purified by dialysis and freeze-dried.

Table 2.4 Experimental and predicted particle size (Z_{ave}) and PDI

Formulation	Emulsifier	Z_{ave} (nm)		
		Experimental (n=3)	**Predicted**	**% Rel. Error**
1S	SDS	44.2 ± 0.7	49.6	12.3
2S	PVA	107.7 ± 5.0	150.9	40.2
3S	Poly-SUS	88.9 ± 10.1	82.0	-7.8
4S	Poly-SUG	79.6 ± 8.9	66.7	-16.2
5S	Poly-L-SULV	92.7 ± 24.1	79.5	-14.3
Formulation	**Emulsifier**	**PDI**		
		Experimental (n=3)	**Predicted**	**% Rel. Error**
1P	SDS	0.130 ± 0.002	0.125	-4.1
2P	PVA	0.044 ± 0.010	0.040	-7.4
3P	Poly-SUS	0.077 ± 0.021	0.059	-23.9
4P	Poly-SUG	0.071 ± 0.004	0.065	-7.4
5P	Poly-L-SULV	0.054 ± 0.004	0.066	-3.8
Note: Formulations 1S-5S represent the optimized experiments leading to the minimum particle sizes; formulations 1P-5P represent the optimized experiments leading to the minimum PDI values.				

The experimental values for the particle size and the PDI values of the PLGA nanoparticles before dialysis, after dialysis, and after freeze-drying are provided in Figure 2.5. After freeze-drying, nanoparticles prepared with SDS could not be re-suspended in aqueous solution due to particle aggregation. However, the particle size slightly decreased after dialysis with a significant increase in PDI value, indicating increased polydispersity of the purified nanoparticles. In contrast, when molecular micelles were used as emulsifiers, the solution

became clearer, as the excess of molecular micelles was removed by dialysis, and the dried nanoparticles could be readily re-suspended in water after freeze-drying.

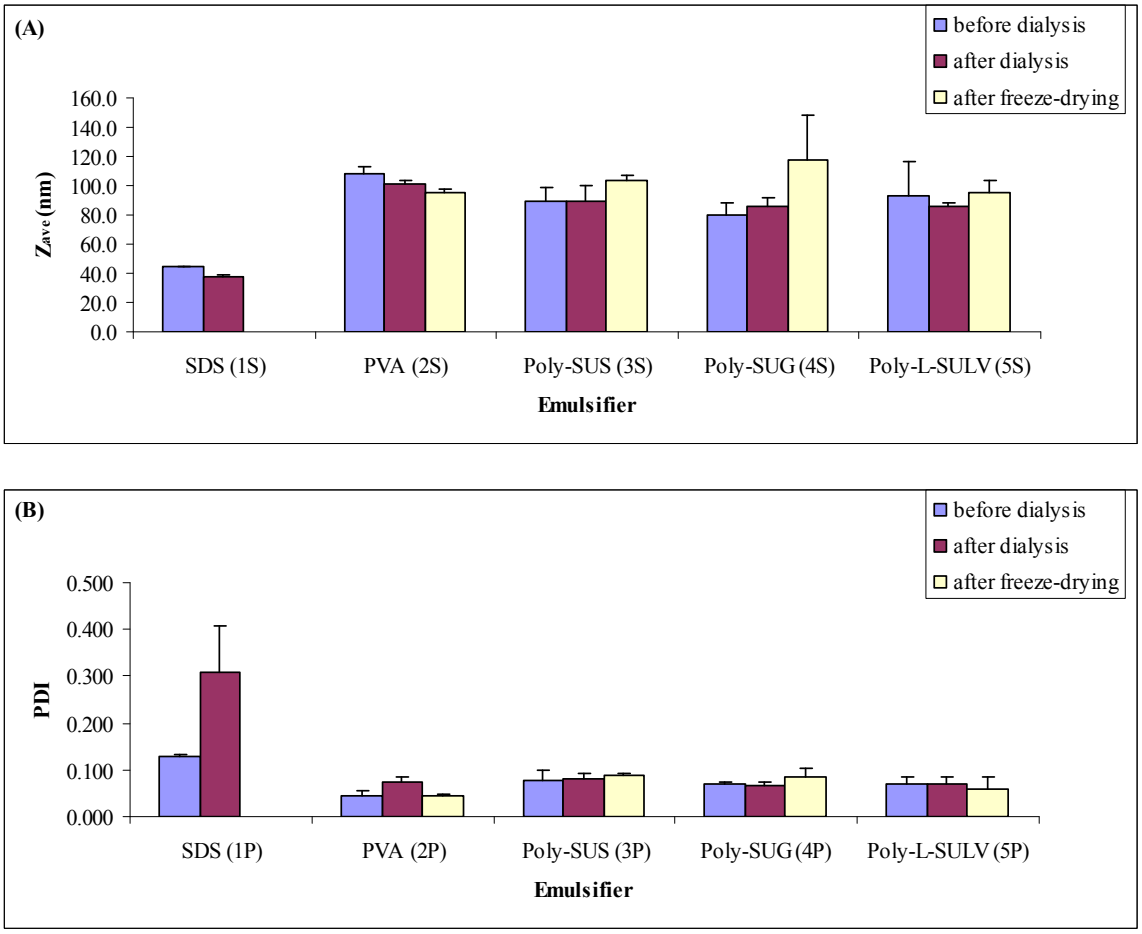

Figure 2.5 Experimental particle size (A) and PDI (B) of PLGA nanoparticles before dialysis, after dialysis and after freeze-drying (n = 3). 1S-5S refer to optimized experiments leading to the minimum particle sizes; 1P-5P refer to optimized experiments leading to the minimum PDI values.

In general, the particle size of PLGA nanoparticles prepared with molecular micelles increased after freeze-drying. However, we were able to obtain a particle size below 100 nm for freeze-dried PLGA nanoparticles using poly-L-SULV as emulsifier. In addition, the PDI values remained within the same range during purification for all molecular micelles, indicating a monodisperse nanoparticle suspension (PDI < 0.100). The nanoparticles prepared with PVA

were also readily re-suspended in water, their particle size and PDI values decreasing after dialysis and freeze-drying.

2.3.2.2 Zeta Potential

The value of the zeta potential for nanoparticles is an indication of suspension stability. An unstable suspension, where aggregates can easily form and precipitate, would have a value of zeta potential close to zero. High positive and low negative zeta potential values indicate a stable suspension because of electrostatic repulsions between charged nanoparticles. The values of zeta potential of synthesized PLGA nanoparticles before dialysis, after dialysis, and after freeze-drying are presented in Table 2.5.

Table 2.5 Experimental zeta potential of PLGA nanoparticles before dialysis, after dialysis and after freeze-drying (n=3)

Formulation	**Emulsifier**	**Zeta potential (mV)**		
		Before dialysis	After dialysis	After freeze-drying
1	SDS	-66.3 ± 3.8	-35.8 ± 6.3	not measured
2	PVA	-2.8 ± 1.0	-27.5 ± 0.7	-29.5 ± 1.0
3	Poly-SUS	-73.1 ± 9.3	-69.5 ± 8.3	-63.2 ± 0.4
4	Poly-SUG	-69.3 ± 7.5	-67.3 ± 7.4	-61.3 ± 5.5
5	Poly-L-SULV	-65.5 ± 1.7	-63.1 ± 5.1	-54.8 ± 1.6

For SDS, the zeta potential increased drastically after dialysis, as SDS was removed from solution, decreasing the negative surface charge of the nanoparticles. Thus, the formation of aggregates took place and consequently it was not possible to re-suspend the nanoparticles in aqueous solution, as previously noted. In contrast, when nanoparticles were synthesized using molecular micelles, the zeta potential remained within the same range after dialysis, slightly

increasing after freeze-drying to - 54 ± 1.6 mV for poly-L-SULV, - 61.3 ± 5.5 mV for poly-SUG and - 63.2 ± 0.4 mV for poly-SUS. This may be attributed to strong hydrophobic interactions between the polymer and the micelle core, the micelle remaining on the surface and intertwined into the nanoparticle. Therefore, the overall micellar surface charge produced a stable suspension, minimizing aggregation in solution after dialysis and freeze-drying. Quantitative methods for the determination of residual molecular micelle concentration in nanoparticle suspension are under development in our laboratory. Further investigation is required to determine the effect of the residual molecular micelle layer on the entrapment efficiency and release rate of active pharmaceutical compounds. When PVA was used as the emulsifier, the zeta potential decreased to a lower negative value after dialysis, since an excess of PVA was likely removed from nanoparticle surface and more negatively charged carboxylic groups of PLGA were uncovered. The zeta potential remained practically the same after freeze-drying, indicating a stable nanoparticle suspension that readily re-suspended in water.

2.3.3 Nanoparticle Morphology

The morphology of purified PLGA nanoparticles was investigated by transmission electron microscopy (TEM). The micrographs of typical nanoparticle suspension obtained with molecular micelles are shown in Figure 2.6. It can be noted that the particle size observed by use of TEM was slightly smaller than the particle size measured by dynamic light scattering. Such disagreement is likely determined by the differences in the sample preparation procedures. The investigated nanoparticles are suspended in aqueous solution for dynamic light scattering measurements, while for TEM imaging the nanoparticles are drop - casted on a grid and let dry before taking their image. However, spherical shape and smooth surface of the PLGA nanoparticles emulsified with molecular micelles were observed. In addition, no aggregates and precipitates were formed during the imaging process.

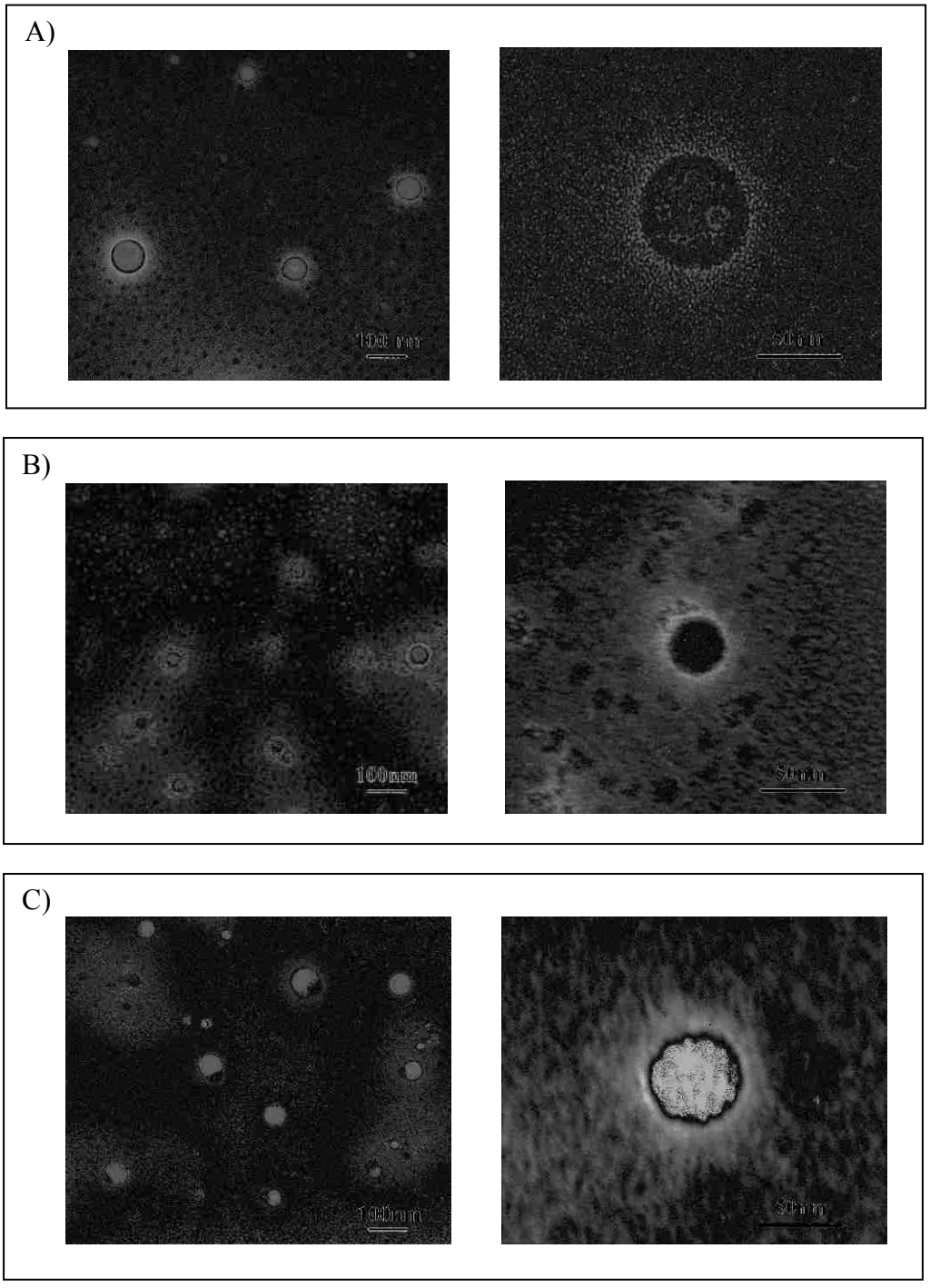

Figure 2.6 Typical micrographs of freeze-dried PLGA nanoparticles obtained with molecular micelles A) poly-SUS; B) poly-SUG; C) poly-L-SULV at 33,000x magnification (right) and 160,000x magnification (left).

2.4 Conclusions

In this study, molecular micelles were successfully used as novel emulsifiers to prepare PLGA nanoparticles. In addition, we were able to control the size and polydispersity of the PLGA nanoparticle suspension by use of a chemometric central composite design (CCD) and by accurate selection of optimal formulation conditions according to the CCD. The predictive ability of the model for particle size and PDI was better for nanoparticles obtained with molecular micelles in comparison with those obtained with conventional emulsifiers. Furthermore, after removal of excess emulsifier, the dried PLGA nanoparticles coated with molecular micelles were readily re-suspended in aqueous solution after purification and freeze-drying without significant modification of their size, shape and surface charge, revealing promising properties as drug delivery systems.

2.5 References

1 Kayser, O.; Lemke, A.; Hernandez-Trejo, N. *Current Pharmaceutical Biotechnology* **2005**, *6*, 3-5.

2 Vogelson, C. T. *Modern Drug Discovery* **2001**, *4*, 49-52.

3 Brannon-Pepas, L. *Medical Plastics and Biomaterials* **1997**, *4*, 34-44.

4 Allemann, E.; Gurny, R.; Doelker, E. *European Journal of Pharmaceutics and Biopharmaceutics* **1993**, *39*, 173-191.

5 Kumar, M. N. V. R. *Journal of Pharmacy & Pharmaceutical Sciences* **2000**, *3*, 234-258.

6 Shikanov, A.; Kumar, N.; Domb, A. J. *Israel Journal of Chemistry* **2005**, *45*, 393-399.

7 Brannon-Pepas, L.; Blanchette, J. O. *Advanced Drug Delivery Reviews* **2004**, *56*, 1649-1659.

8 Brigger, I.; Dubernet, C.; Couvreur, P. *Advanced Drug Delivery Reviews* **2002**, *54*, 631-651.

9 Panyam, J.; Labhasetwar, V. *Advanced Drug Delivery Reviews* **2003**, *55*, 329-347.

10 Delie, F.; Blanco-Prieto, M. J. *Molecules* **2005**, *10*, 65-80.

11 Anderson, J. M.; Shive, M. S. *Advanced Drug Delivery Reviews* **1997**, *28*, 5-24.

12 Bala, I.; Haribaran, S.; Ravi Kumar, M. N. V. *Critical Review in Therapeutic Drug Carrier Systems* **2004**, *21*, 387-422.

13 Hans, M. L.; Lowman, A. M. *Current Opinion in Solid State and Materials Science* **2002**, *6*, 319-327.

14 Quintanar-Guerrero, D.; Alleman, E.; Fessi, H.; Doelker, E. *Drug Develoment and Industrial Pharmacy* **1998**, *24*, 1113-1128.

15 Astete, C. E.; Sabliov, C. M. *Journal of Biomaterials Science, Polymer Edition* **2006**, *17*, 247-289.

16 Song, C. X.; Labhasetwar, V.; Murphy, H.; Qu, X.; Humphrey, W. R.; Shebuski, R. J.; Levy, R. J. *Journal of Controlled Release* **1997**, *43*, 197-212.

17 Birnbaum, D. T.; Kosmala, J. D.; Brannon-Pepas, L. *Journal of Nanoparticle Research* **2000**, *2*, 173-181.

18 Mu, L.; Feng, S.-S. *Pharmaceutical Research* **2003**, *20*, 1864-1872.

19 Kumar, M. N. V. R.; Bakowsky, U.; Lehr, C. M. *Biomaterials* **2004**, *25*, 1771-1777.

20 Panyam, J.; Williams, D.; Dash, A.; Leslie-Pelecky, D.; Labhasetwar, V. *Journal of Pharmaceutical Sciences* **2004**, *93*, 1804-1814.

21 Win, K. Y.; Feng, S.-S. *Biomaterials* **2006**, *27*, 2285-2291.

22 Bilati, U.; Alleman, E.; Doelker, E. *Journal of Microencapsulation* **2005**, *22*, 205-214.

23 Jiao, Y. Y.; Ubrich, N.; Marchand-Arvier, M.; Vigneron, C.; Hoffman, M.; Maincent, P. *Drug Delivery* **2001**, *8*, 135-141.

24 Panyam, J.; Zhou, W.-Z.; Prabha, S.; Sahoo, S. K.; Labhasetwar, V. *FASEB Journal* **2002**, *16*, 1217-1226.

25 Prabha, S.; Zhou, W.-Z.; Panyam, J.; Labhasetwar, V. *International Journal of Pharmaceutics* **2002**, *244*, 105-115.

26 Dillen, K.; Vandervoort, J.; Van den Mooter, G.; Verheyden, L.; Ludwig, A. *International Journal of Pharmaceutics* **2004**, *275*, 171-187.

27 Duan, Y.; Sen, X.; Wang, Q.; Liu, J.; Zhang, Z. *Journal of Materials Science: Materials in Medicine* **2006**, *17*, 559-563.

28 Julienne, M. C.; Alonso, M. J.; Gomez Amoza, J. L.; Benoit, J. P. *Drug Develoment and Industrial Pharmacy* **1992**, *18*, 1063-1077.

29 Prakobvaitayakit, M.; Nimmannit, U. *AAPS PharmSciTech* **2003**, *4*, 1-9.

30 Vandervoort, J.; Ludwig, A. *International Journal of Pharmaceutics* **2002**, *238*, 77-92.

31 Sahoo, S. K.; Panyam, J.; Prabha, S.; Labhasetwar, V. *Journal of Controlled Release* **2002**, *82*, 105-114.

32 Shamsi, S. A.; Palmer C.P.; Warner, I. M. *Analytical Chemistry* **2001**, *73*, 140A-149A.

33 Haddadian, F.; Shamsi, S. A.; Warner, I. M. *Electrophoresis* **1999**, *20*, 3011-3026.

34 Kapnissi-Christodoulou, C. P.; Zhu, X.; Warner, I. M. *Electrophoresis* **2003**, *24*, 3917-3934.

35 Ganea, G. M.; Sabliov, C. M.; Ishola, A. O.; Fakayode, S. O.; Warner, I. M. *Journal of Nanoscience and Nanotechnology* **2008**, *8*, 280-292.

36 Bergstrom, S. Z. *Physiol. Chem.* **1936**, *236*, 163-168.

37 Shamsi, S. A.; Akbay, C.; Warner, I. M. *Analytical Chemistry* **1998**, *70*, 3078-3083.

38 Macossay, J.; Shamsi, S. A.; Warner, I. M. *Tetrahedron Letters* **1999**, *40*, 577-580.

CHAPTER 3

THE EFFECT OF MOLECULAR MICELLES ON SYNTHESIS AND PROPERTIES OF THYMOQUINONE-LOADED POLY(D,L LACTIDE-*CO*-GLYCOLIDE) NANOPARTICLES

3.1 Introduction

Excessive production of free radical species through oxidative processes can lead to alteration of cellular functions responsible for cardiovascular diseases, neurodegenerative diseases, diabetes, cancer, joint diseases, and aging.[1-6] The damaging effect of free radicals is typically counterbalanced by antioxidants acting as free radical suppressors and scavengers.[7, 8] Several examples enzymes such as superoxide dismutase (SOD) and glutathione peroxidase (GSP) as well as tocopherols, flavonoids, polyphenols and quinones.[9] In general, antioxidants play a significant role in disease prevention and treatment. The mechanism against disease depends on antioxidants type and structure. For example, SOD and catalase inhibit the formation of superoxide anion radicals and hydrogen peroxide, while GSP and vitamin E participate in the decomposition of lipid peroxides. In addition, antioxidants can reduce the incidence of cancer, improve immune system, and prevent the development of age-related cataract and macular degeneration. [10-14]

Despite their benefits, many antioxidants present poor water solubility, leading to low absorptivity and bioavailability. In addition, the intended therapeutic role of ingested antioxidants may be different than their *in vivo* activity once the food matrix is disrupted.[15, 16] Therefore, novel antioxidant-loaded drug delivery systems such as polymeric nanoparticles have been identified as alternatives that should provide long-term delivery at the therapeutic level, prevent antioxidant degradation, and increase pharmaceutical activity of such antioxidants.[17, 18]

In recent years, controlled delivery of antioxidants has allowed a new approach for cancer therapy, cardiovascular diseases, neurodegenerative diseases, and ageing.[17-20] Several studies

have reported nanoparticle-based drug delivery systems for controlled delivery of antioxidants. For example, quercetin-loaded nanoparticles have showed excellent free radical scavenging activity and bioavailability.[21, 22] In addition, biodegradable nanoparticles were prepared for poorly soluble ellagic acid demonstrating the importance of synthetic parameters in the physico-chemical and pharmaceutical properties of such drug delivery systems.[23, 24] In other studies, "nanocurcumin" was prepared using polymeric nanoparticles for controlled delivery of natural curcumin with improved anticancer properties.[25, 26] In these studies, as a result of their improved solubility, antioxidant loaded – nanoparticles were demonstrated to have improved antioxidant activity as compared with free antioxidants.

Quinones refer to a group of antioxidants that contain typically a p-benzoquinone structure. Coenzyme Q10, is an lipophilic endogenous p-benzoquinone antioxidant that participates in the mitochondrial respiratory chain.[27, 28] Deficiencies in Q10 and damages of mitochondrial DNA are the main cause of genetic mitochondrial diseases. [29, 30] Currently, the administration of Q10 supplements is the first line therapy for the treatment of mitochondrial encephalomyopathies. Several studies have focused on delivery of coenzyme Q10 using nanoparticles. Such nanoparticles enhanced drug stability and cellular uptake, providing promising routes for administration as compared to regular dietary supplements.[31-33]

In the recent years, benzoquinone-based anticancer drugs have been developed as inhibitors of NADH quinone oxidoreductase (NQO1) involved in quinone metabolism. This strategy is favored by the high concentration of this enzyme in some types of cancer as well as the hypoxic conditions of the solid tumors.[28, 34] Mitomycin C is a classical NQO1 inhibitor and has been used as chemotherapeutic agent for a variety of cancers including head, neck, breast and prostate. However, its lack of specificity accompanied by strong and uncontrollable side effects limit the benefits of this drug. Therefore there is continuous effort for the development of

benzoquinone drugs with improved water solubility and reduced adverse reactions. For example, EOquin is currently used for treatment of superficial bladder cancer, benzoquinone ansamycins such as 17-allylamino-17-demethoxygeldanamycin (17-AAG) and 17-dimethylaminoethylamino -17-demethoxy-geldanamycin (17-DAAG) alone and in combination with other anticancer drugs for the treatment of advanced solid tumors, metastatic renal carcinoma and chemotherapy refractory breast cancer.[35] In addition, natural alkylated and cyclic benzoquinones found in plant extracts presented cytotoxic effects against various cancer cell lines.[36-38]

Thymoquinone (TQ) is the major constituent of *Nigella sativa* black seed oil, a medicinal plant from the *Ranunculaceae* family, which has been used for centuries in Africa, Europe, and Asia for treatment of many diseases including inflammation, asthma, hypertension, gastrointestinal conditions, and skin irritations.[39] Thymoquinone display antioxidant properties by acting as free radical scavengers.[40, 41] In addition, TQ exhibits a protective antioxidant effect against the severe side effects caused by doxorubicin, an anticancer drug, that induces cardiac and renal toxicities during and after chemotherapy.[42, 43] Furthermore, TQ is an emerging anticancer drug, showing cytotoxic activity for human cancer cell lines including colorectal, ovarian, and breast cells.[44-46]

Although thymoquinone is a powerful antioxidant and anticancer drug, its administration is limited due to poor water solubility.[44, 47] In addition, administration of high dosages to rats have resulted in hypoactivity and difficulty in respiration associated with reduced glutathione in the liver and kidney.[48] Another report has shown that TQ is capable of reducing blood glucose levels and allergic dermatitis incidences.[49] To overcome these disadvantages, biodegradable and biocompatible polymeric nanoparticles would be attractive alternatives for TQ delivery. Such nanoparticles would likely provide improved TQ solubility, controlled delivery, and enhanced therapeutic properties.

In the present study, we focused on physico-chemical properties, antioxidant activity, and cytotoxicity of TQ-loaded nanoparticles. Poly(D,L lactide-*co*-glycolide) nanoparticles containing thymoquinone were synthesized by emulsification solvent evaporation method, using molecular micelle poly (sodium *N*-undecenyl-glycinate) (poly-SUG) as emulsifier. The synthetic parameters were investigated using a Box-Behnken experimental design in order to obtain the maximum entrapment efficiency. The individual and combined effects of factors such as PLGA amount, TQ amount and emulsifier concentration (design variables) were established on TQ entrapment efficiency (response).

The surface properties of polymeric nanoparticles are influenced by the emulsifier, which likely plays an important role in their applications as drug delivery systems.[50] Molecular micelles such as poly-SUG represent a novel class of emulsifiers used in nanoparticle synthesis. They have a polymerized hydrophobic core and a critical micelle concentration equal to zero that allow an increased stability and rigidity in comparison with conventional micelles. When used as emulsifiers, molecular micelles strongly interact with PLGA polymer at the organic – aqueous interface. Such interactions are of a hydrophobic nature and provide a reduction in the organic droplet size, resulting in small and monodisperse nanoparticles. Due to their charge, molecular micelles provide sufficient interparticle repulsions in aqueous solutions, leading to increased stability over time.[51] In order to further understand the role of molecular micelles in polymeric nanoparticle synthesis, we investigated the properties of TQ-loaded PLGA nanoparticles prepared using various molecular micelles as emulsifiers. Anionic glycine-based molecular micelles with shorter carbon chains, poly(sodium *N*-heptenyl-glycinate) (poly-SHG), and poly(sodium *N*-decenyl-glycinate) (poly-SDG) were synthesized and used as emulsifiers. In addition, molecular micelles having various amino acid hydrophilic head groups, poly(sodium *N*-undecenyl-alaninate) (poly-SUA), poly(sodium *N*-undecenyl-leucinate) (poly-SUL), and

poly(sodium *N*-undecenyl-valinate) (poly-SUV), were also used as emulsifiers. The effect of the molecular micelles was evaluated by monitoring parameters such as release profile, antioxidant activity, and, cytotoxicity of TQ-loaded PLGA nanoparticles. Controlled release of entrapped TQ was performed by use of the dialysis method under physiological conditions (pH 7.4, 37 ºC) using phosphate buffer as the release medium. A free-radical scavenging assay was used to evaluate the antioxidant activity of TQ and TQ-loaded nanoparticles prepared with various emulsifiers. The cytotoxicity of TQ and TQ-loaded PLGA nanoparticles were assessed using a breast normal cell line (Hs578Bct) and two breast cancer cell lines (hormone-dependent MCF-7 and hormone-independent MDA-MB-231).

3.2 Materials and Methods

3.2.1 Materials

Poly(D,L-lactide-*co*-glycolide) (PLGA, lactide:glycolide 75:25, MW 66-107 kDa), thymoquinone, 2,2-diphenyl-1-picrylhydrazyl (DPPH), and sucrose were purchased from Sigma-Aldrich (St. Louis, MO, USA). Trolox was purchased from Acros Organics (Morris Plains, NJ, USA). Dibasic sodium phosphate was purchased from Mallinckrodt (Hazelwood, MO, USA). Dichloromethane and sodium phosphate monobasic were purchased from EMD Chemicals Inc. (Gibbstown, NJ, USA). All reagents were of analytical grade and used as received.

The monomer forms of sodium *N*-heptenyl-glycinate (SHG), sodium *N*-decenyl-glycinate (SDG), sodium *N*-undecenyl-glycinate [52], sodium *N*-undecenyl-alaninate (SUA), sodium *N*-undecenyl-leucinate (SUL), and sodium *N*-undecenyl-valinate (SUV) were synthesized and characterized according to our previously described procedures [53-57] The corresponding polymers were obtained via polymerization using a ^{60}Co γ-irradiation source. The complete polymerization was confirmed by disappearance of the vinyl protons (δ ~ 6ppm) in the ^{1}H NMR of the resulting polymers. The chemical structures of the molecular micelles used as emulsifiers in the present

study are represented in Figure 3.1. Molecular micelles having glycine as a hydrophilic group and carbon chains ranging from seven (n=3) to eleven (n=7) methylene groups are presented by poly-SHG, poly-SDG and poly-SUG.). In addition, molecular micelles having the same hydrophobic tail and various amino acid hydrophilic head groups are represented by poly-SUA, poly-SUL, and poly-SUV.

3.2.2 Cell Cultures

Normal Hs578Bct human breast fibroblast cells (HTB-125), hormone-dependent MCF-7 (HTB-22), and hormone-independent MDA-MB-231 (MDA, HTB-26) human mammary tumor cells were obtained from the American Tissue Culture Collection (ATCC, Manassas, VA) and grown to 90% confluence according to ATCC's instructions.

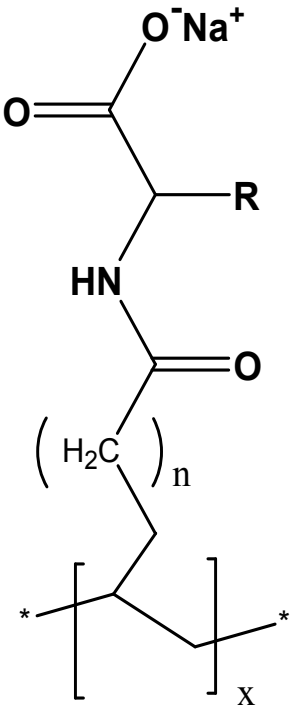

Emulsifier	n	R
Poly-SHG	3	H
Poly-SDG	6	H
Poly-SUG	7	H
Poly-SUA	7	CH_3
Poly-SUL	7	$CH_2CH(CH_3)_2$
Poly-SUV	7	$CH(CH_3)_2$

Figure 3.1 Structures of molecular micelles used as emulsifiers in the nanoparticle synthesis (n is the length of carbon chain; x indicates the polymerization site).

3.2.3 Synthesis of PLGA Nanoparticles

TQ-loaded PLGA nanoparticles were synthesized by use of an emulsification solvent evaporation method (single emulsion). The schematic representation of nanoparticle synthesis is shown in Figure 3.2. Various amounts of PLGA and TQ were dissolved in dichloromethane (DCM) forming an organic phase. The organic phase (1.5 mL) was dispersed into an aqueous phase (8 mL) containing molecular micelles using a homogenizer (model 398, Biospec Products, Inc., Racine, WI, USA) at 20,000 rpm for 2 minutes.

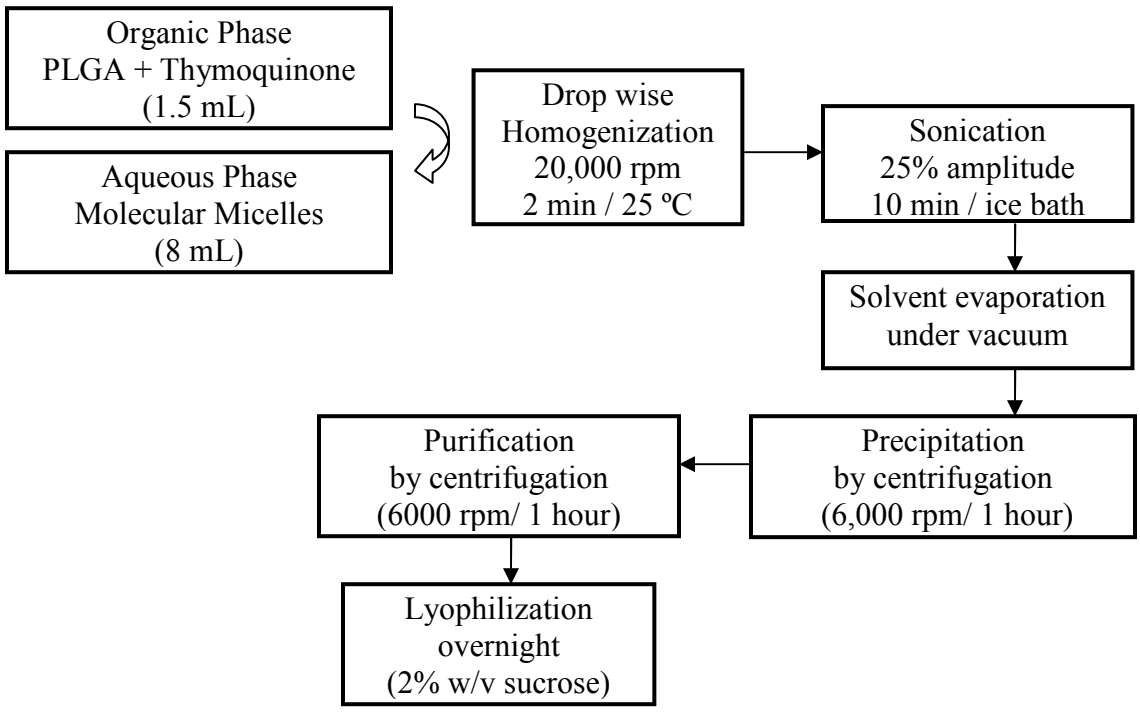

Figure 3.2 Synthesis of TQ-loaded PLGA nanoparticles by emulsification solvent evaporation using molecular micelles as emulsifiers.

The emulsion was further sonicated for 10 minutes in an ice bath using an ultrasound processor (25% amplitude, model VC750, Sonics and Materials Inc., Newton, CT, USA). The solvent was evaporated by rotary evaporation under vacuum (Büchi rotovapor R-200, Brinkmann Instruments, Inc., Westbury, NY, USA). The nanoparticles were precipitated by centrifugation

(6,000 rpm, 1 hour) , and washed using an equal volume of water, in order to eliminate the excess of emulsifier and unentrapped drug. Further, the nanoparticles were lyophilized overnight (Freezone Plus 6, Labconco, Kansas City, MO, USA) and stored in a cool and dry environment until further used. In order to improve the re-suspension of TQ-loaded nanoparticles in aqueous media, cryoprotectant (2% w/v sucrose) was added before freeze-drying. Empty nanoparticles without TQ were synthesized according to the same procedure, involving an organic phase contained only the polymer. All other conditions were held constant.

3.2.4 Nanoparticle Characterization

The nanoparticle size and polydispersity (PDI) were measured using dynamic light scattering (Zetasizer NanoZS, Malvern Instrumets Ltd., Malvern, UK). Zeta potential was measured by laser doppler anemometry (Zetasizer NanoZS, Malvern Instrumets Ltd., Malvern, UK). Nanoparticle morphology was investigated by use of transmission electron microscopy (TEM, JEOL 100CX, Jeol Ltd., Peabody, MA, USA) using uranyl acetate negative staining.

3.2.5 Thymoquinone Quantification

The entrapment efficiency was determined by use of high performance liquid chromatography (HPLC, Shimadzu Scientific Instruments, Columbia, MD, USA, mobile phase 80:20 acetonitrile:water, flow rate 0.5 mL/min, injection volume 20 μL). TQ-loaded PLGA nanoparticles were dissolved in the mobile phase and sonicated in a bath sonicator for sufficient time to ensure complete TQ solubilization. The samples were then filtered through a 0.2 μm syringe filter and injected into the HPLC column (Luna C18(2), Phenomenex Inc., Torrance, CA, USA). The entrapped TQ was quantified using the peak area for each nanoparticle formulation (linear range of the calibration curve was 0.1 – 0.8 mg/mL; LOD 0.0017 mg/mL). The entrapment efficiency (EE %) was calculated as 100 times the ratio of the entrapped TQ amount relative to the known amount of TQ added to each formulation.

3.2.6 Optimization of Entrapment Efficiency

The influence of three synthesis parameters (design variables), PLGA amount, TQ amount, and poly-SUG concentration, on TQ entrapment efficiency (response) was simultaneously investigated using chemometric Box-Behnken experimental design. The design variables were investigated at three levels involving a total number of fifteen experiments including three replicates at the central level. The resultant data analyses were performed using Unscrambler 9.1.2 software. The synthesis conditions were considered optimum for formulations where the maximized entrapment efficiency was obtained. In addition, the influence of other emulsifiers such as poly-SHG, poly-SDG, poly-SUA, poly-SUL and poly-SUV on the TQ entrapment efficiency was further investigated employing the optimum conditions.

3.2.7 *In vitro* Controlled Release

In vitro controlled release was performed using a dialysis method. Specifically, a known amount of solid nanoparticles (6 mg), containing a TQ amount established by the method described above, were re-suspended in phosphate buffer (2mL of 0.1M Na_2HPO_4-NaH_2PO_4, pH 7.4). This suspension was placed in a dialysis bag (Specta/Por, MWCO 1000Da, Spectrum Laboratories, Rancho-Dominguez, CA, USA) that was further placed in the phosphate buffer release medium (15 mL) and incubated at 37 ºC in a refrigerated orbital shaker (CO24, Edison, NJ, USA). Various time intervals were investigated. At each time point, the release medium was completely replaced with fresh release medium, and placed back in the shaker chamber for further TQ release. The sink conditions calculated based on TQ solubility, TQ amount contained in the nanoparticles, and the total volume of release medium, were maintained throughout the experimental time. The percentage (%) release for every time point was calculated as percentage of total entrapped drug. Following the same procedure, a control experiment was performed using TQ suspension in phosphate buffer.

3.2.8 Antioxidant Activity of TQ-loaded Nanoparticles

The antioxidant activity of TQ-loaded nanoparticles was determined by use of 2,2-diphenyl-1-picrylhydrazyl (DPPH) assay. [21, 40] Briefly, in a 96-well plate, 100 μL of 100 μM DPPH solution in methanol was incubated with 100 μL of aqueous suspensions of TQ-loaded nanoparticles prepared with different molecular micelles as well as solutions of TQ dissolved in methanol. Methanol and empty nanoparticles (synthesized without TQ) were also incubated with DPPH solution, and used as controls. After 30 minutes, the absorbance was read at 517 nm using a microplate spectrophotometer (Model 680, Bio-Rad Laboratories, Hercules, CA, USA). The scavenging activity for each sample was calculated as DPPH scavenging (%) = 100 x $[(A_{control}-A_{sample})/A_{control}]$, where A_{sample} is the absorbance of DPPH in the presence of TQ-containing samples, and $A_{control}$ is the absorbance of DPPH for control samples in the absence of TQ. The concentration of TQ in each nanoparticle sample and in free TQ solution for which 50% DPPH scavenging is achieved (IC50), was used to compare the scavenging activity. In addition, Trolox, a powerful water soluble antioxidant, was used as standard in the DPPH assay. Trolox Equivalents were calculated as the ratio between the IC50 for Trolox and the IC50 for each sample, and expressed as μmol Trolox/ g TQ. All experiments were performed in triplicate.

3.2.9 Cytotoxicity of TQ-loaded Nanoparticles

The cytotoxic effect of TQ and TQ-loaded nanoparticles on breast normal and cancer cell lines was determined by use of CellTiter 96® AQ_{ueous} One Solution Cell Proliferation Assay (Promega Corporation, Madison, Wisconsin, USA). Normal breast (Hs578Bct) and breast cancer (hormone-dependent MCF-7 and hormone independent MDA-MB-231) cell cultures ($1x10^4$ cells/well, 50 μL) were incubated at 37 ºC, in 5% CO_2, with TQ solutions containing less than 1% DMSO, and TQ-loaded nanoparticles (3 mg/mL) suspended in the culture media (50 μL) for 24, 48 and 72 hours. At the end of the incubation period, the cells were treated with 3-(4,5-di-

methylthiazol-2-yl)-5-(3-carboxymethoxyphenyl)-2-(4-sulfo-phenyl)-2H-tetrazolium salt (MTS) (20 μL), according to the manufacturer's instructions (CellTiter 96® AQ_{ueous} One Solution Cell Proliferation Assay, Promega, Madison, WI). After 1 hour, the absorbance was read at 490 nm using a microplate spectrophotometer (Benchmark Plus, Bio-Rad Laboratories, Hercules, CA, USA). Blank nanoparticles prepared by emulsification solvent evaporation, without adding TQ to the formulation, were used as controls. Percentage cell viability was calculated as 100 times the ratio of absorbance in the presence of TQ and TQ-loaded nanoparticles and absorbance for TQ-free control samples. All experiments were performed in triplicate.

3.3. Results and Discussion

3.3.1 Nanoparticle Characterization

TQ-loaded PLGA nanoparticles were synthesized by emulsification evaporation using molecular micelles as emulsifiers. In our previous studies, molecular micelles demonstrated excellent emulsifying properties offering uniform and nanometer size nanoparticles. In addition, nanoparticle high surface charge conferred by molecular micelles allowed enhanced stability in aqueous solution.[51] The physico-chemical properties of TQ-loaded nanoparticles prepared with molecular micelles as emulsifiers are presented in Table 3.1. TQ-loaded PLGA nanoparticle sizes ranged from 123.5 to 187.4 nm, depending on the micelle structure. The particle sizes for nanoparticles emulsified with poly-SHG and poly-SUV were significantly higher (p-value = 0.05) than the other nanoparticles. It should be mentioned that micelles with short carbon chain (C7) such as poly-SHG were likely more flexible and less hydrophobic than micelles containing longer carbon chains (C11) such as poly-SUG. Therefore, their interactions with PLGA were likely reduced leading to an increase in particle size. In addition, micelles having larger hydrophilic head groups such as poly-SUV likely preferred in the aqueous phase as compared to organic phase. Such interactions likely lead to an increase in particle size as well. For closely

related molecular micelles such as poly-SDG, poly-SUG, and poly-SUA, the particle size remained approximately the same. In contrast, polydispersity indicated by polydispersity index (PDI) remained constant and below 0.100, indicating monodisperse nanoparticle suspensions for all micelles. In addition, molecular micelles conferred high negative charge on the nanoparticle surface as indicated by the values of zeta potential. Statistical analysis revealed that both the PDI and zeta potential remained unchanged (p-value = 0.05) regardless of the investigated emulsifier.

Table 3.1 Physico-chemical properties of TQ-loaded PLGA nanoparticles (n=4)

Emulsifier	Size	PDI	Zeta potential (mV)
Poly-SHG	177.7 ± 9.7	0.054 ± 0.010	-60.8 ± 2.6
Poly-SDG	146.5 ± 19.5	0.083 ± 0.024	-59.1 ± 4.8
Poly-SUG	164.1 ± 15.5	0.083 ± 0.003	-60.0 ± 5.2
Poly-SUA	149.3 ± 9.5	0.071 ± 0.012	-60.7 ± 3.1
Poly-SUL	144.8 ± 21.3	0.061 ± 0.011	-62.4 ± 1.9
Poly-SUV	173.1 ± 8.8	0.091 ± 0.070	-60.9 ± 8.0

Note: Other conditions were PLGA (100 mg); TQ (15 mg), and emulsifier (0.5% w/v).

Furthermore, TQ-loaded PLGA nanoparticles presented uniform well-defined spherical shape as shown in Figure 3.3. Our results indicated that all molecular micelles used in this study provided excellent emulsifier properties, leading to small monodisperse particle size, highly negative surface charge, and uniform spherical shapes.

3.3.2 Optimization of TQ Entrapment Efficiency

The entrapment efficiency of TQ-loaded nanoparticles was investigated using a Box-Behnken optimization design. Compared with other designs, Box-Behnken design presents

several advantages such as pre-established limits of design variables, and a reduced number of experiments [58]. The experimental design involved fifteen experiments including three central level experiments for reproducibility purposes. The design allowed an investigation of the simultaneous effects of PLGA amount (mg), TQ amount (mg), and poly-SUG concentration (% w/v) (design variables) on the entrapment efficiency (response). The limits of design variable ranges were selected based on preliminary experiments that indicated that TQ is more compatible with high molecular weight polymers than low molecular weight polymers. In addition, we found that drug precipitation occurred at a drug loading higher than 25 mg. therefore, in our further experiments, high molecular weight PLGA polymer (MW 66-107 kDa) and a drug loading less than 25 mg were used.

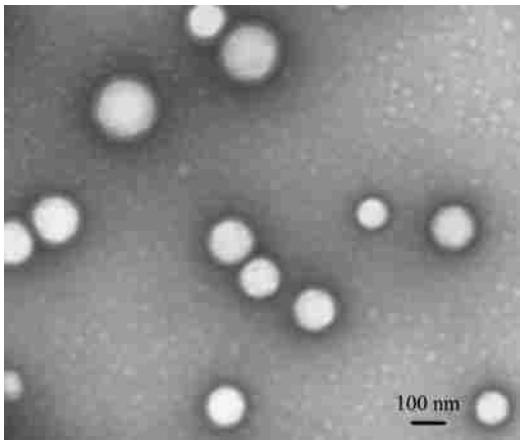

Figure 3.3 Transmission electron micrograph of TQ-loaded PLGA nanoparticles (magnification 33,000x) prepared with poly-SHG.

In addition, poly-SUG was selected as emulsifier for optimization due to its high availability, and easy synthesis. Detailed experimental conditions are presented in Table 3.2. For all experiments included in the Box-Behnken optimization design, the particle size of TQ-loaded PLGA nanoparticles containing various amounts of TQ varied between approximately 123 and 167 nm, likely due to various amounts of poly-SUG used in each formulation. Monodisperse

nanoparticle suspensions were obtained for all fifteen experiments used in the design, as shown by a polydispersity index (PDI) lower than 0.100.

Table 3.2 Experimental conditions used in Box-Behnken experimental design

Exp. No.	PLGA (mg)	TQ (mg)	Poly-SUG (%w/v)	EE %	Size	PDI
1	50	25	0.75	10.8	158.0	0.063
2	75	15	0.75	21.9	164.9	0.054
3	75	5	0.5	28.4	167.4	0.071
4	50	5	0.75	10.5	123.4	0.070
5	75	15	0.75	27.3	162.8	0.064
6	50	15	0.5	21.3	141.5	0.050
7	100	15	0.5	35.1	157.0	0.059
8	75	25	0.5	20.9	130.2	0.049
9	100	5	0.75	26.7	142.8	0.062
10	50	15	1	10.5	127.3	0.073
11	75	15	0.75	24.3	129.8	0.050
12	100	25	0.75	25.6	143.6	0.051
13	75	5	1	32.7	127.6	0.047
14	100	15	1	29.8	132.7	0.047
15	75	25	1	22.3	125.2	0.068

The investigated variables strongly influenced the entrapment efficiency as indicated by the response surface represented in Figure 3.4. When the entrapment efficiency was represented as a function of PLGA amount and TQ amount (Figure 3.4.A), the highest entrapment efficiency range was obtained for increased amounts of PLGA (above 80 mg) and TQ amounts lower than 20 mg, possibly due to increased viscosity of the organic phase that would retain greater amounts of TQ. The effect of emulsifier on the entrapment efficiency is shown in Figure 3.4.B.

A)

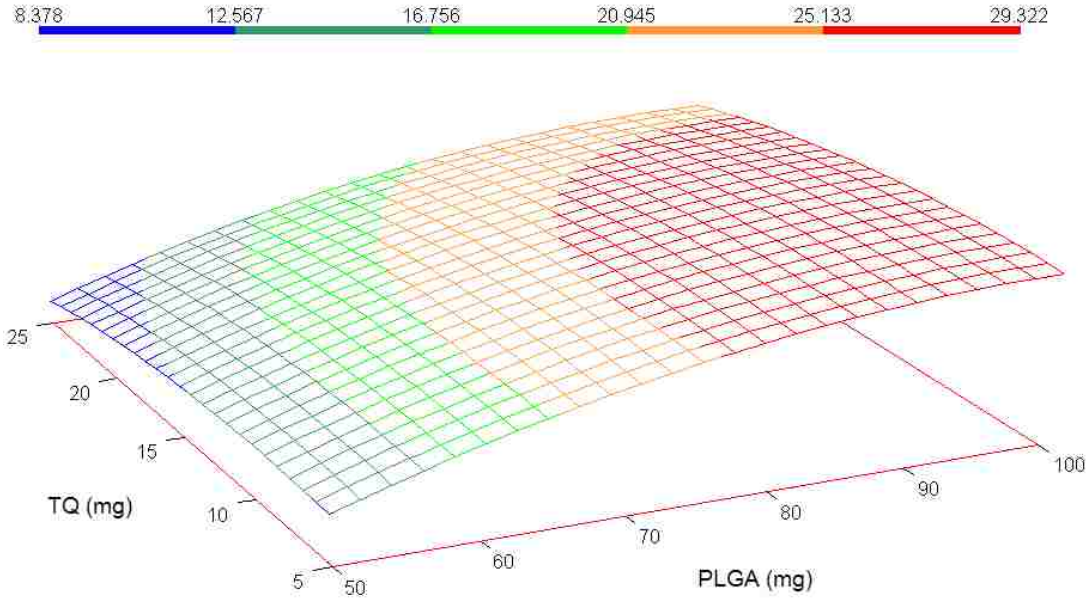

B)

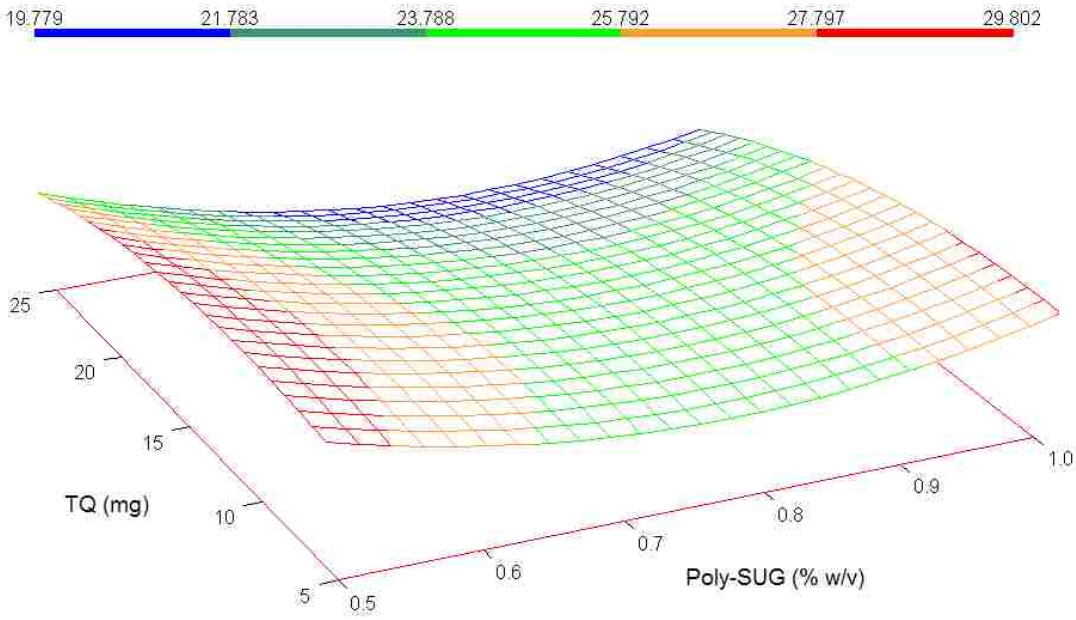

Figure 3.4 Response surface for entrapment efficiency represented as a function of A) TQ (mg) and PLGA (mg); and B) TQ (mg) and poly-SUG (% w/v). The highest entrapment efficiency is shown by the red zones.

The entrapment efficiency increased with the decrease of poly-SUG concentration. The highest entrapment efficiency was obtained for poly-SUG concentrations lower than 0.55 % w/v. Larger values of entrapment efficiency were obtained for a poly-SUG concentrations higher than 0.55 % w/v as well. It should be noted that molecular micelles have the ability to incorporate hydrophobic compounds [56, 59-61] In molecular micelle-assisted nanoparticle synthesis, a biphasic system containing a micellar aqueous solution and an organic polymeric phase was involved. Therefore, the partition of the drug between the two phases likely affected the drug entrapment into the polymeric matrix.

When molecular micelles are present at the aqueous-organic interface in order to stabilize the emulsion, they would likely incorporate a portion of the TQ. Such TQ portion was eliminated in the precipitation and purification steps by centrifugation. In addition, the TQ phase partition can be changed towards organic phase by decreasing the molecular micelle concentration. However, the decrease is limited by the minimum micelle concentration necessary for synthesis of stable, and uniform particle sizes. Therefore, we found that the maximum entrapment efficiency was obtained for 100 mg PLGA, 15 mg TQ and 0.5 % w/v poly-SUG, and these conditions were considered as optimum for further experiments.

Multivariate regression was used to correlate the investigated design variables with the entrapment efficiency. A quadratic model was constructed based on experimental data and is described by equation 3.1:

$$EE\% = b_0+b_1[PLGA]+b_2[TQ]+b_3[MM]+b_4[PLGA]^2+b_5[TQ]^2+b_6[MM]^2 \qquad 3.1$$

where *EE%* is the entrapment efficiency, described above; *[PLGA]* is the amount of PLGA (mg); *[TQ]* is the amount of TQ (mg); *[MM]* is the emulsifier concentration (% w/v); b_0 is the intercept; and b_1- b_6 are the correlation coefficients for each of the equation terms.

Analysis of variance (ANOVA) was further used to establish the significance of design variables and their interactions with the response. The results of analysis of variance of the regression model are presented in Table 3.3. The design variables were considered significant for a p-value lower than 0.05. ANOVA results indicated that the most significant variable influencing the entrapment efficiency is the PLGA amount (p-value 0.0004), followed by TQ amount and molecular micelle concentration.

Table 3.3 Analysis of variance for Box-Behnken model

Variables	**p-value**	***b*-coefficients**	
Intercept	0.2653	b_0	7.905
[PLGA]	0.0004	b_1	0.32
[TQ]	0.1278	b_2	-0.234
[MM]	0.3731	b_3	-5.203
$[PLGA]^2$	0.0823	b_4	-2.303
$[TQ]^2$	0.3335	b_5	-1.194
$[MM]^2$	0.1053	b_6	2.118

In addition, validation of the regression model was achieved by comparing the predicted response with the response values of the central samples of the design as well as independent optimum experiments separated from the experimental design. The predicted and the experimental entrapment efficiencies as well as the levels of the investigated variables are presented in Table 3.4. It can be noted that the predicted and measured values were identical for central samples presenting a percent relative error of 0.00 % and good predictive ability of the

model. In case of experiments performed at the optimum conditions, the percent relative error was 2.39 % suggesting high predictability of the model.

Table 3.4 Predictability of Box-Behnken model

Experiments	PLGA (mg)	TQ (mg)	Poly-SUG (%w/v)	Predicted EE%	Measured EE%	% RE
Central	75	15	0.75	24.49	24.49	0.00
Optimum	100	15	0.5	33.46	34.26	2.39

Note: Percent relative error (% RE) = 100*(Predicted EE – Measured EE)/Predicted EE; EE = entrapment efficiency

3.3.3 The Effect of Molecular Micelles on the Entrapment Efficiency

In order to evaluate the effect of the molecular micelles on entrapment efficiency of TQ-loaded PLGA nanoparticles, the short chain molecular micelles poly-SHG and poly-SDG as well as micelles having various amino acid head group such as poly-SUA, poly-SUL, and poly-SUV were used as emulsifiers. The nanoparticles were synthesized using optimum conditions as determined using Box-Behnken design: 100 mg PLGA, 15 mg TQ, and 0.5 % w/v emulsifier, respectively. The values of TQ entrapment efficiency for TQ-loaded PLGA nanoparticles prepared with various micelles are presented in Table 3.5. The values of entrapment efficiency were similar for all molecular micelles, regardless of their structure, indicating that the type of the micelle was not a significant factor in the Box Behnken optimization design.

3.3.4 Release Profile of Optimized TQ-loaded PLGA Nanoparticles

TQ-loaded PLGA nanoparticles were synthesized at the optimum conditions using various molecular micelles as emulsifiers. The TQ release from these nanoparticles was investigated for a period of 72 hours.

Table 3.5 Effect of emulsifier on entrapment efficiency of TQ-loaded PLGA nanoparticles (n=4)

Emulsifier	Poly-SHG	Poly-SDG	Poly-SUG	Poly-SUA	Poly-SUL	Poly-SUV
EE%	32.09 ± 2.85	34.63 ± 2.96	34.26 ± 1.08	33.69 ± 4.72	35.17 ± 4.90	37.20 ± 8.65

The release occurred based on the diffusion of TQ from the TQ-loaded nanoparticles placed in a dialysis bag to an external aqueous phase. The release profiles for the first 8 hours are shown in Figure 3.5. It was observed that the TQ release levels were strongly influenced by the emulsifier used in the nanoparticle synthesis. TQ-loaded nanoparticles had a release of 30-60% for the first hour depending on the emulsifier while a control sample containing equivalent TQ showed a release level of 80% within the same period of time. However, all nanoparticle formulations showed a rapid release in the first 8 hours with similar release rates followed by a plateau at different release levels. It is possible that TQ was not uniformly distributed in the nanoparticle matrix, a portion being situated near the surface of the nanoparticles rather than inside, and therefore leading to a rapid release in the first hours.

The nanoparticles prepared with poly-SHG and poly-SUG showed a similar release of approximately 75% of the drug for the same period of time (8 hours). Thus, a shorter carbon chain of the molecular micelles did not change the release profile. The lowest released amount was given by the nanoparticles prepared with poly-SUA. Varying the amino acid head group of the micelles from alanine to valine resulted in higher release level for poly-SUV-emulsified nanoparticles as compared to poly-SUA. In addition, it is possible that molecular micelles with longer carbon chains adhered stronger to the nanoparticle surface as compared with shorter carbon chains. Furthermore, the interface micelle layer could be of a different density in case of poly-SUA as compared with poly-SUG likely determining a slower release.

After eight hours, there was no significant release observed, and the amount of released drug remained approximately constant until 72 hours (the total investigated time).

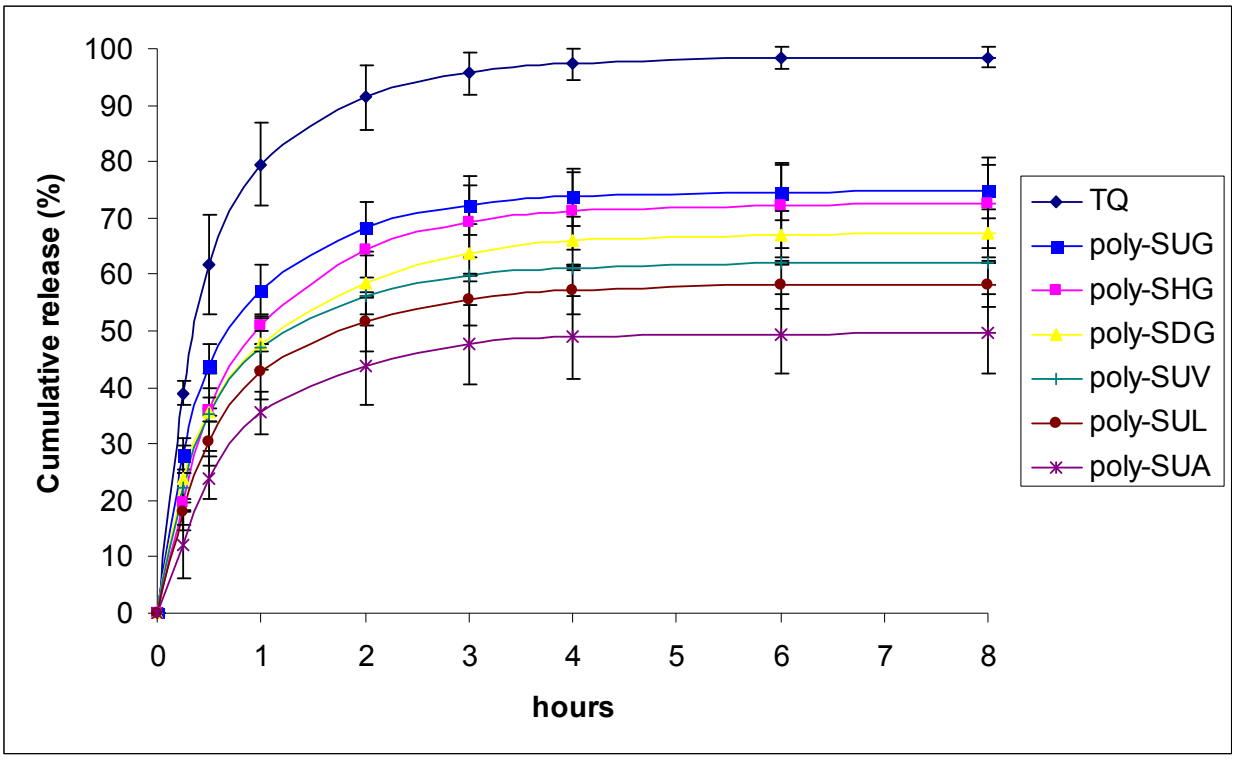

Figure 3.5 Release profile of TQ-loaded nanoparticles prepared with various molecular micelles.

3.3.5 Antioxidant Activity of Optimized TQ-loaded PLGA Nanoparticles

The antioxidant activities of TQ and TQ-loaded PLGA nanoparticles synthesized at the optimum conditions were evaluated by use of the DPPH scavenging assay. The concentration of TQ (mg/mL) for which 50% inhibition was reached was expressed as IC50 (mg TQ/mL). In general, a high scavenging activity is indicated by a small IC50. The DPPH scavenging activities of TQ and TQ-loaded PLGA nanoparticles are presented in Table 3.6. The IC50 for the free drug was 0.132 ± 0.003 mg/mL while the TQ-loaded PLGA nanoparticles presented a smaller IC50. For example, the IC50 for TQ-loaded nanoparticles emulsified with poly-SUA was 0.023 ± 0.001 mg/mL, representing an improved antioxidant activity. A lower antioxidant activity of

nanoparticles was obtained for poly-SHG (IC50 = 0.107 ± 0.020 mg/mL), but comparable with the one of free TQ.

In addition, Trolox Equivalents were calculated based on the ratio between IC 50 of Trolox and the IC50 of each sample. A high Trolox Equivalents number indicates a high antioxidant activity as compared to a powerful antioxidant such as Trolox. Similarly, Trolox Equivalents were the highest for poly-SUA (753.73 ± 18.39 μmol Trolox/g TQ), closely followed by poly-SUV–emulsified nanoparticles (597.48 ± 42.96 μmol Trolox/g TQ).

Table 3.6 DPPH scavenging activity of TQ and TQ-loaded PLGA nanoparticles (n=3)

Sample	IC50 (mg/mLTQ)	Trolox Equivalents (μmol Trolox/g TQ)
TQ	0.132 ± 0.003	132.25 ± 4.22
Poly-SHG	0.107 ± 0.020	168.56 ± 29.91
Poly-SDG	0.044 ± 0.004	404.36 ± 32.99
Poly-SUG	0.052 ± 0.002	341.65 ± 14.07
Poly-SUA	0.023 ± 0.001	753.73 ± 18.39
Poly-SUL	0.036 ± 0.005	494.74 ± 69.38
Poly-SUV	0.030 ± 0.002	597.48 ± 42.96

In addition, we observed that the DPPH scavenging activity inversely correlated with the release profile of TQ-loaded nanoparticles, as the slowest release of poly-SUA–emulsified nanoparticles had shown the highest antioxidant activity. It should be mentioned that DPPH radical is not soluble in water, and likely can diffuse into a more hydrophobic environment offered by nanoparticles. Therefore, assuming that the reaction with DPPH radicals can take place inside the PLGA nanoparticles, it is possible that the TQ present in the PLGA nanoparticle

environment had better solubility in case of poly-SUA as compared to other micelles. However, all TQ-loaded nanoparticles showed improved DPPH scavenging activity as compared with free TQ indicating that such nanoparticle systems could be excellent candidates as free radical scavengers.

3.3.6 Cytotoxicity of TQ and Optimized TQ-loaded PLGA Nanoparticles

In general, cell viability refers to the number of cells that remain viable after the treatment with a drug or drug delivery system. Cytotoxicity is the property of a drug that induces cell death, preferably in cancer cells for anticancer drugs. Cytotoxic properties of drugs and drug delivery systems are typically measured by cell viability assays. In this study, MTS assay was used to evaluate the cell viabilities of TQ and optimized TQ-loaded PLGA nanoparticles for normal breast cells (Hs578Bct), and cancer breast cells (MCF-7 and MDA-MB-231) at 24, 48 and 72 hours. In cytotoxicity studies of polymeric nanoparticles, several important aspects should be taken into consideration. First, the components of nanoparticles, including the polymer, the drug, and the emulsifier should not present any toxicity against both normal and cancer cells. Second, the desired effect for cancer cells is typically to obtain low cell viability within a short period of time, using drug concentrations that should not significantly affect the viability of normal cells.

Cell viability results for normal breast (Hs578Bct), and cancer breast cells (MCF-7 and MDA-MB-231) in the presence of TQ are presented in Figure 3.6. It can be noticed that a low concentration of free TQ (50 μM) did not affect cell viability of both normal and cancer cells irrespective of incubation time (24, 48 and 72 hours). However, at an increased concentration of TQ (200 μM), the cell viability critically decreased to 12.03 ± 0.67 % for normal cells in the first 24 hours, and remained fairly constant afterwards (48 and 72 hours). This like suggests that such high TQ concentration was toxic to the cells.

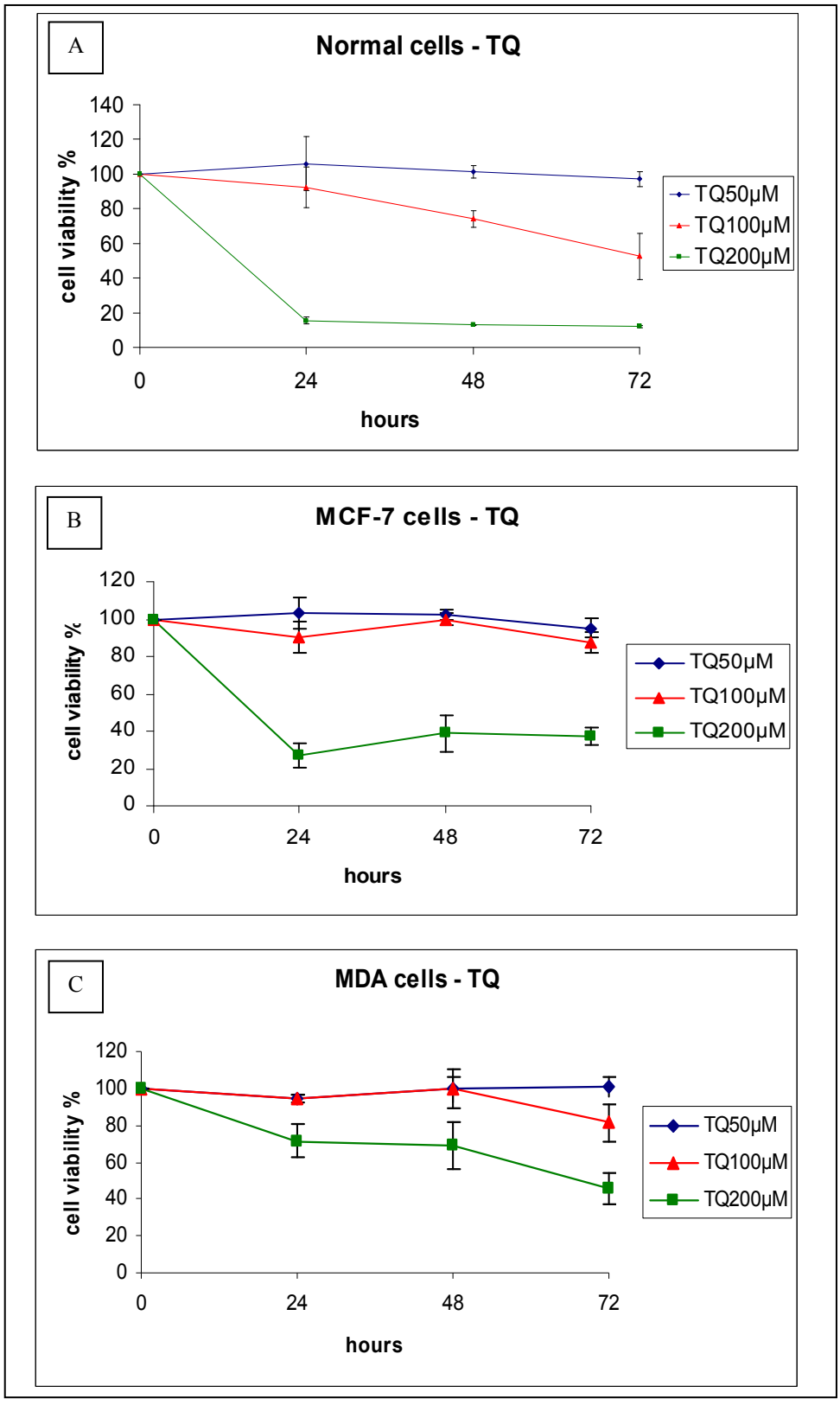

Figure 3.6 Cell viability of A) Hs578Bct normal breast cells; B) MCF-7 breast cancer cells; and C) MDA-MB-231 breast cancer cells incubated with TQ.

In the case of cancer cells, low concentrations of TQ (50 and 100 μM) did not have a significant reduction in the cell viability for both MCF-7 and MDA-MB-231 cancer cells within the investigated period of time (72 hours). However, when the TQ concentration increased to 200μM, the MCF-7 cell viability decreased to 27.29 ± 6.52 % after 24 hours, and slightly increased to 37.42 ± 4.83 % after 72 hours. With regard to MDA-MB-231 cancer cells, the viability decreased progressively in time to 45.5 ± 8.58 % after 72 hours for 200 μM TQ indicating that such cells are more resistant to TQ treatment than MCF-7 cells. Although a high dosage of TQ (200 μM) was useful for breast cancer inhibition, it was toxic to normal cells. Such effects were not desirable because at this concentration the toxicity of TQ was higher for normal cells than for cancer cells.

Optimized TQ-loaded PLGA nanoparticles as well as blank nanoparticles prepared without TQ and (containing an average of 279.1 ± 47.7 μM TQ) were also incubated with normal breast cells (Hs578Bct) and cancer breast cells (MCF-7 and MDA-MB-231). The cell viabilities of normal cells in the presence of blank and TQ-loaded nanoparticles are presented in Figure 3.7. The lowest cell viabilities were obtained for poly-SUL - emulsified blank nanoparticles (71.52 ± 2.11 %), followed closely by poly-SUA - emulsified blank nanoparticles (72.14 ± 4.61 %) at 72 hours. It can be noted that cell viability remained above 90 % for all blank nanoparticles emulsified with the other molecular micelles used in this study, irrespective of emulsifier. This indicates that the polymer and the emulsifier had no cytotoxic effect on normal cells. In the case of TQ – loaded nanoparticles incubated with normal cells, the cell viability decreased progressively in time from ~ 80 – 100 % after 24 hours to ~ 40 – 80% after 48 hours. After 72 hours, the lowest cell viability was obtained for poly-SDG–emulsified nanoparticles (30.95 ± 7.48 %) and poly-SUL–emulsified nanoparticles (37.05 ± 13.29 %). This effect was not observed for empty nanoparticles emulsified with the same molecular micelles.

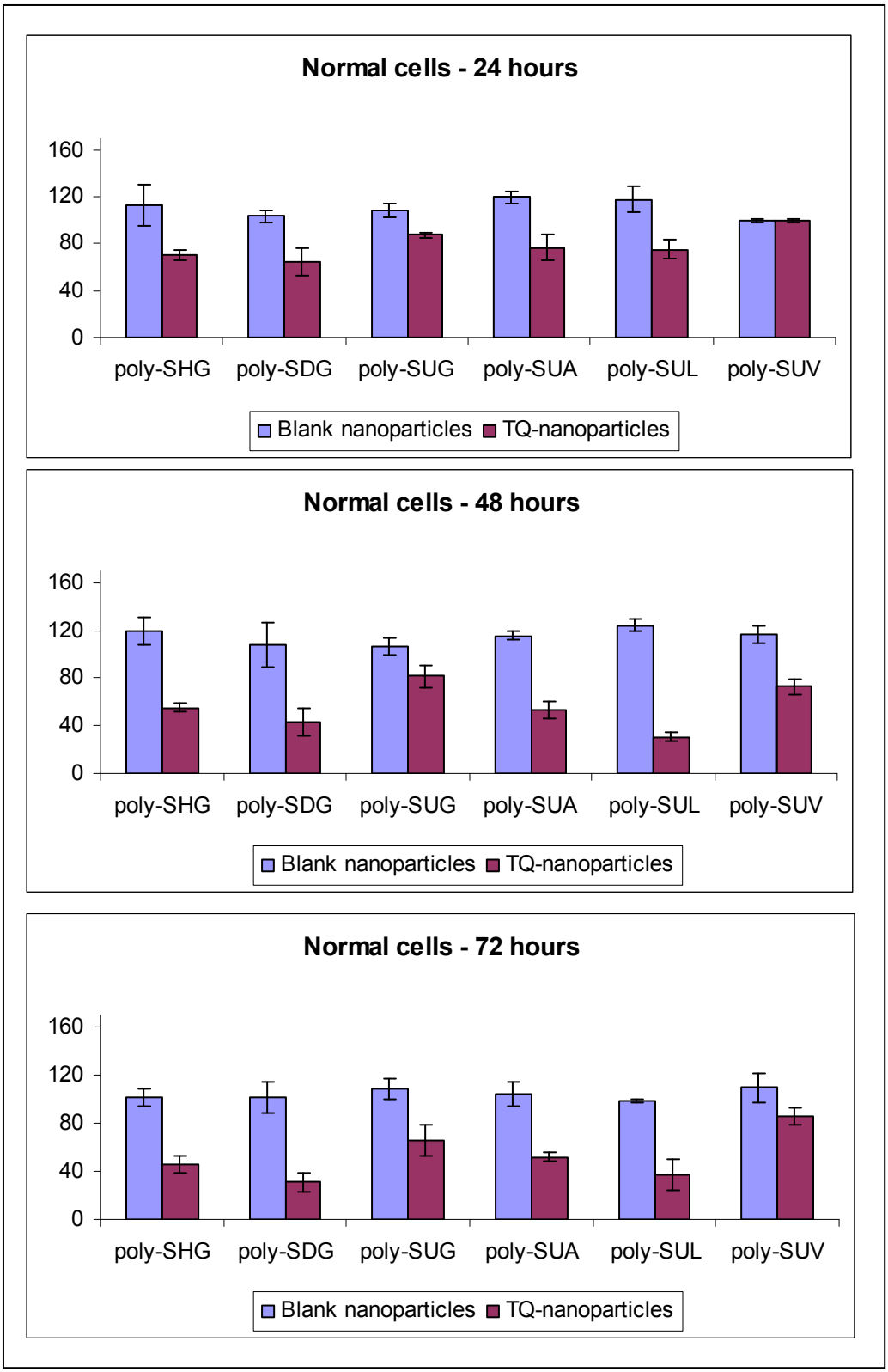

Figure 3.7 Cell viability of Hs578Bct normal breast cells in the presence of blank and TQ-loaded nanoparticles.

Therefore, the decrease in the cell viability was likely due to nanoparticle cell uptake and TQ release in the cellular media. In contrast, poly-SUV emulsified TQ-loaded nanoparticles provided the highest cell viability (85.79 ± 7.04 %) after 72 hours having the desired effect of low toxicity for normal cells.

The results for cell viability of MCF-7 and MDA-MB-231 cancer cells incubated with TQ-loaded nanoparticles are presented in Figure 3.8. For these nanoparticles, we did not observe a significant decrease in the cell viability after 24 and 48 hours for any of the nanoparticles. Such effect can be determined by insufficient cellular uptake and metabolism of the cells after the incubation with nanoparticles. We observed an overgrowth of both cancer cell lines incubated with TQ-loaded poly-SDG–emulsified nanoparticles. Similar effect was observed in case of blank poly-SDG–emulsified nanoparticles incubated with the cancer cells, indicating that such effect is likely induced by the emulsifier and not by the entrapped TQ. The MCF-7 cell viability decreased for all TQ-loaded nanoparticles at 72 hours. The lowest cell viability was obtained for poly-SUL–emulsified nanoparticles (43.26 ± 9.45 %), which is comparable with that obtained for equivalent free TQ (37.42 ± 4.83 %). For MDA-MB-231 breast cancer cells incubated with poly-SUL–emulsified nanoparticles, the cell viability was slightly higher (59.16 ± 4.52 %) than for MCF-7 cells, likely due to the drug-resistance of such cells. However, it should be noted that TQ-loaded nanoparticles emulsified with poly-SUV reached a cell viability of 68.47 ± 8.42 % for MDA-MB-231 cells, while the cell viability was higher for normal cells (85.79 ± 7.04 %) treated with the same nanoparticles. Although TQ-loaded nanoparticles emulsified with poly-SUV did not affect the cell viability of MCF-7 cells, their performance was improved for MDA-MB-231 cells. Considering that free TQ generated a low cell viability for both normal and cancer cells, TQ-loaded nanoparticles emulsified with poly-SUV can be potentially used as drug delivery systems for breast cancer inhibition.

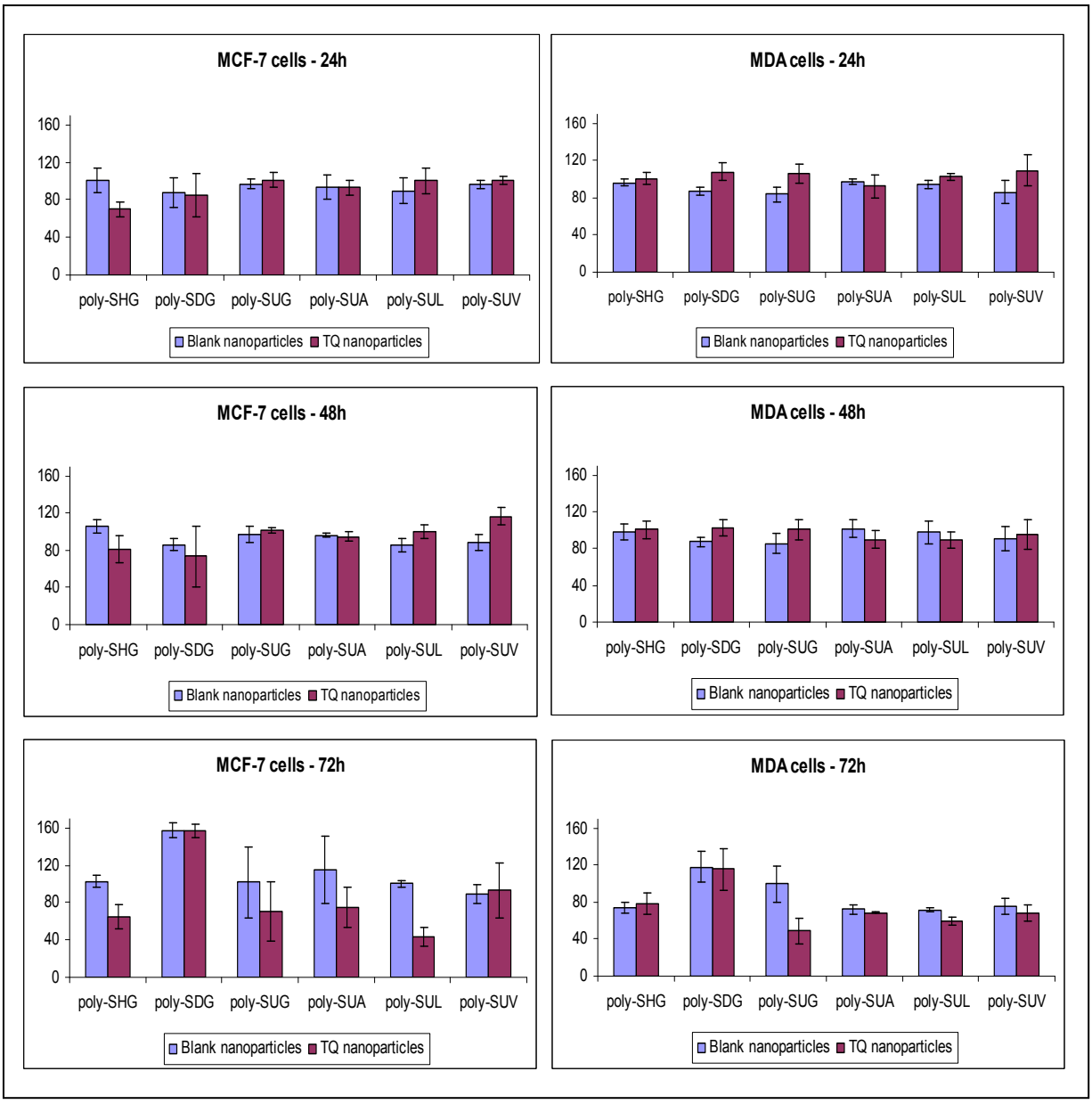

Figure 3.8 Cell viability of MCF-7 cancer cells (left); and MDA-MB-231 cancer cells (right) incubated with blank PLGA nanoparticles and TQ-loaded PLGA nanoparticles

3.4 Conclusions

TQ-loaded PLGA nanoparticles were successfully synthesized by use of an emulsification solvent evaporation technique using various molecular micelles as emulsifiers. The TQ entrapment efficiency was optimized using a Box-Behnken experimental design, and the

optimum synthetic conditions such as PLGA amount, TQ amount, and emulsifier concentration were obtained for maximum entrapment efficiency.

The molecular micelles strongly influenced the TQ release profile, the antioxidant and cytotoxic properties of TQ-loaded PLGA nanoparticles. Molecular micelles offered high flexibility to nanoparticle physico-chemical and biological properties and, therefore, can be used in the synthesis of drug-loaded nanoparticles depending on the desired properties. In addition, such nanoparticles are promising as free radical scavengers and inhibitors of breast cancer cells.

3.5. References

1 Dalle-Donne, I.; Rossi, R.; Colombo, R.; Giustarini, D.; Milzani, A. *Clinical Chemistry* **2006**, *52*, 601-623.

2 Molavi, B.; Mehta Jawahar, L. *Current Opinion in Cardiology* **2004**, *19*, 488-493.

3 Passi, S.; Gianni, G.; Cocchi, M. *Progress in Nutrition* **2006**, *8*, 241-256.

4 Manea, A.; Constantinescu, E.; Popov, D.; Raicu, M. *Journal of Cellular and Molecular Medicine* **2004**, *8*, 117-126.

5 Goetz, M. E.; Luch, A. *Cancer Letters* **2008**, *266*, 73-83.

6 Afonso, V.; Champy, R.; Mitrovic, D.; Collin, P.; Lomri, A. *Joint, Bone, Spine* **2007**, *74*, 324-329.

7 Sorg, O. *Comptes Rendus Biologies* **2004**, *327*, 649-662.

8 Kohen, R.; Nyska, A. *Toxicologic Pathology* **2002**, *30*, 620-650.

9 Pokorny, J.; Yanishlieva, N.; Gordon, M. *Antioxidants in food* **2001**, CRC Press LLC, Boca Raton, Forida, 87-249.

10 Bland, J. S. *Alternative Therapies* **1996**, *2*, 73-76.

11 Zhou, B.; Liu, Z.-L. *Pure Applied Chemistry* **2005**, *77*, 1887-1903.

12 Borek, C. *Integrative Cancer Therapies* **2004**, *3*, 333-341.

13 Garewal, H. S. *Antioxidants and disease prevention* **1997**, CRC Press LLC, Boca Raton, Florida, 3-177.

14 Milbury, P. E.; Richer, A. C. *Understanding the antioxidant controversy: scrutinizing the "fountain of youth"* **2008**, Praeger Publishers, Westport, Connecticut, 1-14.

15 Parada, J.; J.M., A. *Journal of Food Science* **2007**, *7*, R21-R32.

16 Shoji, Y.; Nakashima, H. *Journal of Drug Targeting* **2004**, *12*, 385-391.

17 Kaur, I. P.; Kapila, M.; Agrawal, R. *Ageing Research Reviews* **2007**, *6*, 271-288.

18 Dziubla, T.; Muro, S.; Muzykantov, V. R.; Koval, M. *Oxidative Stress, Disease and Cancer* **2006**, 1023-1043.

19 Sheu, S. S.; Nauduri, D.; Anders, M. W. *Biochimica Et Biophysica Acta-Molecular Basis of Disease* **2006**, *1762*, 256-265.

20 Ratnam, D. V.; Ankola, D. D.; Bhardwaj, V.; Sahana, D. K.; Kumar, M. *Journal of Controlled Release* **2006**, *113*, 189-207.

21 Wu, T. H.; Yen, F. L.; Lin, L. T.; Tsai, T. R.; Lin, C. C.; Cham, T. M. *International Journal of Pharmaceutics* **2008**, *346*, 160-168.

22 Zhang, Y.; Yang, Y.; Tang, K.; Hu, X.; Zou, G. *Journal of Applied Polymer Science* **2008**, *107*, 891-897.

23 Bala, I.; Bhardwaj, V.; Hariharan, S.; Sitterberg, J.; Bakowsky, U.; Kumar, M. *Nanotechnology* **2005**, *16*, 2819-2822.

24 Bala, I.; Bhardwaj, V.; Hariharan, S.; Kharade, S. V.; Roy, N.; Kumar, M. N. V. R. *Journal of Drug Targeting* **2006**, *14*, 27-34.

25 Bisht, S.; Feldmann, G.; Soni, S.; Ravi, R.; Karikar, C.; Maitra, A.; Maitra, A. *Journal of Nanobiotechnology* **2007**, *5:3*, 1-18.

26 Kurzrock, R.; Li, L.; Mehta, K.; Aggarwai, B. B.; Liposomal curcumin for treatment of cancer: WO/2004/080396, 2004, pp 66.

27 Trumpower, B. L. *Journal of Bioenergetics and Biomembranes* **1981**, *13*, 1-24.

28 Gutierrez, P. L. *Frontiers in Bioscience* **2000**, *5*, 629-638.

29 Horvath, R.; Gorman, G.; Chinnery, P. F. *Neurotherapeutics* **2008**, *5*, 558-568.

30 Quinzii, C. M.; Lopez, L. C.; Naini, A.; DiMauro, S.; Hirano, A. *Biofactors* **2008**, *32*, 113-118.

31 Ankola, D. D.; Viswanad, B.; Bhardwaj, V.; Ramarao, P.; Ravi Kumar, M. N. V. *European Journal of Pharmaceutics and Biopharmaceutics* **2007**, *67*, 361-369.

32 Hsu, C.-H., Coenzyme Q10 nanoparticles engineered from microemulsion precursors for oral delivery, 2004.

33 Nehilla, B. J.; Bergkvist, M.; Popat, K. C.; Desai, T. A. *International Journal of Pharmaceutics* **2008**, *348*, 107-114.

34 Alcain, F. J.; Villalba, J. M. *Expert Opinion on Therapeutic Patents* **2007**, *17*, 649-665.

35 Neckers, L.; Neckers, K. *Expert Opin Emerg Drugs* **2005**, *10*, 137-149.

36 Dettrakul, S.; Surerum, S.; Rajviroongit, S.; Kittakoop, P. *Journal of Natural Products* **2009**, *72*, 861-865.

37 Muhammad, I.; Takamatsu, S.; Walker, L. A.; Mossa, J. S.; Fong, H. H. S.; El-Feraly, F. S. *Phytotherapy Research* **2003**, *17*, 887-891.

38 Snader, K. M. *Anticancer agents from natural products* **2005**, CRC Press Boca Raton, Florida, 339-356.

39 Salem, M. L. *International Immunopharmacology* **2005**, *5*, 1749-1770.

40 Badary, O. A.; Taha, R. A.; El-Din, A. M. G.; Abdel-Wahab, M. H. *Drug and Chemical Toxicology* **2003**, *26*, 87-98.

41 Burits, M.; Bucar, F. *Phytotherapy Research* **2000**, *14*, 323-328.

42 Badary, O. A.; Abdel-Naim, A. B.; Adel-Wahab, M. H.; Hamada, F. M. A. *Toxicology* **2000**, *143*, 219-226.

43 Nagi, M. N.; Mansour, M. A. *Pharmacological Research* **2000**, *41*, 283-289.

44 Gali-Muhtasib, H.; Roessner, A.; Schneider-Stock, R. *International Journal of Biochemistry & Cell Biology* **2006**, *38*, 1249-1253.

45 Shoieb, A. M.; Elgayyar, M.; Dudrick, P. S.; Bell, J. L.; Tithof, P. K. *International Journal of Oncology* **2003**, *22*, 107-113.

46 Gali-Muhtasib, H.; Diab-Assaf, M.; Boltze, C.; Al-Hmaira, J.; Hartig, R.; Roessner, A.; Schneider-Stock, R. *International Journal of Oncology* **2004**, *25*, 857-866.

47 Scifinder *Scifinder Scholar, Advanced Chemistry Development (ACD/Labs) software, V8.14 for Solaris* **2007**, accessed September 2007.

48 Badary, O. A.; Al-Shabanah, O. A.; Nagi, M. N.; Al-Bekairi, A. M.; Elmazar, M. M. A. *Drug Development Research* **1998**, *44*, 56-61.

49 Ali, B. H.; Blunden, G. *Phytotherapy Research* **2003**, *17*, 299-305.

50 Esmaeili, F.; Ghahremani, M. H.; Esmaeili, B.; Khoshayand, M. R.; Atyabi, F.; Dinarvand, R. *International Journal of Pharmaceutics* **2008**, *349*, 249-255.

51 Ganea, G. M.; Sabliov, C. M.; Ishola, A. O.; Fakayode, S. O.; Warner, I. M. *Journal of Nanoscience and Nanotechnology* **2008**, *8*, 280-292.

52 Zhao, Y. F.; Sugiyama, S.; Miller, T.; Miao, X. G. *Expert Review of Medical Devices* **2008**, *5*, 395-405.

53 Macossay, J.; Shamsi, S. A.; Warner, I. M. *Tetrahedron Letters* **1999**, *40*, 577-580.

54 Akbay, C.; Gill, N. L.; Powe, A.; Warner, I. M. *Electrophoresis* **2005**, *26*, 415-425.

55 Billiot, F. H.; Billiot, E. J.; Warner, I. M. *Journal of Chromatography A* **2001**, *922*, 329-338.

56 Thibodeaux, S. J.; Billiot, E.; Warner, I. M. *Journal of Chromatography A* **2002**, *966*, 179-186.

57 Akbay, C.; Gill, N. L.; Agbaria, R. A.; Warner, I. M. *Electrophoresis* **2003**, *24*, 4209-4220.

58 Govender, S.; Pillay, V.; Chetty, D. J.; Essack, S. Y.; Dangor, C. M.; Govender, T. *International Journal of Pharmaceutics* **2005**, *306*, 24-40.

59 Akbay, C.; Gill, N. L.; Warner, I. M. *Electrophoresis* **2007**, *28*, 1752-1761.

60 Shamsi, S. A.; Palmer, C. P.; Warner, I. M. *Analytical Chemistry* **2001**, *73*, 140A-149A.

61 Valle, B. C.; Morris, K. F.; Fletcher, K. A.; Fernand, V.; Sword, D. M.; Eldridge, S.; Larive, C. K.; Warner, I. M. *Langmuir* **2007**, *23*, 425-435.

CHAPTER 4

FLUORESCENT RATIOMETRIC MOLECULAR MICELLE - MODIFIED POLY(D,L LACTIDE-*CO*-GLYCOLIDE) NANOPARTICLES FOR DETECTION OF HYDROXYL RADICALS

4.1 Introduction

Aerobic organisms produce the energy necessary for their life by oxidation of biological substrates in the presence of oxygen. Complete oxygen reduction takes place in mitochondria involving a series of redox reactions controlled by a complex enzymatic mechanism. Such reactions generate radical and non-radical reactive oxygen species, i.e. superoxide anion ($O_2^{\bullet -}$), hydroxyl radical ($OH^{\bullet}$), singlet oxygen ($^1O_2$), and hydrogen peroxide (H_2O_2). The cells are exposed to oxidative stress when an unbalance exists between the free radical production of their elimination by various reducing agents, enzymes, and other antioxidants.[1-3] Reactive oxygen species are involved in many metabolic processes, including signal transduction, carcinogenesis, and inflammatory response. In addition, excessive production of radical species can lead to alteration of cellular functions responsible for cardiovascular diseases, neurodegenerative diseases, diabetes, cancer, joint diseases, and aging.[4-9]

In the cellular oxidation process, hydroxyl radical can be produced by Fenton and Habber-Weiss reactions of hydrogen peroxide with transition metals such as iron and copper.[2, 8] Hydroxyl radical has a short half-life, and is considered the most aggressive free radical, mainly due to its high reactivity. It is able to react with lipids, amino acids, proteins, DNA, and sugars at extremely high rates, leading to cell damage and even cell death.[10] Other exogenous sources such as ozone and ionization radiation lead to hydroxyl radical generation as well.

Reactive oxygen species can be detected by a variety of methods, including electron spin resonance (ESR), UV-Vis, fluorescence, and luminescence spectroscopy.[11] Compared to the other methods, fluorescence sensors provide several advantages such as high specificity,

localized information at the target site, versatility of detection scheme, including fluorescence spectroscopy and fluorescence microscopy for both *in vitro* and *in vivo* detection.[12-14] In particular, coumarin 3-carboxylic acid (C3C) has been used as a fluorescent sensor for detection of hydroxyl radical.[15] The non-fluorescent C3C molecule reacts with hydroxyl radical and undergoes hydroxylation at position C7 of the coumarin structure, producing a highly fluorescent compound, 7-hydroxy coumarin 3-carboxylic acid (7-OH C3C) with the emission at 450 nm when excited in the 400-410 nm region.[15-17] In the chemical structure of C3C, the carboxylic group in the C3 position can be easily coupled with other molecules via a peptide bond. Therefore, other coumarin derivatives such as the succinimidyl ester of C3C (SECCA), phospholipid - linked coumarins, and C3C – derivatized amino acids and peptides were used for the detection of hydroxyl radicals.[18-20]

Although fluorescent probes have been successfully used to detect hydroxyl radicals, several limitations should be taken into consideration. For example, the changes in the fluorescence intensity of a single fluorophore that reacts with a specific radical can be affected by variations in radical and probe concentrations, instrumental artifacts and sensitivity to other environmental factors such as temperature and pH. In addition, real time *in vivo* imaging becomes challenging if the probe reacts with other molecules present in the cellular media, undergoes photobleaching or generates other secondary radicals.[11] A novel approach for detection of hydroxyl radicals is the use of fluorescence ratiometric detection that likely reduces such limitations. In this case, the ratio between the fluorescence intensity of a reporting molecule and the fluorescence intensity of a reference molecule can be used. Such ratiometric fluorescent sensors were reported for the detection of hydrogen peroxide and hydroxyl radicals using coumarin-coupled dyes.[21, 22] Another interesting approach is the use of ratiometric nanoparticles. For example, C3C-coupled polyacrylamide nanoparticles incorporating Texas Red as reference

dye were used as ratiometric nanoparticles, and hydroxyl radicals were detected based on the fluorescence intensity ratio between the two dyes.[23] Although such ratiometric sensors were used for the detection of free radicals, their limited solubility in aqueous media required the use of organic solvents that can act as radical scavengers. In addition, the compatibility of nanoparticle sensors with biological samples should be addressed in case of *in vitro* detection of hydroxyl radicals.

In this study, we adopted a strategy where biocompatible poly-lactide-co-glycolide (PLGA) nanoparticles were used as ratiometric fluorescent nanosensors for hydroxyl radical detection. The design of the ratiometric nanosensor is illustrated in Figure 4.1. Novel lysine-based molecular micelles containing a C3C moiety as the hydrophilic head group were synthesized and used as emulsifiers in the synthesis of PLGA nanoparticles by emulsification solvent evaporation. Such micelles have a polymerized highly hydrophobic core that strongly interacts with polymeric nanoparticles while the hydrophilic head group remains at the interface with aqueous solutions. The coumarin moiety is covalently bound to the lysine-based hydrophilic group that is present exclusively on the surface of the nanosensors and in direct contact with hydroxyl radicals present in the investigated samples. In order to complete the ratiometric scheme, neutral red dye was encapsulated into the nanoparticle matrix, protected from potential side reactions with free radicals. Other nanoparticles containing only C3C moiety or only NeR dye were also synthesized using emulsification solvent evaporation, and used as controls in the detection of hydroxyl radicals. The fluorescence intensity ratio between coumarin and neutral red was dependent on reaction time, nanoparticle concentration, and hydroxyl radical concentration. In addition, the response of C3C-poly-Nε-SUK – modified NeR – loaded PLGA nanoparticles was investigated in the presence of other reactive oxygen species such as superoxide anion radical, hydrogen peroxide, hypochlorite and singlet oxygen. Furthermore, the ratiometric

nanoparticles were incubated with MCF-7 breast tumor cells that were exposed to H_2O_2 – induced oxidative stress, and the detection of hydroxyl radicals was observed using fluorescence microscopy.

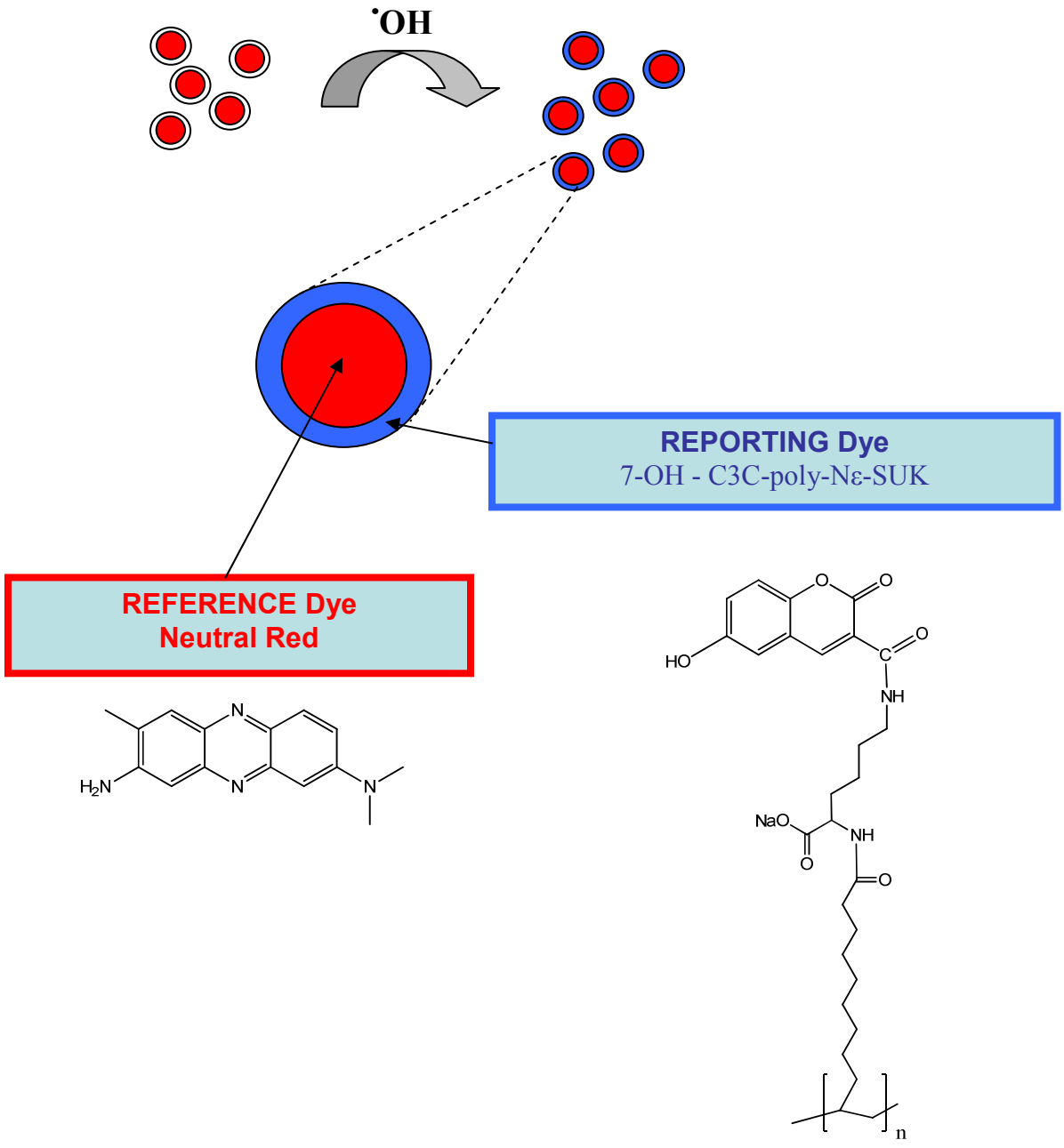

Figure 4.1 Design of the ratiometric nanosensor.

4.2 Experimental

4.2.1 Materials

Poly (D,L-lactide-*co*-glycolide) (PLGA, lactide:glycolide 50:50, MW 40,000-75,000), sodium dodecyl sulfate (SDS), undecylenic acid, ethyl acetate, trifluoroacetic acid (TFA), sodium carbonate, coumarin 3-carboxylic acid, Nε-Boc lysine, dimethyl sulfoxide (DMSO), anhydrous dimethyl formamide (DMF), sucrose, hydrogen peroxide, and neutral red (NeR) were purchased from Sigma-Aldrich (St. Louis, MO, USA). NeR was neutralized with NaOH in water, resulting into a red precipitate that was freeze-dried and used further in nanoparticle synthesis. Dibasic sodium phosphate was purchased from Mallinckrodt (Hazelwood, MO, USA). *N*-hydroxysuccinimide (NHS), *N,N'*-dicyclohexylcarbodiimide (DCC), and cuprous sulfate were purchased from Fluka (Milwaukee, WI, USA). Dichloromethane (DCM), sodium phosphate monobasic, isopropyl alcohol, tetrahydrofuran, and hexanes were purchased from EMD Chemicals Inc. (Gibbstown, NJ, USA). Sodium bicarbonate and sodium hydroxide were purchased from Fisher Scientific (Pittsburgh, PA, USA). Doubly-distilled deionized water was obtained from an ELGA PURELAB Ultra water polishing system (US Filter, Lowell, MA, USA). All reagents were of analytical grade and were used as received.

4.2.2 Synthesis of Coumarin Functionalized Molecular Micelles

The amino acid based molecular micelle poly (sodium *N*-undecenyl-Nε-Boc lysinate) (poly- Nε-Boc-SUK) was synthesized according to the procedure described by Macossay et al.[24] The deprotection of Boc group was achieved in a mixture of DCM and TFA 1:1 v/v for 4 hours at room temperature. The synthesis scheme of C3C-poly-Nε-SUK is presented in Figure 4.2. The first step is represented by the activation of carboxylic group of C3C, resulting in the succinimidyl ester of C3C (SECCA), according to an modified procedure described by Bardajee et al.[25] The unprotected poly-Nε-SUK (100 mg) was dissolved in sodium carbonate 0.1 M (5mL)

followed by the addition of SECCA dissolved in 1:4 v/v DMSO:DMF (5 mL) and allowed to react overnight. The solvent was removed by dialysis (cellulose ester membrane, MWCO 1000 Da, Spectrum Laboratories, Inc., Rancho Dominguez, CA, USA) for 24 hours. The final product, C3C-poly-Nε-SUK, was freeze-dried and refrigerated. Proton NMR indicated the completion of the coupling reaction by the presence of coumarin chemical shifts in the 7-9 ppm region.

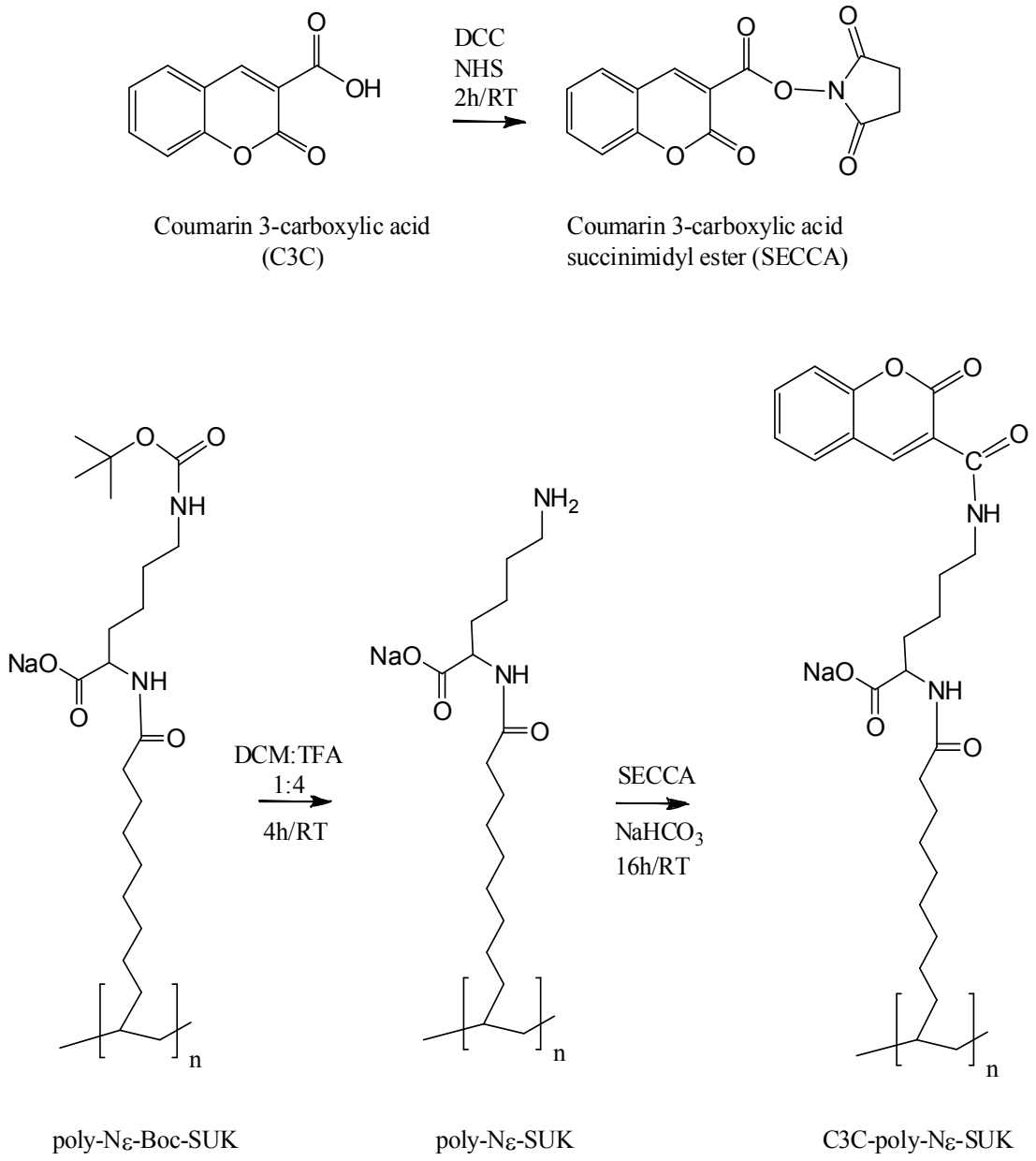

Figure 4.2 Synthesis of C3C-poly-Nε-SUK micelle.

4.2.3 Nanoparticle Synthesis

PLGA nanoparticles were synthesized by use of an emulsification solvent evaporation method. Briefly 0.5 mL of 1 mg/mL NeR in DCM was added to 0.5 mL DCM solution containing 50 mg of PLGA. In case of blank nanoparticles, the dye solution was replaced with DCM. An aqueous phase was prepared by dissolving C3C-poly-Nε-SUK in 5 mL water. For non-C3C-functionalized neutral red loaded nanoparticles, C3C-poly-Nε-SUK was replaced with a non-functionalized Boc-protected poly-Nε-Boc-SUK molecular micelle. The organic phase was added dropwise to the aqueous phase under stirring conditions using a homogenizer (model 398, Biospec Products, Inc., Racine, WI, USA), at 15,000 rpm for 2 minutes, resulting in a single o/w emulsion. The emulsion droplets were further reduced by sonication using a probe ultrasound processor (model VC750, Sonics and Materials Inc., Newton, CT, USA), operating at an amplitude intensity of 35 %, for 10 minutes. The solvent was evaporated using a rotary evaporator (Büchi rotovapor R-200, Brinkmann Instruments, Inc., Westbury, NY, USA). The nanoparticles were centrifuged at 10,000 rpm for 30 minutes, followed by washing by centrifugation in the same conditions. The nanoparticle suspension was stored at 4 ºC until further use.

4.2.4 Nanoparticle Characterization

Average particle diameter (Z_{ave}) and size distribution indicated by the polydispersity index (PDI) were measured by use of dynamic light scattering (DLS) (Zetasizer NanoZS, Malvern Instrumets Ltd., Malvern, UK) and reported as intensity distribution. Nanoparticle surface charge indicated by zeta potential was measured by use of laser doppler anemometry (Zetasizer NanoZS, Malvern Instrumets Ltd., Malvern, UK) using a capillary cell. The reported values of particle size, PDI, and zeta potential represent the average of three different nanoparticle batches. Nanoparticle morphology were investigated using transmission electron

microscopy (TEM) (JEOL 100CX, JEOL USA Inc., Peabody, MA, USA) operating at 80kV. A drop of nanoparticle suspension was dried at room temperature on a carbon coated copper grid and negatively stained using a 2 % solution of uranyl acetate.

4.2.5 Dye Content

The dye content was determined in the supernatant resulted from the centrifugation steps using absorbance spectroscopy (UV-3101PC UV-Vis-near-IR scanning spectrometer, Shimadzu, Columbia, MD) using a reduced volume (1.4 mL) quartz cuvet. A calibration curve was constructed for C3C by representing the absorbance intensity at 290 nm as a function of C3C concentration ($y = 0.0111x-0.0258$, $R^2 = 0.9927$). Similarly, a calibration curve was constructed for NeR by representing the absorbance intensity at 530 nm as a function of NeR concentration ($y = 1.1178x-0.0019$, $R^2 = 0.9989$). The NeR entrapment efficiency was calculated by difference between found amount in the supernatant and the theoretical amount added to the formulation. The C3C coverage was calculated based on the C3C content of poly-Nε-SUK attached on the surface of nanoparticles after purification.

4.2.6 Hydroxyl Radical Generation

Hydroxyl radicals were generated in phosphate buffer (pH=7.4) based on the reaction of cuprous sulfate and hydrogen peroxide in the presence of ascorbic acid, as described by equations 4.1 and 4.2. The reduction of Cu^{2+} takes place in the presence of ascorbic acid resulting into Cu^{+} that further reacts with hydrogen peroxide leading to the formation of hydroxyl radicals. The concentration of $OH^{\bullet}$ was varied by varying the concentration of cuprous sulfate added to the reaction. For various experiments, the reaction was stopped at various time intervals using DMSO as $OH^{\bullet}$ scavenger.

$$Cu^{2+} \xrightarrow{ascorbic\ acid} Cu^{+} \quad 4.1$$

$$Cu^{+} + H_2O_2 \rightarrow Cu^{2+} + OH^{\bullet} + OH^{-} \quad 4.2$$

4.2.7 Fluorescence Spectroscopy

Steady-state fluorescence spectra were recorded using Fluorolog-3 spectrometer (model FL1073, Horiba Jobin Yvon, Edison, NJ) operated in the front face mode, at 25 ºC as provided by a temperature control chamber. The samples were prepared in phosphate buffer (pH 7.4), and a short path (0.4 cm^2) cuvette was used. The excitation and emission slit widths were both set at 5 nm, respectively. The samples were excited at 410 nm, and the emission was collected from 420 to 700 nm. The blanks containing all reagents except nanoparticles were subtracted for each sample. All measurements were performed in triplicate.

4.2.8 *In vitro* Detection of Hydroxyl Radicals

Human mammary MCF-7 tumor cells (HTB-22, American Tissue Culture Collection, ATCC, Manassas, VA) were grown to 90% confluence according to ATCC's instructions and used for *in vitro* detection of $OH^{\bullet}$ radicals. Specifically, the cells were incubated with nanoparticle suspension (0.07 mg/ mL cell suspension) in a 6-well plate at 10,000 cells/ well. After two hours of incubation, the cells were washed with growth media to eliminate the excess of nanoparticles. The cells were then exposed to H_2O_2-induced oxidative stress (400 μM) for 40 minutes, and washed with phosphate buffer. Fluorescence images were taken before and after exposure, using a Leica DM RXA2 upright microscope (Leica Microsystems Inc., Bannockburn, IL) equipped with GFP and TRITC filter cubes, and an immersion 40X objective.

4.3 Results and Discussion

4.3.1 Nanoparticle Characterization

In this study, C3C-poly-Nε-SUK – modified NeR loaded PLGA nanoparticles were prepared by emulsification solvent evaporation using fluorescent molecular micelles as emulsifiers. Previously, PLGA nanoparticles were successfully synthesized in our laboratory using molecular micelles as emulsifiers, offering great advantages such as small size,

monodisperse suspension, and excellent stability.[26] The C3C-poly-Nε-SUK – modified NeR loaded PLGA nanoparticles synthesized in this study had a size of 124 ± 0.7 nm. In addition, the nanoparticle suspension was monodisperse as expressed by a PDI value of 0.052 ± 0.012. The anionic molecular micelle present on the nanoparticle surface conferred a zeta potential of -52.77 ± 0.76 mV, indicating high stability of nanoparticles in solution. Individual nanoparticles having spherical shape were observed by TEM, their micrograph being illustrated in Figure 4.3.

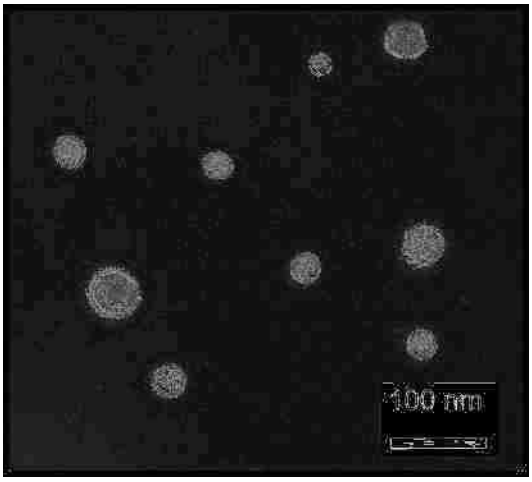

Figure 4.3 TEM micrograph of C3C-poly-Nε-SUK – modified PLGA nanoparticles.

Commercially available NeR is delivered as a chloride that is highly water soluble. In order to encapsulate it into PLGA nanoparticles, neutralization with NaOH was performed, and it resulted into a red precipitate consisting of highly hydrophobic neutralized NeR. The hydrophobic NeR dye was thus encapsulated in PLGA nanoparticles by an emulsification solvent evaporation method using C3C-poly-Nε-SUK as an emulsifier. The content of NeR was determined by UV spectroscopy, based on a calibration curve as described above. Taking into consideration the initial NeR amount added to the formulation, it was found that the NeR content was 83.9 ± 0.8%. Similarly, the C3C content given by the presence of C3C-poly-Nε-SUK was determined by UV spectroscopy. The C3C content was found to be 48.4 ± 0.9%, representing the

fraction of C3C amount present in the initial C3C-poly-Nε-SUK micelle used as emulsifier in the nanoparticle synthesis.

4.3.2 Nanoparticle Reaction with Hydroxyl Radicals

Hydroxyl radicals were detected using ratiometric fluorescence spectroscopy. Compared with variations of a single signal, ratiometric detection involves changes in the ratio of two signals. The first signal is given by a reporting dye that reacts with the molecule of interest, while the second signal is given by a reference dye that corrects for instrumental artifacts. Nanoparticles that contain both reference and reporting dyes can be used in the ratiometric detection scheme. In case of C3C-poly-Nε-SUK – modified NeR – loaded PLGA nanoparticles, NeR was the reference dye, and was encapsulated into PLGA nanoparticles. In addition, the reporting dye was 7-OH C3C-poly-Nε-SUK that resulted from the reaction with $OH^{\bullet}$ radicals of C3C-poly-Nε-SUK molecular micelle present on the nanoparticle surface. The product of such reaction presented a fluorescent signal at 450 nm when excited at 410 nm. At the same time, the reference dye, NeR, offered a separate fluorescent signal as shown in Figure 4.4.

In order to demonstrate that the two fluorescent peaks were generated by C3C and NeR respectively, blank nanoparticles were prepared without NeR. These nanoparticles contained C3C-poly-Nε-SUK molecular micelle on the surface. In addition, NeR-loaded nanoparticles were prepared using a non-functionalized Boc-protected poly-Nε-Boc-SUK molecular micelle as emulsifier. The fluorescence spectrum of C3C-poly-Nε-SUK – modified blank nanoparticles presented the peak at 450 nm as a result of the reaction of $OH^{\bullet}$ radicals with C3C, while the fluorescence peak at 540 nm is absent. In contrast, the spectrum of Boc-protected poly-Nε-Boc-SUK – modified NeR – loaded nanoparticles contained exclusively the fluorescence of reference dye NeR. Therefore, it was confirmed that the two peaks at 450 nm and 535 nm were generated by the reference and the reporting dyes, respectively.

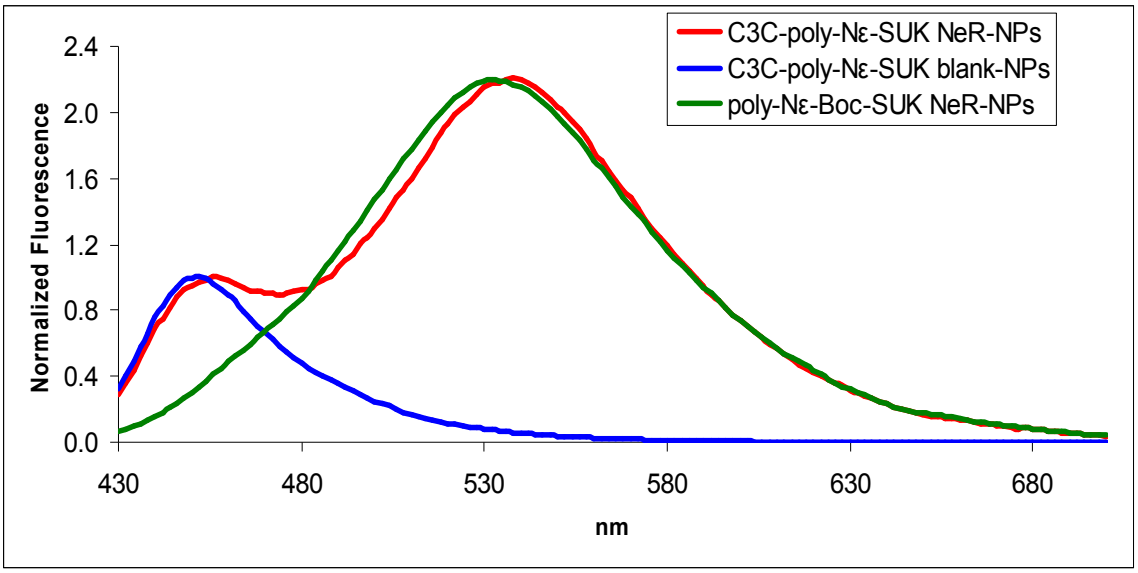

Figure 4.4 Normalized fluorescence of nanoparticles after the reaction with $OH^{\bullet}$ (0.07 mg/mL nanoparticles, 200 μM $CuSO_4$, 20 mM H_2O_2 and 200 μM ascorbic acid; 5 minutes; total volume was 500 mL).

4.3.2.1 Effect of Coumarin Location

The reaction between $OH^{\bullet}$ radicals and C3C likely depends on the availability of the reagents. In the case of C3C-poly-Nε-SUK – modified NeR – loaded PLGA nanoparticles, C3C was placed near the surface of the nanoparticle, directly exposed to the environment containing $OH^{\bullet}$ radicals and readily available for the reaction. The effect of C3C location on the fluorescence response was observed by changing the position of C3C within the ratiometric nanosesor. Nanoparticles containing both C3C and NeR in the polymeric matrix were synthesized using non-fluorescent poly-Nε-Boc-SUK as emulsifier (poly-Nε-Boc-SUK – modified NeRSec – loaded PLGA nanoparticles). However, the succinimidyl ester of C3C (SECCA) was used instead of C3C, due to its higher hydrophobicity. It should be mentioned that SECCA readily reacts with $OH^{\bullet}$ radicals resulting in a fluorescent product having the intensity maximum at 450 nm.[15, 18] The fluorescence spectra of C3C-poly-Nε-SUK – modified NeR –

loaded PLGA nanoparticles (red spectrum) and poly-Nε-Boc-SUK – modified NeRSec – loaded PLGA nanoparticles (blue and green spectra) are shown in Figure 4.5. The nanoparticles containing an equal molar ratio of SECCA and NeR within the polymer matrix presented a peak in the fluorescence spectrum at 538 nm likely due to NeR fluorescence, and no evident intensity of 7-OH C3C at 450 nm, as it can be noted in Figure 4.5 (blue spectrum).

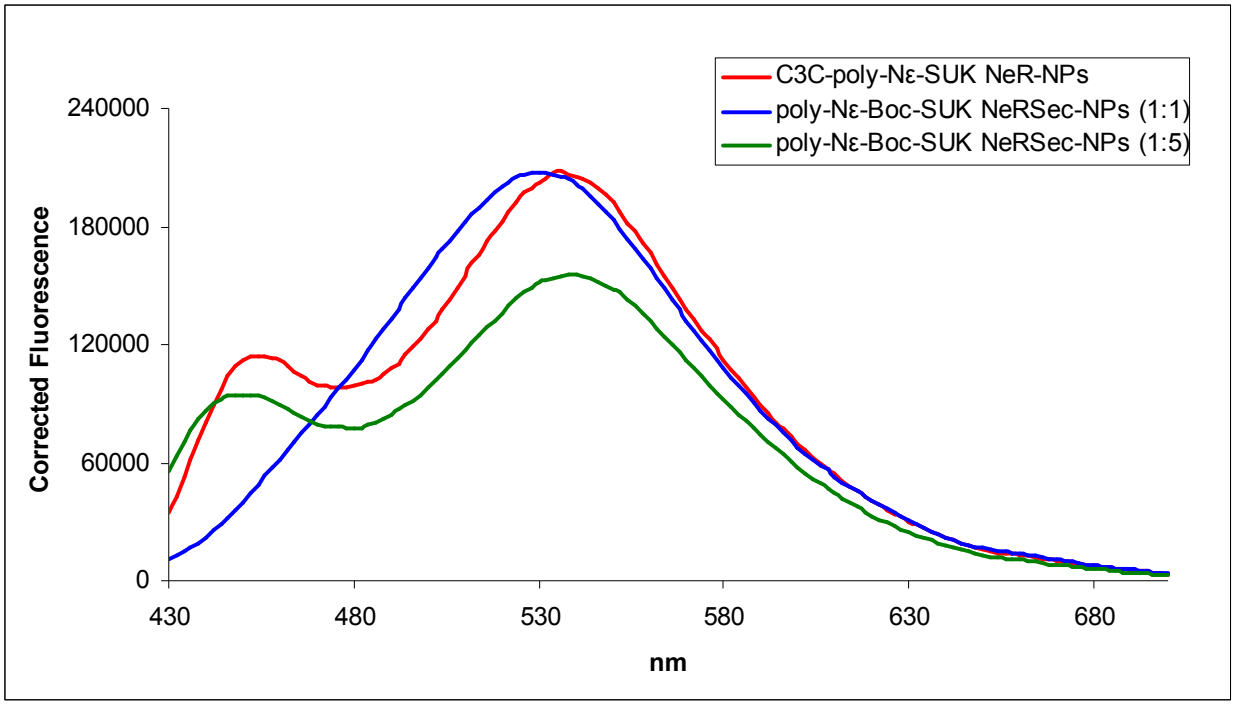

Figure 4.5 Effect of C3C location. Corrected fluorescence of nanoparticles after the reaction with $OH^{\bullet}$ (0.07 mg/mL nanoparticles, 200 µM $CuSO_4$, 20 mM H_2O_2 and 200 µM ascorbic acid; 5 minutes; total volume was 500 mL).

As the amount of SECCA added to the nanoparticles increased to a 1:5 molar ratio, a portion of the dye was likely situated near the nanoparticle surface. Therefore, the reaction between SECCA and $OH^{\bullet}$ radicals readily occurred, and the peak at 450 nm appeared in the fluorescence spectrum. However, the overall fluorescence signal was lower for poly-Nε-Boc-SUK – modified NeRSec – loaded PLGA nanoparticles than for C3C-poly-Nε-SUK – modified

NeR – loaded PLGA nanoparticles. Such results suggested that the presence of coumarin moiety on the surface of the nanoparticles generated the highest signal, likely due to availability of C3C for the reaction with $OH^{\bullet}$ radicals.

4.3.2.2 Effect of Reaction Time

In general, hydroxyl radicals have a short life-time in solution and rapidly react with surrounding molecules. Due to sample preparation and instrumental limitation, the time needed for nanoparticle reaction with $OH^{\bullet}$ radicals was established by stopping the reaction at various time intervals using DMSO as $OH^{\bullet}$ scavenger. DMSO rapidly reacts with hydroxyl radicals and likely eliminates their presence in solution. In Figure 4.6, the I_{450}/I_{528} ratio between C3C fluorescence intensity at 450 nm and NeR fluorescence intensity at 528 nm is represented as a function of time.

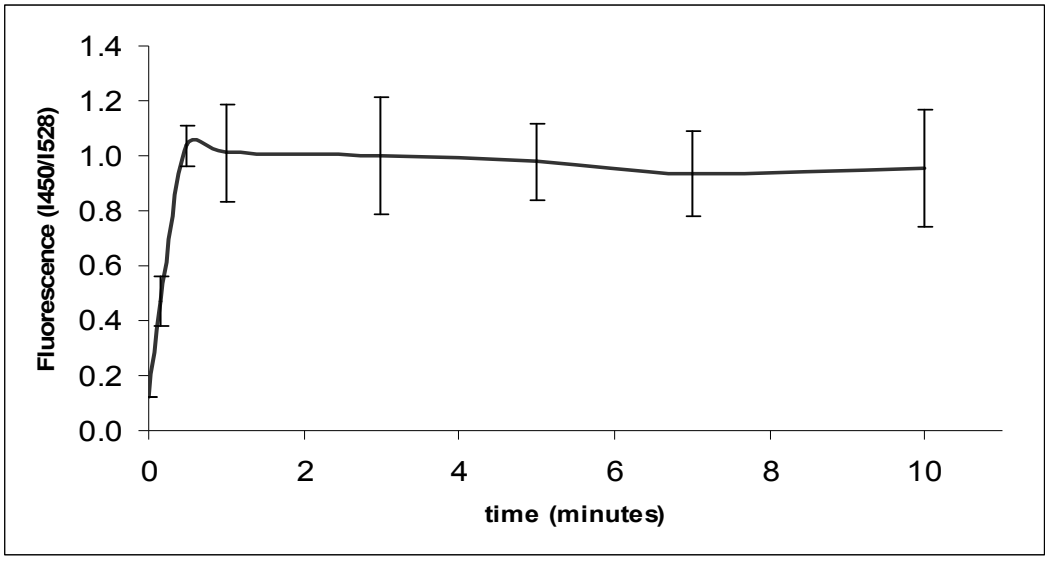

Figure 4.6 Effect of reaction time on fluorescence ratio after the reaction of nanoparticles with $OH^{\bullet}$ (0.07 mg/mL nanoparticles, 200 μM $CuSO_4$, 20 mM H_2O_2 and 200 μM ascorbic acid; total volume 500 mL).

A linear increase of I_{450}/I_{528} is observed in the first minute, indicating that the radicals were rapidly consumed in the reaction with C3C. It is worth mentioning that the reaction of $OH^{\bullet}$

with C3C is irreversible, and limited by the concentration of radicals. After one minute, it is possible that $OH^{\bullet}$ radical concentration decreased. Therefore, further increase in the fluorescent ratiometric signal was not observed with increase in the reaction time. For further experiments, the reaction was stopped at 5 minutes in order to ensure the complete reaction.

4.3.2.3 Effect of Nanoparticle Concentration

Spectroscopic analyses using nanoparticle reactions with various molecules are limited by their scattering effect. Therefore, a minimum nanoparticle concentration is desirable that would be sufficient for the reaction and at the same time remains within the instrumental limitations. Figure 4.7 represents the fluorescence spectra of increasing concentrations of nanoparticle suspensions reacting with $OH^{\bullet}$ radicals. All other conditions were kept constant. It can be noted that the intensity of NeR at 528 nm increased with the increase in nanoparticle concentration.

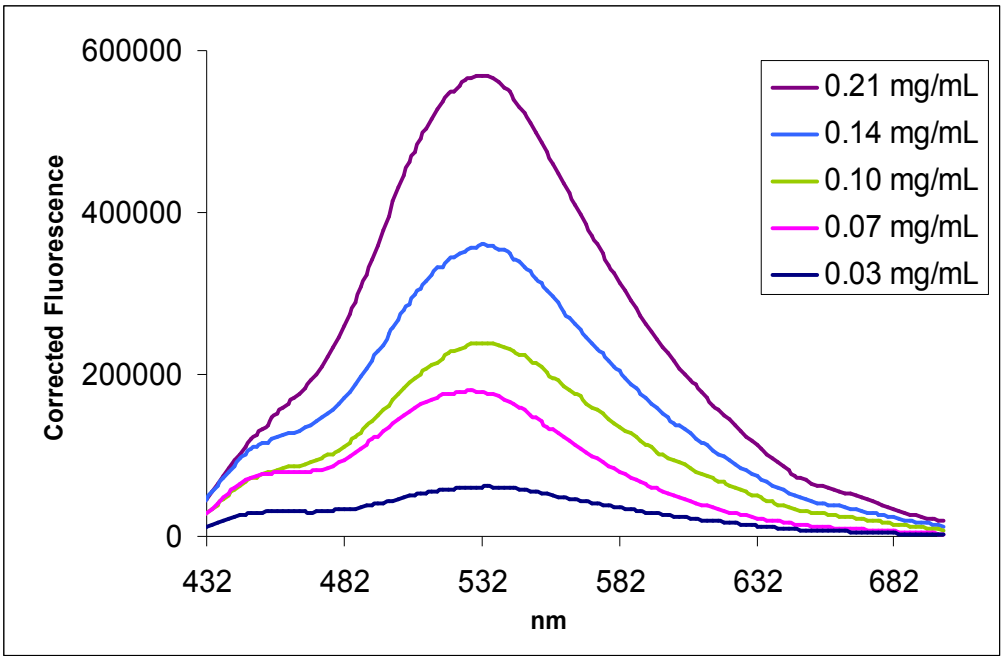

Figure 4.7 Fluorescence spectra of nanoparticles after the reaction with $OH^{\bullet}$ (0.03, 0.07, 0.10, 0.14, 0.21 mg/mL nanoparticles, 400 µM $CuSO_4$, 20 mM H_2O_2 and 200 µM ascorbic acid, incubated for 5 min; total volume 500 mL).

However, as more nanoparticles were used in the reaction, the peak corresponding to 7-OH C3C started to disappear under the NeR peak. Since the concentration of $OH^{\bullet}$ radicals remained constant, an increase in nanoparticle concentration did not produce an increase of 7-OH peak, but resulted in an increase of only NeR peak. In addition, a significant cloudiness of reaction medium was observed at concentrations above 0.1 mg/mL nanoparticle solution. A minimum concentration of 0.07 mg/mL nanoparticles was considered optimum for ratiometric experiments, firstly to produce a clear response at 450 and 528 nm, and secondly to minimize the scattering effect.

4.3.2.4 Effect of Hydroxyl Radical Concentration

Increasing concentrations of $OH^{\bullet}$ radicals were incubated with C3C-poly-Nε-SUK – modified NeR – loaded PLGA nanoparticles. In case of ratiometric sensors, if the reporting and reference dyes are in close proximity, and there is an overlap between the fluorescence of the reporting dye and the absorbance of the reference dye, fluorescence resonance energy transfer (FRET) occurs. In this case, the signal of the reporting dye decreases and the one of the reference dye increases. The reporting dye signal strictly depends on the reaction with $OH^{\bullet}$ radicals, and an increase in radical concentration would likely produce an increase in the reporting dye signal. The response of C3C-poly-Nε-SUK – modified NeR – loaded PLGA nanoparticles to different concentrations of $OH^{\bullet}$ radicals is illustrated in Figure 4.8(A).

In this experiment, the concentration of $OH^{\bullet}$ was changed by changing the concentration of $CuSO_4$, according to equations 4.1 and 4.2. The other conditions were maintained constant. As the $OH^{\bullet}$ concentration increases, it is expected that C3C present on the surface of nanoparticles to generate an increase in the fluorescence intensity at 450 nm. However, an increase in NeR signal was observed while the signal from 7-OH C3C decreased due to a fluorescence energy transfer between the coumarin and the reference dye.

(A)

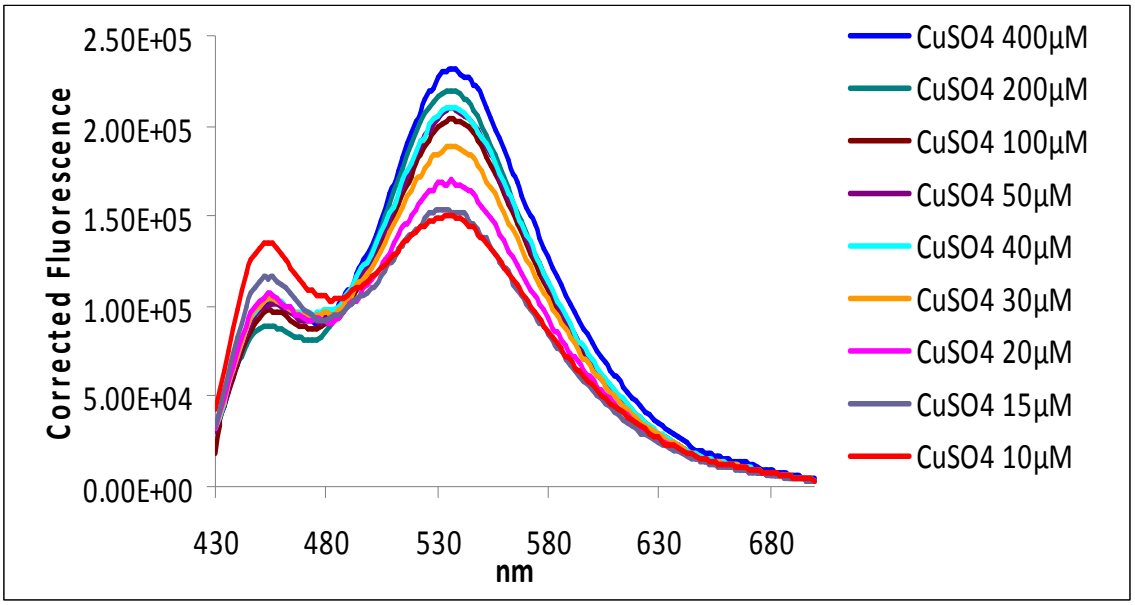

(B)

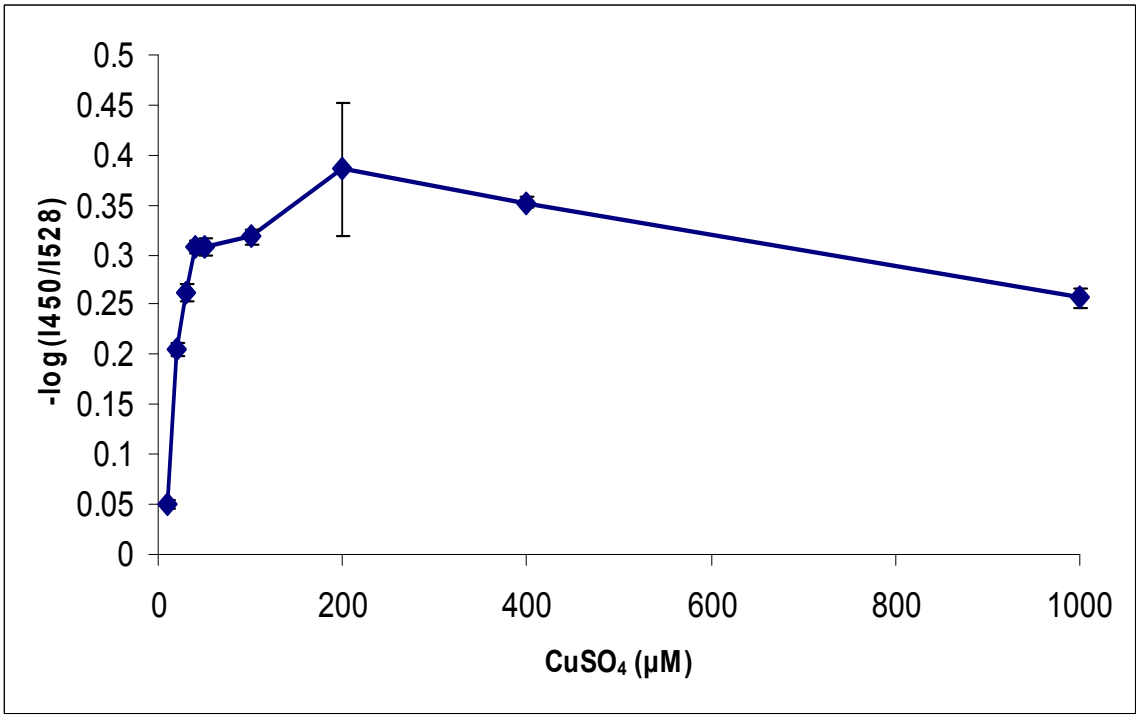

Figure 4.8 (A) Fluorescence spectra of nanoparticles after the reaction with $OH^{\bullet}$ (0.07mg/mL nanoparticles, 20 mM H_2O_2, 200 µM ascorbic acid, and 10, 20, 30, 40, 50, 100, 200, 400, and 1000 µM $CuSO_4$, incubated for 5 min; total volume 500 mL); (B) logarithmic I450/I528 ratio as a function of $CuSO_4$ concentration.

In addition, the observed FRET phenomenon was favored by the spectral overlap and short spatial distance between the reporting and reference dyes. The I_{450}/I_{528} ratio between C3C fluorescence intensity at 450 nm and NeR fluorescence intensity at 528 nm is represented as a function of $CuSO_4$ concentration in Figure 4.8(B) on a logarithmic scale. It can be observed that the fluorescence intensity ratio increases as the concentration $OH^{\bullet}$ radicals increases. In order to verify that the increase in the NeR signal was determined by FRET, NeR – loaded PLGA nanoparticles modified with poly-N-Boc-SUK micelles were also incubated with increasing concentrations of hydroxyl radicals, and compared with C3C-poly-Nε-SUK – modified NeR – loaded PLGA nanoparticles. We noticed an insignificant increase in the NeR peak as compared with the increase determined by the presence of C3C (as shown in Appendix IV.A).

4.3.3 Reaction with Other Radicals

The selectivity of nanoparticles for $OH^{\bullet}$ radicals is important in particular for radical detection in biological samples. NeR-loaded PLGA nanoparticles modified with C3C-poly-Nε-SUK were exposed to various radical and non-radical reactive species such as superoxide anion ($O_2^{\bullet -}$), hydrogen peroxide (H_2O_2), singlet oxygen ($^1O_2$), and hypochlorite anion (OCl^-). The reactions took place in phosphate buffer using the same nanoparticle concentration, reaction volume and reaction time. DMSO was used only for the detection of hydroxyl radicals. The ratio between C3C fluorescence intensity at 450 nm and NeR fluorescence intensity at 528 nm (I_{450}/I_{528}) is represented in Figure 4.9 for each radical. It can be noted that the I_{450}/I_{528} ratio was significantly higher for $OH^{\bullet}$ than for the other radicals, indicating increased nanosensor selectivity towards hydroxyl radical likely determined by the selectivity of C3C.

4.3.4 *In vitro* Detection of Hydroxyl Radicals

Aerobic organisms are complicated machines that produce energy based on oxidation reactions. Such reactions generate reactive oxygen species that are involved in diseases such as

cancer, diabetes and ageing. In comparison with other reactive oxygen species, hydroxyl radical is a short life radical. In addition, it can react with numerous biological molecules including lipids, proteins and DNA. In order to verify the ability of C3C-poly-Nε-SUK – modified NeR – loaded PLGA nanoparticles to react with $OH^{\bullet}$ radicals generated in cell cultures, MCF-7 breast tumor cells were incubated with ratiometric nanoparticles for 2 hours.

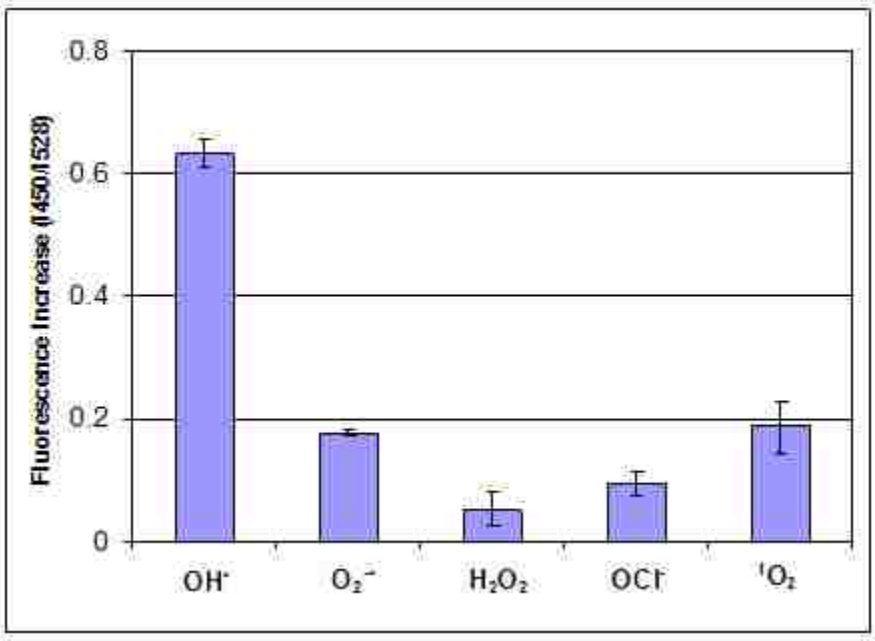

Figure 4.9 Fluorescence spectra of nanoparticles after the reaction with various radicals (0.07 mg/mL nanoparticles, and $OH^{\bullet}$ (400 μM $CuSO_4$, 20 mM H_2O_2 and 200 μM ascorbic acid), $O_2^{-\bullet}$ (200 μM KO_2), H_2O_2 (20 mM), OCl^- (200 μM NaOCl), $^1O_2$ (200 μM H_2O_2 + 200 μM NaOCl).

After the nanoparticle cell uptake took place, the cells were washed in order to eliminate the excess of nanoparticles. The cells were further exposed to oxidative stress using hydrogen peroxide as initiator. In the cellular environment, hydroxyl radicals are mainly generated by the reaction of hydrogen peroxide with metals, and likely contained the transition metals necessary for the reaction with hydrogen peroxide. The fluorescent signal was observed by fluorescence

microscopy at different incubation times as shown in Figure 4.10. Initially the cells appeared red likely due to the NeR signal. As the $OH^{\bullet}$ radicals became available in the cell environment at 10, 20 and 40 minutes, the cells started to turn green possibly as a result of 7-OH C3C fluorescence signal. Therefore, ratiometric C3C-poly-Nε-SUK – modified NeR – loaded PLGA nanoparticles were able to detect free radicals in stressed cells. It should be mentioned that C3C can react with $OH^{\bullet}$ radicals that are also produced through natural metabolism of viable cells. However, their presence did not generate green fluorescence during the nanoparticle cellular uptake. In oxidative stress conditions, the concentration of $OH^{\bullet}$ radicals is higher as compared with normal conditions, allowing their rapid detection in viable cells using ratiometric nanoparticles.

The MCF-7 cells were also incubated with NeR-loaded nanoparticles modified with a non-fluorescent Boc-protected poly-SUK. In this experiment, the cells appeared red before the exposure to oxidative stress, and remained mainly red after the exposure to oxidative stress, the weak green color being observed likely due to cell autofluorescence. Similarly, the cells were incubated with C3C-poly-Nε-SUK – modified blank PLGA nanoparticles. No fluorescence was observed before the exposure to oxidative stress. However, the cells became green after the exposure to oxidative stress, likely due to coumarin reaction with hydroxyl radicals (as shown in Appendix IV.B).

4.4 Conclusions

Detection of reactive oxygen species is critical for the investigation of their role in biological systems, and a suitable analytical method is desirable for their rapid detection. Hydroxyl radical is one of the most important radical involved in oxidative stress, mainly due to its high reactivity. In this study, C3C-poly-Nε-SUK – modified NeR – loaded PLGA nanoparticles were used to successfully detect hydroxyl radicals by fluorescence ratiometric detection conferred by 7-OH C3C reporting dye and NeR reference dye. In addition, the

ratiometric nanoparticles were sensitive and selective for hydroxyl radicals as compared to other reactive oxygen species such as superoxide anion ($O_2^{\bullet-}$), hydrogen peroxide (H_2O_2), singlet oxygen ($^1O_2$), and hypochlorite (OCl^-). Furthermore, C3C-poly-Nε-SUK – modified NeR – loaded PLGA nanoparticles were able to detect hydroxyl radicals in viable cells exposed to oxidative stress allowing their potential use in the study of other living systems.

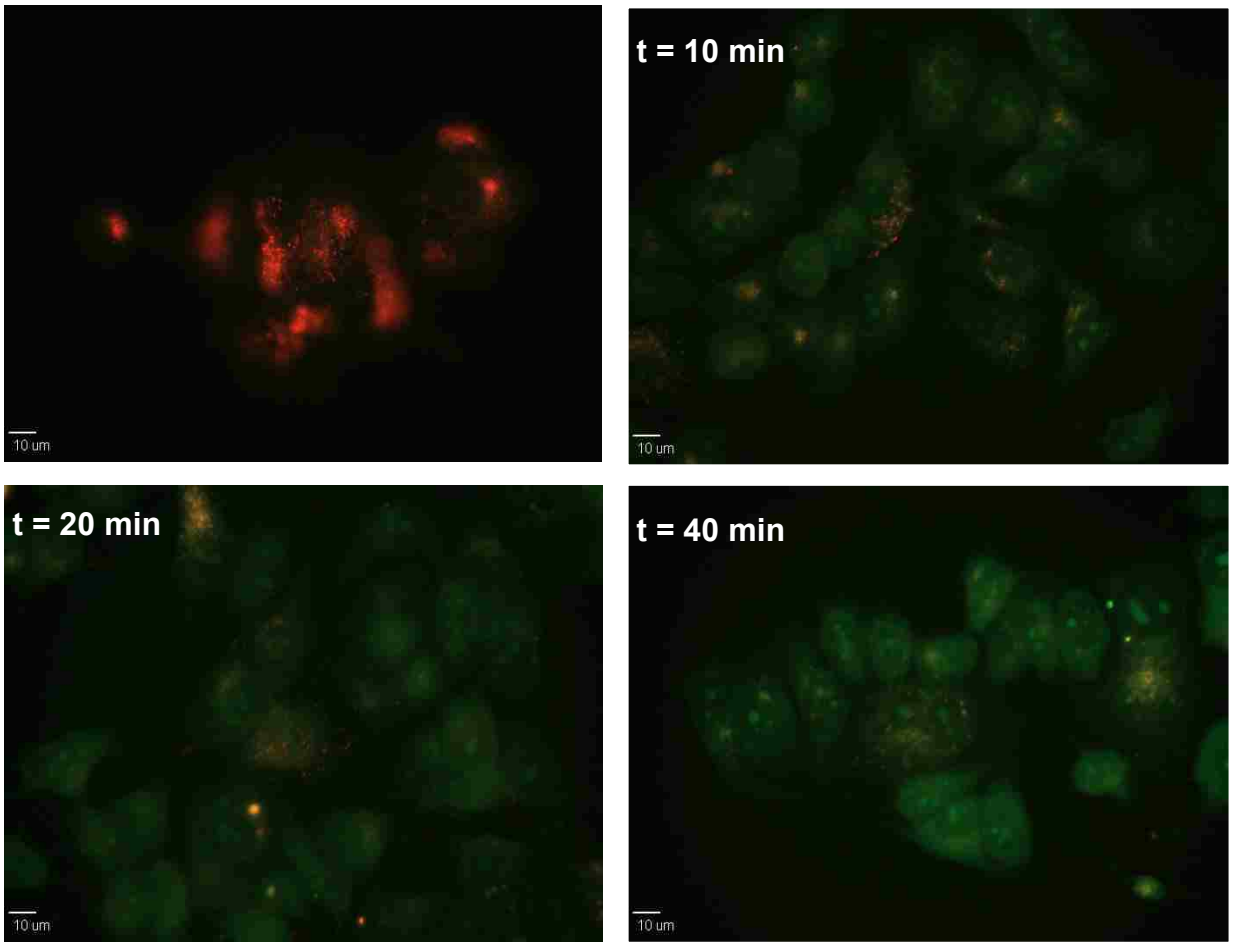

Figure 4.10 Fluorescence micrographs of nanoparticle response in MCF-7 cells exposed to H_2O_2 – induced oxidative stress (400 μM), before the addition of H_2O_2 (top left corner), at t = 10, 20, and 40 minutes after the addition of H_2O_2.

4.5 References

1 Sorg, O. *Comptes Rendus Biologies* **2004**, *327*, 649-662.

2 Kohen, R.; Nyska, A. *Toxicologic Pathology* **2002**, *30*, 620-650.

3 Jones, D. P. *Antioxidants & Redox Signaling* **2006**, *8*, 1865-1879.

4 Dalle-Donne, I.; Rossi, R.; Colombo, R.; Giustarini, D.; Milzani, A. *Clinical Chemistry* **2006**, *52*, 601-623.

5 Molavi, B.; Mehta Jawahar, L. *Current Opinion in Cardiology* **2004**, *19*, 488-493.

6 Passi, S.; Gianni, G.; Cocchi, M. *Progress in Nutrition* **2006**, *8*, 241-256.

7 Manea, A.; Constantinescu, E.; Popov, D.; Raicu, M. *Journal of Cellular and Molecular Medicine* **2004**, *8*, 117-126.

8 Goetz, M. E.; Luch, A. *Cancer Letters* **2008**, *266*, 73-83.

9 Afonso, V.; Champy, R.; Mitrovic, D.; Collin, P.; Lomri, A. *Joint, Bone, Spine* **2007**, *74*, 324-329.

10 Halliwell, B.; Gutteridge, J. M. C. *Free radicals in biology and medicine* **1989**, Oxford University Press, 2nd edition, 1-81.

11 Bartosz, G. *Clinica Chimica Acta* **2006**, *368*, 53-76.

12 Gomes, A.; Fernandes, E.; Lima, J. L. F. C. *Journal of Biochemical and Biophysical Methods* **2005**, *65*, 45-80.

13 Soh, N.; Imato, T. *Current Bioactive Compounds* **2006**, *2*, 409-430.

14 Soh, N. *Analytical and Bioanalytical Chemistry* **2006**, *386*, 532-543.

15 Manevich, Y.; Held, K. D.; Biaglow, J. E. *Radiation Research* **1997**, *148*, 580-591.

16 Martin-Aragon, S.; Benedi, J.; Villar, A. *Phytotherapy Research* **1996**, *10*, S75-S78.

17 Newton, G. L.; Milligan, J. R. *Radiation Physics and Chemistry* **2006**, *75*, 473-478.

18 Makrigiorgos, G. M.; Baranowska-Kortylewicz, J.; Bump, E.; Sahu, S. K.; Berman, R. M.; Kassis, A. I. *International Journal of Radiation Biology* **1993**, *63*, 445-458.

19 Soh, N.; Makihara, K.; Ariyoshi, T.; Seto, D.; Maki, T.; Nakajima, H.; Nakano, K.; Imato, T. *Analytical Sciences* **2008**, *24*, 293-296.

20 Ghosh, S. C.; Auzenne, E.; Farquhar, D.; Klostergaard, J. *Bioconjugate Chemistry* **2007**, 731-735.

21 Albers, A. E.; Okreglak, V. S.; Chang, C. J. *Journal of American Society* **2006**, 9640-9641.

22 Soh, N.; Makihara, K.; Sakoda, E.; Imato, T. *Chemical Communications (Cambridge, United Kingdom)* **2004**, 496-497.

23 King, M.; Kopelman, R. *Sensors and Actuators, B: Chemical* **2003**, *B90*, 76-81.

24 Macossay, J.; Shamsi, S. A.; Warner, I. M. *Tetrahedron Letters* **1999**, *40*, 577-580.

25 Bardajee, G. R.; Winnik, M. A.; Lough, A. J. *Acta Crystallographica Section E-Structure Reports Online* **2007**, *63*, o1513-o1514.

26 Ganea, G. M.; Sabliov, C. M.; Ishola, A. O.; Fakayode, S. O.; Warner, I. M. *Journal of Nanoscience and Nanotechnology* **2008**, *8*, 280-292.

CHAPTER 5
CONCLUSIONS AND FUTURE STUDIES

The major goal of this dissertation was to demonstrate the utility of molecular micelles in nanoparticle synthesis. Molecular micelle – modified polymeric nanoparticles can be used as drug delivery systems for delivery of antioxidants. In addition, they can serve as nanoparticle – based analytical sensors for detection of free radicals. The importance of drug delivery systems and the use of polymeric nanoparticles as drug delivery systems were emphasized in the first chapter of this dissertation. In addition, methods of nanoparticle synthesis and nanoparticle characterization were described in detail. Molecular micelles were compared with conventional micelles, and their utility in nanoparticle synthesis was revealed. The concepts of antioxidants, oxidative stress and free radicals were introduced as well. Chemometrics and optimization designs played an important role in the research included in this dissertation and were described in the first chapter as well.

In the second chapter, molecular micelles were used as novel emulsifiers in the synthesis of poly (D,L lactide-*co*-glycolide) (PLGA) nanoparticles by emulsification solvent evaporation. Examples of such micelles include poly (sodium *N*-undecenyl sulfate) (poly-SUS), poly (sodium *N*-undecenyl-glycinate) (poly-SUG) and poly (sodium *N*-undecenyl-L-leucyl-valinate) (poly-L-SULV). Other emulsifiers, such as anionic sodium dodecyl sulfate (SDS) and non-ionic poly (vinyl alcohol) (PVA) were used for comparison. The optimization of nanoparticle synthesis was achieved by the use of a central composite experimental design (CCD). The individual and combined effects of PLGA concentration, emulsifier concentration, homogenization speed, and sonication time (design variables) on particle size and polydispersity index (responses) were investigated using multivariate analysis. The most significant design variables influencing the nanoparticle size and size distribution were PLGA concentration and emulsifier concentration (*p*

< 0.05) in comparison to the other design variables. The quadratic model demonstrated the highest predictive ability when the molecular micelles were used as emulsifiers. The PLGA nanoparticles optimally synthesized according to the CCD were further purified by dialysis and then freeze-dried. Dried nanoparticles synthesized with molecular micelles and PVA were readily re-suspended in water, as compared with SDS for which nanoparticle aggregation occurred. The size of PLGA nanoparticles synthesized using molecular micelles increased after freeze-drying, but remained below 100 nm when poly-L-SULV was used as emulsifier. The PDI values indicated monodisperse nanoparticle suspensions after purification and freeze-drying for all investigated molecular micelles (PDI < 0.100). The nanoparticle suspensions synthesized using molecular micelles were the most stable after dialysis and freeze-drying, having low negative zeta potential values ranging from - 54 ± 1.6 mV for poly-L-SULV to - 63.2 ± 0.4 mV for poly-SUS. Transmission electron microscopy (TEM) micrographs showed spherical shapes and smooth surfaces for the molecular micelle – modified PLGA nanoparticles.

In the third chapter of this dissertation, anionic amino acid - based molecular micelles were used as emulsifiers in the synthesis of thymoquinone (TQ)-loaded PLGA nanoparticles by use of an emulsification solvent evaporation method. The nanoparticle synthesis was optimized for maximum entrapment efficiency using a Box-Behnken experimental design. Optimum conditions were found to be 100 mg PLGA, 15 mg TQ and 0.5% w/v emulsifier [poly(sodium *N*-undecenyl-glycinate) (poly-SUG)]. In addition, other structurally related molecular micelles having various amino acid head groups and different hydrophobic carbon chain lengths were also examined as emulsifiers, and provided excellent emulsifier properties, leading to monodispersed particle sizes below 200 nm, and maximum entrapment efficiency. *In vitro* release studies revealed a rapid TQ release in the first 8 hours, the highest release levels being obtained for poly-SUG and poly(sodium *N*-heptenyl-glycinate) (poly-SHG). The antioxidant activity of TQ-

loaded nanoparticles, indicated by IC50 (mg/mL TQ for 50% 2,2-diphenyl-1-picrylhydrazyl (DPPH) scavenging activity), was the highest for poly(sodium *N*-undecenyl-alaninate) (poly-SUA)-emulsified nanoparticles (0.023±0.001 mg/mL), representing an improvement factor of 5.7 as compared to free TQ. In addition, TQ-loaded nanoparticles showed lower cytotoxic effects than the equivalent free TQ for normal (Hs578Bct) breast cells, indicating a protective effect provided by the nanoparticles. For MCF-7 breast cancer cells, the lowest cell viability was obtained for poly(sodium *N*-undecenyl-leucinate) (poly-SUL) – emulsified nanoparticles (43.26±9.45%), which is comparable to free TQ (37.42±4.83%). In addition, TQ-loaded nanoparticles emulsified with poly(sodium *N*-undecenyl-valinate) (poly-SUV) were more effective for MDA-MB-231 breast cancer cell inhibition (68.47±8.42%) than free TQ. Molecular micelles offered high flexibility to nanoparticle physico-chemical and biological properties and, therefore, can be used in the synthesis of drug-loaded nanoparticles depending on the desired properties. In addition, such nanoparticles are promising as free radical scavengers and inhibitors of breast cancer cells.

Molecular micelle – modified nanoparticles are not only an example of drug delivery systems, but nanosensors that can be used for detection of various molecules. In the fourth chapter of this dissertation, polymeric nanoparticles were synthesized using fluorescent labeled molecular micelles that served as detectors for hydroxyl radicals. Specifically, poly (sodium N-undecenyl - Nε - lysinate) (poly-Nε-SUK) functionalized with coumarin 3-carboxylic acid (C3C) was used as emulsifier in the synthesis of neutral red (NeR) - loaded PLGA nanoparticles by emulsification – solvent evaporation. Ratiometric fluorescence spectroscopy was applied for the detection of hydroxyl radicals based on the intensity ratios of a reporting and reference dyes, respectively. The product of C3C reaction with hydroxyl radical, 7-hydroxy coumarin 3-carboxylic acid (7-OH C3C) represented the reporting dye, while NeR encapsulated into the

nanoparticles was the reference dye. Other fluorescent and non-fluorescent molecular micelles were used in the synthesis of control nanoparticles. C3C-poly-Nε-SUK – modified NeR-loaded nanoparticles were able to detect hydroxyl radicals in simulated samples as well as biological samples exposed to oxidative stress. Furthermore, the ratiometric nanoparticles were selective for hydroxyl radicals as compared to other reactive oxygen species including superoxide anion ($O_2^{\bullet-}$), hydrogen peroxide (H_2O_2), singlet oxygen ($^1O_2$), and hypochlorite (OCl^-). In addition to nanosensor spectral properties, their low toxicity and fast cellular uptake allow their potential use in the study of other living systems.

The research presented in this dissertation demonstrated the utility of molecular micelles in nanoparticle synthesis, their versatility that conferred tunable properties for drug loaded nanoparticles, and their ability to offer functional groups for analytical purposes. Molecular micelle – modified nanoparticles are not only an example of drug delivery systems, but nanosensors that can be used for detection of various molecules. Their biodegradability and biocompatibility represent great advantages as compared with toxicity of other nanoparticles used for analytical purposes.

There are multiple possibilities for further use of molecular micelle – modified nanoparticles. Taking into consideration the fact that many antioxidants exhibit protective effects in chemotherapy and some of them have anticancer properties, the co-entrapment of multiple antioxidants and anticancer drugs having both scavenging and anticancer properties can be studied as potential treatment for various cancers. In addition, there is a large variety of molecules that can be covalently attached to molecular micelles. Several examples include fluorescent dyes, near infrared dyes, folate-based conjugates, aptamers, and others. Such molecules can serve multiple purposes ranging from targeted delivery to detection of small reactants and disease biomarkers in biological systems.

APPENDIX I

GENERAL SYNTHESIS SCHEME OF MOLECULAR MICELLES

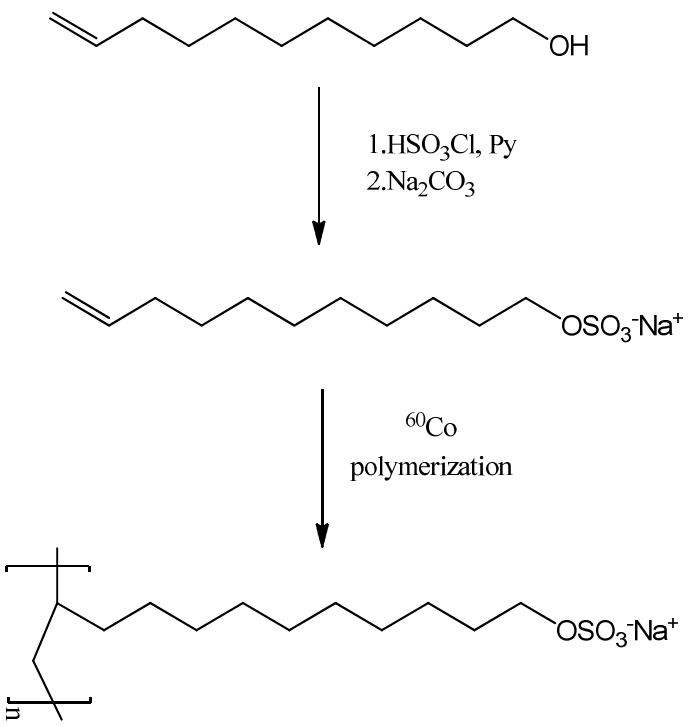

Appendix I.A Synthesis of Poly-SUS.

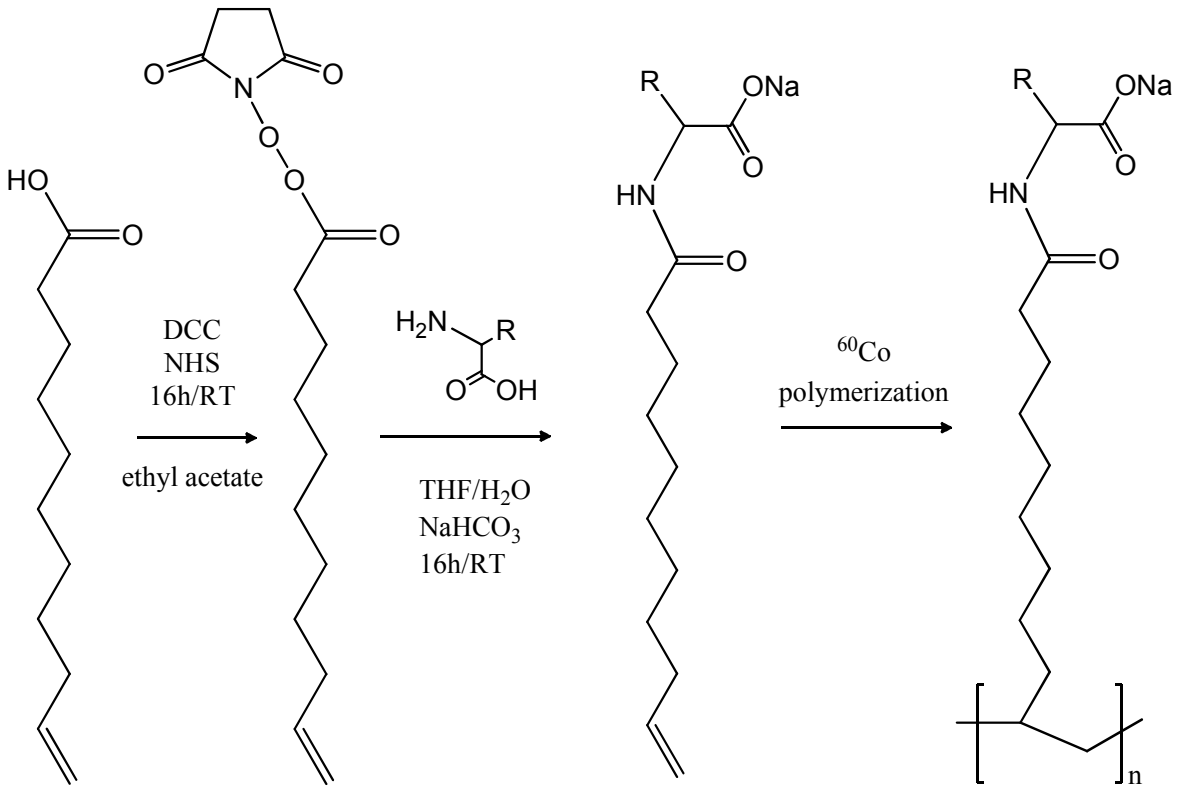

Appendix I.B Synthesis of amino acid and dipeptide based molecular micelles.

APPENDIX II
EXPERIMENTAL CONDITIONS USED IN THE CENTRAL COMPOSITE DESIGN

Exp. No.	Experimental conditions			
	PLGA (% (w/v))	Emulsifier (% (w/v))	H. speed (rpm)	S. time (min)
1	5.0	1.00	10,000	5
2	3.5	0.55	15,000	10
3	5.0	1.00	20,000	15
4	5.0	1.00	10,000	15
5	0.5	0.55	15,000	10
6	2.0	1.00	20,000	15
7	2.0	0.10	10,000	15
8	5.0	1.00	20,000	5
9	2.0	0.10	10,000	5
10	3.5	0.55	25,000	10
11	6.5	0.55	15,000	10
12	2.0	0.10	20,000	5
13	2.0	1.00	10,000	5
14	3.5	0.05	15,000	10
15	3.5	0.55	15,000	20
16	3.5	0.55	15,000	10
17	3.5	0.55	5,000	10
18	3.5	0.55	5,000	0
19	3.5	1.45	15,000	10
20	3.5	0.55	15,000	10
21	2.0	1.00	10,000	15
22	5.0	0.10	20,000	15
23	3.5	0.55	15,000	10
24	2.0	0.10	20,000	15
25	5.0	0.10	20,000	5
26	2.0	1.00	20,000	5
27	3.5	0.55	15,000	10
28	5.0	0.10	10,000	5
29	5.0	0.10	10,000	15

APPENDIX III
RESULTS OF ANALYSIS OF VARIANCE FOR CENTRAL COMPOSITE DESIGN

Particle size (Z_{ave})										
	SDS		**PVA**		**Poly-SUS**		**Poly-SUG**		**Poly-L-SULV**	
R^2	0.953		0.933		0.937		0.966		0.985	
	p	b_{xy}	*p*	b_{xy}	*p*	b_{xy}	*p*	b_{xy}	*p*	b_{xy}
b_0	0.00	55.77	0.00	312.74	0.00	126.14	0.00	134.69	0.00	139.01
X_1	0.00	4.38	0.00	21.95	0.00	8.77	0.00	5.47	0.00	9.94
X_2	0.00	-26.82	0.00	-266.23	0.00	-52.20	0.00	-76.95	0.00	-49.84
X_3	0.46	0.00	0.45	0.00	0.83	0.00	0.25	0.00	0.12	0.00
X_4	0.13	-0.33	0.02	-5.90	0.01	-1.35	0.00	-1.54	0.00	-1.99
X_1X_2	0.00	-4.21	0.02	-26.11	0.44	-1.60	0.51	1.34	0.59	-0.54
X_1X_3	0.50	0.69	0.46	-7.93	0.70	0.85	0.32	2.24	0.15	-1.76
X_1X_4	0.89	-0.13	0.34	-9.40	0.29	2.16	0.05	4.32	0.00	4.01
X_2X_3	0.27	1.07	0.29	10.83	0.49	-1.43	0.79	-0.53	0.00	3.77
X_2X_4	0.11	1.44	0.18	12.60	0.26	2.15	0.03	4.55	0.00	-4.40
X_3X_4	0.15	-1.35	0.18	13.27	0.32	1.99	0.18	2.79	0.06	2.23
X_1^2	0.16	1.16	0.73	2.87	0.49	-1.19	0.63	0.86	0.01	-2.80
X_2^2	0.00	6.13	0.00	44.11	0.00	9.70	0.00	10.72	0.00	10.75
X_3^2	0.86	-0.14	0.43	6.62	0.80	0.44	0.09	3.21	0.37	0.79
X_4^2	0.06	1.74	0.04	19.79	0.12	2.98	0.03	4.68	0.45	0.78

Appendix III.A Analysis of variance for particle size.

Polydispersity Index (PDI)										
	SDS		**PVA**		**Poly-SUS**		**Poly-SUG**		**Poly-L-SULV**	
R^2	0.872		0.970		0.773		0.743		0.914	
	p	b_{xy}	p	b_{xy}	p	b_{xy}	p	b_{xy}	p	b_{xy}
b_0	0.00	0.00	0.13	0.00	0.14	0.00	0.09	0.00	0.11	0.00
X_1	0.00	0.00	-0.01	0.01	0.01	0.41	0.00	0.31	0.00	0.05
X_2	0.00	0.00	0.04	0.00	-0.22	0.00	0.06	0.00	0.04	0.00
X_3	0.46	0.02	0.00	0.34	0.00	0.53	0.00	0.37	0.00	0.68
X_4	0.13	0.74	0.00	0.53	0.00	0.95	0.00	0.52	0.00	0.66
X_1X_2	0.00	0.00	-0.02	0.00	-0.02	0.40	0.00	0.14	-0.01	0.06
X_1X_3	0.50	0.04	-0.01	0.94	0.00	0.30	0.00	0.36	0.00	0.66
X_1X_4	0.89	0.48	0.00	0.92	0.00	0.90	0.00	0.46	0.00	0.61
X_2X_3	0.27	0.67	0.00	0.34	0.01	0.80	0.00	0.51	0.00	0.53
X_2X_4	0.11	1.00	0.00	0.30	0.01	0.51	0.00	0.23	0.01	0.19
X_3X_4	0.15	0.41	0.00	0.23	0.01	0.21	-0.01	0.77	0.00	0.91
X_1^2	0.16	0.04	0.01	0.84	0.00	0.73	0.00	0.27	0.00	0.02
X_2^2	0.00	0.69	0.00	0.00	0.04	0.05	-0.01	0.12	-0.01	0.00
X_3^2	0.86	0.11	0.01	0.45	0.00	0.73	0.00	0.92	0.00	0.93
X_4^2	0.06	0.49	0.00	0.00	0.03	0.22	0.00	0.10	-0.01	0.23

Appendix III.B Analysis of variance for polydispersity index.

APPENDIX IV
FLUORESCENCE OF NEUTRAL RED LOADED PLGA NANOPARTICLES

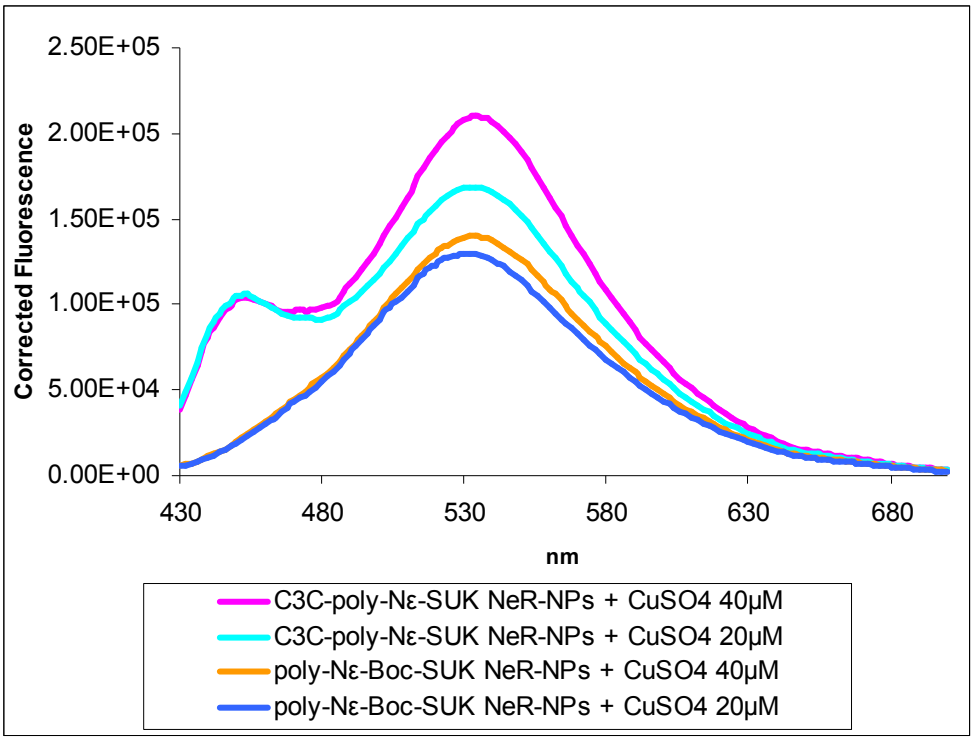

Appendix IV.A Fluorescence spectra of nanoparticles after the reaction with $OH^{\bullet}$ (0.07 mg/mL nanoparticles, 20 mM H_2O_2, 200 μM ascorbic acid, 20 and 40 μM $CuSO_4$, incubated for 5 min; total volume 500 mL)

Before reaction with OH• **After reaction with OH•**

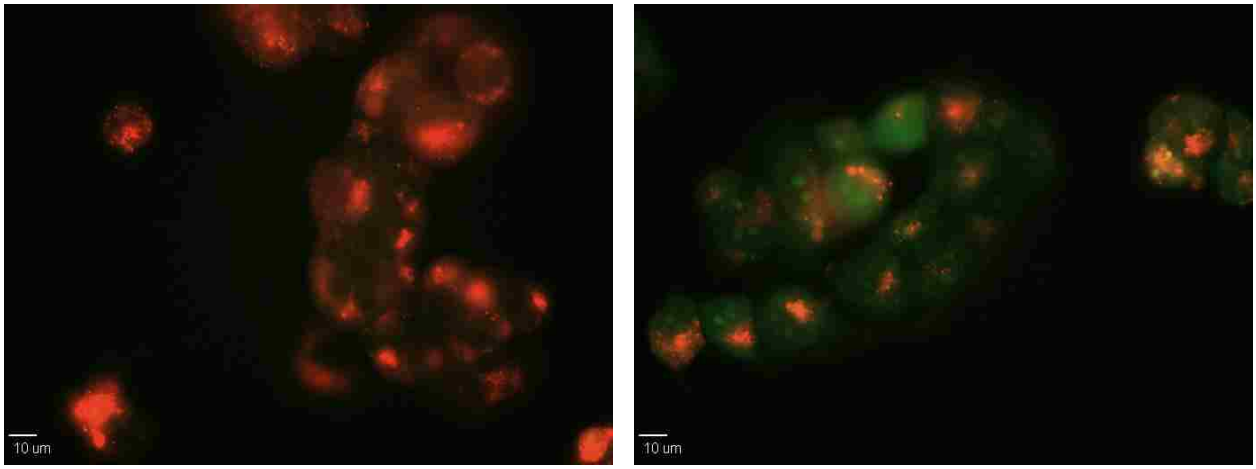

C3C-poly-Nε-SUK – modified NeR-loaded PLGA nanoparticles

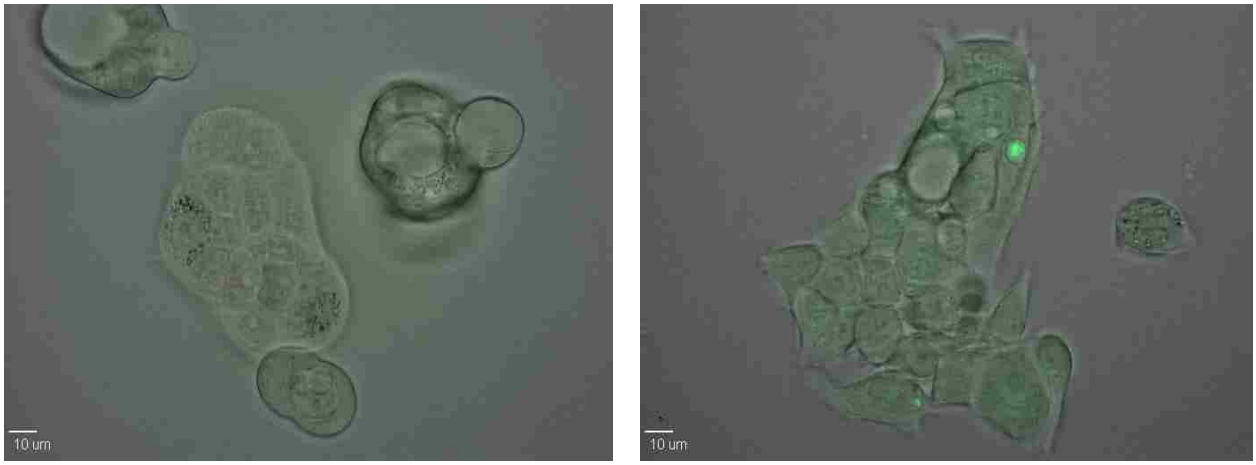

C3C-poly-Nε-SUK – modified blank PLGA nanoparticles

Appendix IV.B Fluorescence micrographs of nanoparticle response in MCF-7 cells before and after exposure to H_2O_2 – induced oxidative stress (400 μM).

APPENDIX V
COPYRIGHT AGREEMENT LETTER

Re: copyright agreement for doctoral thesis

1 message

nalwa@mindspring.com <nalwa@mindspring.com> **Tue, Oct 20, 2009 at 10:11 AM**
Reply-To: nalwa@mindspring.com
To: Gabriela Visser <gganea1@tigers.lsu.edu>

Hi Gabriela:

American Scientific Publishers grants permission to use text, data, figures and tables into your PhD thesis. from the following article.

Ganea G. M., Sabliov C. M., Ishola A., Fakayode S. O., Warner I. M., *Experimental design and multivariate analysis for optimizing poly(D,L-lactide-co-glycolide) (PLGA) nanoparticle synthesis using molecular micelles*, Journal of Nanoscience and Nanotechnology, volume 8, number 1, January 2008, pages 280–292

Please make sure to cite the reference.

Best regards,

H. S. Nalwa

-----Original Message-----
From: Gabriela Visser
Sent: Oct 20, 2009 10:03 AM
To: jnn@aspbs.com, weichen@uta.edu
Subject: copyright agreement for doctoral thesis

Dear Sirs,
My name is Gabriela M Ganea (married Visser) and I am currently writing my doctoral thesis. I hereby request the permission to reproduce text, data, figures and tables in my thesis from the publication listed below:
Ganea G. M., Sabliov C. M., Ishola A., Fakayode S. O., Warner I. M., *Experimental design and multivariate analysis for optimizing poly(D,L-lactide-co-glycolide) (PLGA) nanoparticle synthesis using molecular micelles*, Journal of Nanoscience and Nanotechnology, volume 8, number 1, January 2008, pages 280–292
Thank you for your consideration on my request.
Sincerely,

Gabriela M Visser
PhD candidate, Analytical Chemistry
Warner Research Group
Chemistry Department
Louisiana State University
Baton Rouge, LA, 70803
225-578-3919
gganea1@tigers.lsu.edu

VITA

Gabriela was born in Galati, Romania, in the wonderful family of Aurelian and Cristinica Ganea. Her primary, middle and high school education took place in Galati. Her passion for chemistry started in the seventh grade when she was the first in her class to get an A on a chemistry test. Her high school education focused on science subjects such as mathematics, physics and chemistry. She also participated in local and national competitions such as chemistry and biology Olympiads. Her college education took place in Bucharest, the capital of Romania, at the University of Bucharest, College of Chemistry. As an undergraduate student, Gabriela participated in research programs within the National Dairy Institute, and Microbiology Center of the University of Bucharest. She also received a summer internship at the Immunology Cantacuzino Institute in Bucharest. She received a bachelor's degree in biochemistry, and throughout her college she was the recipient of an undergraduate scholarship granted by the Romanian Ministry of Education. After her college, Gabriela returned to Galati to work as a chemist in the Environmental Protection Department of Ispat Sidex, Galati. The experience gained in the industry encouraged her to pursue her graduate studies. In 2002, she returned to the University of Bucharest to earn her master's degree in bioanalytical chemistry. Her research involved the development of analytical sensors for the detection of genetically modified organisms. During her graduate studies, she received a graduate assistantship granted by the Romanian Ministry of Education. Immediately after that, in 2004, Gabriela went to the United States to continue her graduate studies at Louisiana State University under the guidance of Dr. Isiah Warner. As a doctoral candidate, Gabriela was presented with Outstanding Research Assistant Award in 2009 granted by Chemistry Department, Louisiana State University. Gabriela graduated with the degree of Doctor of Philosophy in chemistry from Louisiana State University in December 2009. Publications and conference presentations include:

Ganea G. M., Sabliov C. M., Ishola A., Fakayode S. O., Warner I. M., *Experimental design and multivariate analysis for optimizing poly(D,L-lactide-co-glycolide) (PLGA) nanoparticle synthesis using molecular micelles*, Journal of Nanoscience and Nanotechnology, 8, 280–292 (2008)

Gates A. T., Fakayode S. O., Lowry M., **Ganea G. M.**, Murugeshu A., Robinson J.W., Strongin R. M., Warner I. M. *Gold nanoparticle sensor for homocysteine thiolactone-induced protein modification* – Langmuir, 24 (8), 4107 - 4113, (2008)

Ganea G. M., Fakayode S. O., Losso J. N., van Nostrum C. F., Sabliov C. M., Warner I. M. *The effect of molecular micelles on synthesis and properties of thymoquinone-loaded poly(d,l lactide-co-glycolide) nanoparticles,* Pharmaceutical Research, submitted (2009)

Ganea G. M., Kolic P., Losso J. N., Warner I. M. *Fluorescent ratiometric molecular micelle - modified poly(d,l lactide-co-glycolide) nanoparticles for detection of hydroxyl radicals,* in preparation for submission (2009)

2006 - Poster presentation at local CBM^2 competition, Baton Rouge, LA

2008 - Poster presentation at Pittcon Analytical Chemistry Conference, New Orleans, LA

2008 - Poster presentation at ACS National Conference, New Orleans, LA

2008 - Poster presentation at ACS National Conference, Philadelphia, PA, 2008